



MARTIN-LUTHER-UNIVERSITÄT

HALLE-WITTENBERG

Synthesis and Aggregation Behavior of Poly(propylene oxide)-Based Amphiphilic and Triphilic Block Copolymers

Dissertation

Zur Erlangung des akademischen Grades

Doctor rerum naturalium (Dr. rer. nat.)

vorgelegt der

Naturwissenschaftlichen Fakultät II–Chemie und Physik

der Martin-Luther-Universität Halle-Wittenberg

von

von Herrn Samuel Oppong Kyeremateng

geb. am 21. August 1978 in Kumasi, Ghana

Gutachter:

1. Prof. Dr. Jörg Kressler

2. Prof. Dr. Karl-Friedrich Arndt

Halle (Saale), den 11 August, 2010

DEDICATION

To my Lord, the author and finisher of my faith.....

Abbreviations

AFM	Atomic Force Microscopy
AIBN	2,2'-Azo-bis(isobutyronitrile)
ATRA	Atom Transfer Radical Addition
ATRP	Atom Transfer Radical Polymerization
BIB	2-Bromoisobutyryl bromide
bpy	2, 2'-Bipyridine
Cmc	Critical Micellization Concentration
Cmt	Critical Micellization Temperature
CRP	Controlled Radical Polymerization
CryoSEM	Cryogenic Scanning Electron Microscopy
CTA	Chain Transfer Agent
CuAAC	Copper(I)-Catalyzed Alkyne-Azide Cycloaddition
DCC	N, N'-(dicyclohexyl)carbodiimide (DCC)
DIPEA	N-Ethyl-diisopropylamine
DMAP	4-(Dimethylamino) pyridine
DMF	Dimethylformamide
DMSO- <i>d</i> ₆	Deuterated Dimethyl sulfoxide
DP	Degree of Polymerization
DSC	Differential Scanning Calorimetry
Et ₃ N	Triethylamine
FT-IR	Fourier Transform Infrared
GMA	Glycerol monomethacrylate
HSDSC	High Sensitivity Differential Scanning Calorimetry
ITC	Isothermal Titration Calorimetry
LCST	Lower Critical Solution Temperature
<i>M</i> _n	Number Average Molar Mass
<i>M</i> _w	Weight Average Molar Mass
MADIX	Macromolecular Design via Interchange of Xanthates
NMP	Nitroxide Mediated Polymerization
NMR	Nuclear Magnetic Resonance
PB	Poly(butadiene)
PBO	Poly(butylene oxide)
PDI	Polydispersity Index

PEE	Poly(ethyl ethylene)
PEEP	Poly(ethyl ethylene phosphate)
PEO	Poly(ethylene oxide)
PFO	Poly(perfluoropropylene oxide)
PG	Poly(glycidol)
PGMA	Poly(glycerol methacrylate)
PPO	Poly(propylene oxide)
PS	Poly(styrene)
PSMA	Poly(solketal methacrylate)
PVCL	Poly(<i>N</i> -vinyl caprolactam)
PVME	Poly(vinyl methyl ether)
py	Pyridine
RAFT	Reversible Addition Fragmentation Chain Transfer
R–X	Alkyl Halide
SEC	Size Exclusion Chromatography
SMA	Solketal methacrylate
SPAAC	Strain-Promoted Azide-Alkyne Cycloaddition
TBTA	Tris-(benzyltriazolylmethyl)amine
TEM	Transmission Electron Spectroscopy
TEMPO	2,2,6,6-Tetramethyl-1-piperidinoxyl
TFB	Tetrafluorobenzene
TFT	α,α,α -Trifluorotoluene
THF	Tetrahydrofuran
TLC	Thin Layer Chromatography

Symbols

I^\bullet	Radical initiator
R^\bullet	Radical specie
P_m^\bullet	Propagating specie
f	Initiator efficiency
D_{app}	Apparent diffusion coefficient
Γ	Characteristic decay rate
q	Scattering vector
n_o	Refractive index
θ	Scattering angle
λ	Wavelength
r_o	Core radius
R_h	Apparent hydrodynamic radius
$[\eta]$	Intrinsic viscosity
η	Viscosity
T	Absolute temperature
R	Molar gas constant
γ	Surface tension
N_A	Avogadro's number
k	Boltzmann constant
τ_c	Closing required for loop formation
b	Kuhn's length
l_p	Persistence length
l	Length of monomeric unit
r	End-to-end distance
L	Length of polymer chain
N	Degree of polymerization
C_∞	Characteristic ratio
ΔG°_{mic}	Standard free energy of micellization
ΔH°_{mic}	Standard ethalpy of micellization
ΔS°_{mic}	Standard entropy of micellization
ΔH_t	Endothermic transfer enthalpy

Contents	Page
List of Abbreviations	iii
List of Symbols	v
Chapter 1 – General Introduction	1
1.1 Current Techniques for Block Copolymer Synthesis	1
1.2 Methods of Controlled Radical Polymerization (CRP)	4
1.2.1 Polymerization by Reversible Addition Fragmentation Chain Transfer (RAFT)	4
1.2.2 Nitroxide Mediated Polymerization (NMP)	5
1.2.3 Atom Transfer Radical Polymerization (ATRP)	7
1.3 ‘Click’ Chemistry in Macromolecular Synthesis	9
1.4 Block Copolymers in Aqueous Medium	13
1.5 Motivation and Objectives of this Work	15
1.6 References and Notes	17
Chapter 2 – Synthesis of Amphiphilic and Triphilic Block Copolymers by ATRP and Copper(I)-Catalyzed Alkyne-Azide Cycloaddition (CuAAC) ‘Click’ Reaction	23
2.1 Introduction	23
2.2 Synthesis of Monomer (Solketal Methacrylate)	24
2.3 ATRP Initiators Synthesis	25
2.4 Synthesis of Alkyne-End Functionalized Compounds	27
2.5 Synthesis of Polymers by ATRP	28
2.6 Copper(I)-Catalyzed Alkyne-Azide Cycloaddition (CuAAC) ‘Click’ Reactions	35
2.7 Acidic Hydrolysis of Block Copolymers	36
2.8 Conclusions	38
2.9 References	39

Chapter 3 – Aggregation Behavior of Amphiphilic PPO/PGMA and PPO/PEO Block Copolymers in Water	41
3.1 Introduction	41
3.2. Experimental Part	43
3.2.1 Materials	43
3.2.2 Characterization	43
3.2.2.1 Dynamic Light Scattering (DLS)	43
3.2.2.2 ¹ H NMR Spectroscopy	44
3.2.2.3 Small Angle Neutron Scattering (SANS)	44
3.2.2.4 Surface Tension	44
3.2.2.5 Isothermal Titration Calorimetry (ITC)	45
3.3 Results and Discussion	45
3.3.1 Temperature-Dependent DLS Studies	45
3.3.2 Temperature-Dependent ¹ H NMR Studies	47
3.3.3 Temperature-Dependent Surface Tension Measurements	51
3.3.4 Isothermal Titration Calorimetry Studies	56
3.3.5 Temperature-Dependent SANS Studies	59
3.4 Conclusions	61
3.5 References	62
Chapter 4 – Effect of Hydrophilic Block Length-A on the Aggregation Behavior of Triphilic CABAC Pentablock Copolymer Analogues in Water	66
4.1 Introduction	66
4.2. Experimental Part	67
4.2.1 Materials	67
4.2.2 Characterization	68
4.2.2.1 NMR Spectroscopy	68

4.2.2.2 Surface Tension Measurement	68
4.2.2.3 Dynamic Light Scattering (DLS)	69
4.2.2.4 Tetrafluorobenzene (TFB) Solubilization Experiments	69
4.2.2.5 Atomic Force Microscopy (AFM)	70
4.2.2.6 Transmission Electron Microscopy (TEM)	70
4.3 Results and Discussion	70
4.3.1 Surface Tension Measurements	70
4.3.2 DLS Studies	71
4.3.3 NMR Spectroscopy Studies	76
4.3.4 Aggregation Mechanism and Loop Formation	81
4.3.5 AFM and TEM Investigations on Polymer Aggregates	85
4.3.6 TFB Uptake-Capabilities of Block Copolymer Micelles	87
4.4 Conclusions	89
4.5 References	90
Chapter 5 – Aggregation Behavior of Triphilic CAB Triblock Copolymer Analogues in Water: Comparison with Triphilic CBA and Amphiphilic BA Counterparts	93
5.1 Introduction	93
5.2. Experimental Part	95
5.2.1 Materials	95
5.2.2 Characterization	96
5.2.2.1 Surface Tension Measurement	96
5.2.2.2 Dynamic Light Scattering (DLS)	96
5.2.2.3 Atomic Force Microscopy (AFM)	97
5.2.2.4 Transmission Electron Microscopy (TEM)	97
5.3 Results and Discussion	97
5.3.1 Surface Tension Measurements	97
5.3.2 DLS Studies	100
5.3.3 AFM and TEM Investigations on Polymer Aggregates	105
5.4. Conclusions	108
5.5 References	109

Chapter 6 – Summary	111
Chapter 7 – Experimental Procedures for Synthesis of Block Copolymers	114
7.1 Materials	114
7.2 Synthesis of Monomer (Solketal Methacrylate)	114
7.3 ATRP Initiators Synthesis	115
7.4 Synthesis of Alkyne-End Functionalized Compounds	117
7.5 Synthesis of BA ABA and CA Block Copolymers by ATRP	118
7.6 Replacement of Br Chain-End Functionality with N ₃ (Azidation Reaction)	119
7.7 Copper(I)-Catalyzed Alkyne-Azide Cycloaddition (CuAAC) ‘Click’ Reactions	120
7.8 Acidic Hydrolysis of the Acetonide Groups of the Block Copolymers	120
7.9 References	121
Appendix	122
Acknowledgements	129
Publications	130
Curriculum Vitae	131

Chapter 1

General Introduction

1.1 Current Techniques for Block Copolymer Synthesis

Specific polymers exhibit different intrinsic characteristics and properties due to their different constituent monomer units. Covalently linking two or more different polymer blocks in a polymer chain, results in a block copolymer. Recent advances in polymer synthesis techniques allow almost complete freedom in selecting the polymer for each block. Thus, by tailoring the blocks lengths, sequence, and architecture, block copolymers may exhibit new and interesting properties which are the resultant effect of the combined characteristics and properties of the individual blocks. These resultant properties attract great attention in high technological fields such as nanotechnology, optics and biomaterials.^{1,2} Therefore, the synthesis of tailor-made macromolecules with desired molecular design and consequently, the understanding of the quantitative structure-property relationships have become the main focus of polymer chemists.

The first way to block copolymer synthesis was opened with the invention of anionic polymerization by Szwarc et al. in 1956.³ This enabled polymer chemist for the first time to gain control over the degree of polymerization (DP), number average molar mass (M_n), and polydispersity index (PDI). Due to the livingness of macroanions formed during the polymerization, block copolymers became accessible upon addition of the second monomer after the full consumption of the first monomer batch. About 30 years after Szwarc's work, the controlled/living routes for cationic polymerization were discovered. The highlights of the living cationic polymerization are presented in an elegant review by Kennedy, whose fundamental contributions to the field led to novel block copolymer structures based on monomers not susceptible to anionic polymerization.⁴ However, preparation of block copolymers by means of anionic or cationic polymerization is rather problematic due to reactivity restrictions of the monomers and demanding requirements.⁵ This directed synthetic chemists to focus on other polymerization techniques that require less stringent conditions and have wide monomer applicability.

The mid to late 1990s saw the start and growth of new polymerization methods for preparation of block copolymers with sufficient control over DP, M_n and PDI similar to ionic

polymerization methods. These new methods called controlled radical polymerization (CRP) techniques have opened new opportunities in block copolymer synthesis. In principle, the CRP techniques are based on the delicate balance between dormant and active species. Their success lies in the ability to introduce relatively stable chain end functionalities that can be reactivated for subsequent block copolymerization or post-polymerization modifications. Since polymerization, in this case, proceeds by radicals rather than ions as with the case of ionic polymerization, CRP techniques show tolerance to functional groups and can be used on a wide variety of monomers. Therefore, CRP techniques enable the synthesis of many well-defined copolymers with controlled architectures, compositions, and functionalities. Currently, the three main CRP techniques which have attracted the most attention are atom transfer radical polymerization (ATRP), reversible addition-fragmentation chain transfer polymerization (RAFT) and nitroxide-mediated radical polymerization (NMP). The ever-growing application of these techniques in polymer synthesis is reflected in the yearly increase in their number of scientific publications as shown in Figure 1.1.

Post-polymerization modification reactions are also considered as a successful tool for the synthesis of functional polymers which can be covalently attached to inorganic, natural product molecules, natural polymer or another synthetic polymer to yield materials with previously unattainable properties. In 2002, the Nobel Prize laureate, K.B Sharpless, introduced the concept of ‘click’ chemistry that is based on highly efficient organic reactions between two easily accessible functional groups, azides and alkynes.⁷ Following this concept, several ‘click’ reactions in combination with CRP techniques have been described in the literature, thus, expanding the scope of tailor-made macromolecular topologies for advanced applications.⁸⁻¹⁶ In this thesis, such a combination with the ATRP technique has been employed to create novel perfluorocarbon-encapped di- and triblock copolymers. In addition, these novel block copolymers are investigated extensively with a wide array of polymer characterization techniques for their solution and bulk properties.

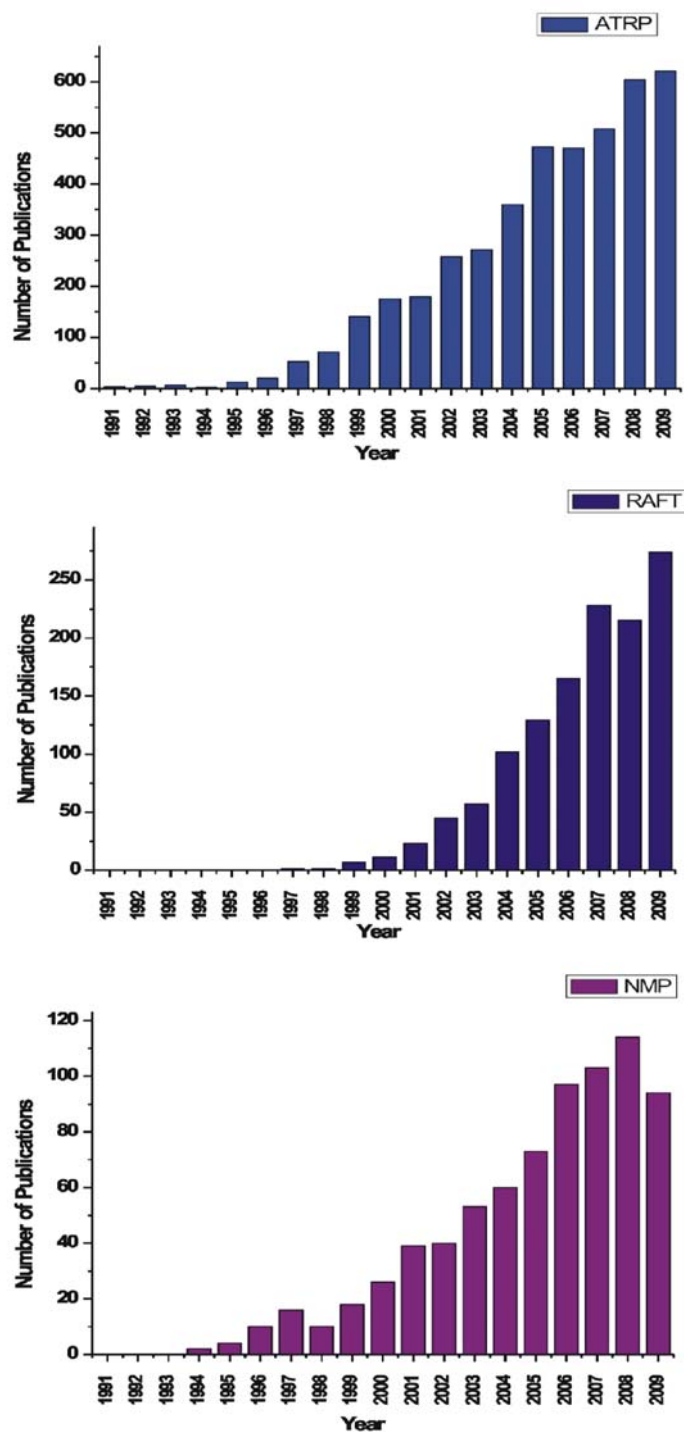


Figure 1.1 Number of publications in each year for the three main controlled radical polymerization techniques.⁶

1.2 Methods of Controlled Radical Polymerization (CRP)

1.2.1 Polymerization by Reversible Addition Fragmentation Chain Transfer (RAFT)

The reversible addition-fragmentation chain transfer (RAFT) polymerization technique was invented by Rizzardo et al. in 1998.¹⁷⁻¹⁹ Another group reported a similar technique known as MADIX (Macromolecular Design via the Interchange of Xanthates)^{20,21} RAFT polymerization works under conditions very similar to those of conventional free-radical polymerization. The major difference is the addition of certain thiocarbonylthio derivatives to an otherwise conventional free-radical polymerization mixture. These compounds contain an activated C=S double bond and act as reversible Chain Transfer Agents (CTA). The general structure of a CTA is depicted in Figure 1.2.

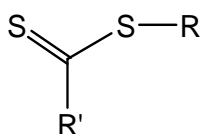


Figure 1.2 General chemical structure of a Chain Transfer Agent (CTA)

RAFT polymerization is carried out with a conventional initiator such as a peroxide or 2,2'-azo-bis(isobutyronitrile) (AIBN) in the presence of the CTA. Initiation, propagation and termination reactions are therefore the same as in conventional free-radical polymerization.²²

The polymerization process is controlled by the equilibrium between propagating and dormant chains as illustrated in Figure 1.3. In the pre-equilibrium (during the early stages of the polymerization), the oligomeric radical species, P_n^\bullet adds to the CTA to form an intermediate radical. This intermediate radical then fragments into an oligomeric thiocarbonylthio compound [$P_n\text{S}(\text{R}')\text{C}=\text{S}$], which constitutes the dormant species, and a new radical, R^\bullet . The R^\bullet radical re-initiates polymerization to generate a new propagating radical P_m^\bullet . In the main-equilibrium (after all of the CTA is consumed) the polymer chains change between the active state (during which they can add monomer) and the dormant state. This results in equilibrium between dormant polymer chains and propagating radicals, which gives a control character to the polymerization process. As a result, the polymer chains grow in

parallel, and the polymer has predictable molar mass and narrow molar mass distribution or polydispersity.

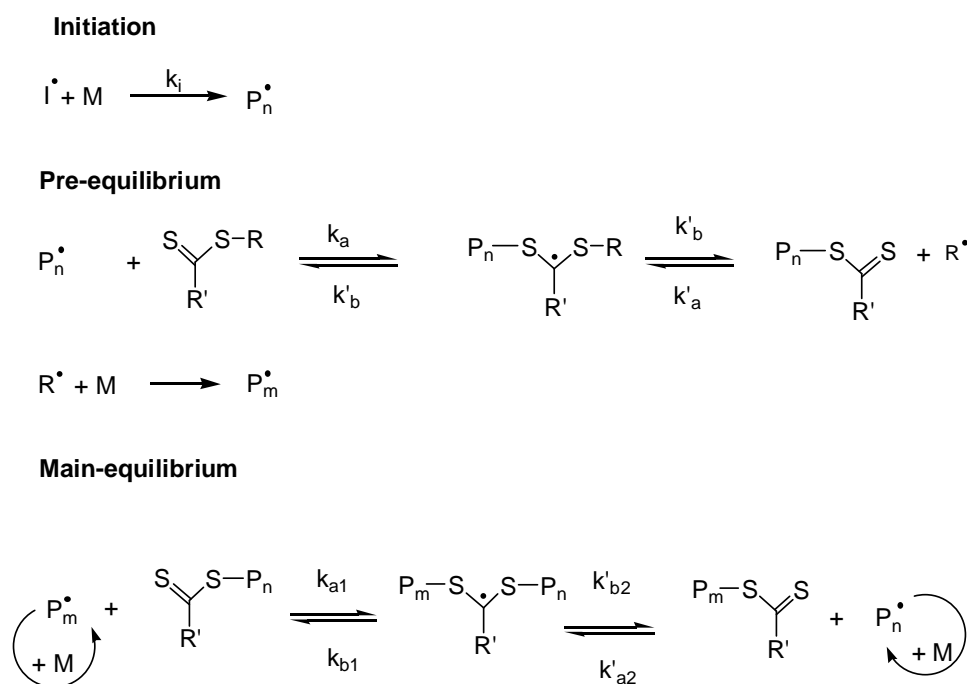


Figure 1.3 General mechanism of RAFT polymerization

The key that makes RAFT a controlled polymerization is the choice of the CTA. Controlled polymerization occurs with dithioesters because the transferred end group in the polymeric dithioester is as labile as the dithioester group in R'CSSR. A significant advantage of RAFT polymerization over other CRP techniques is that, it can be performed for a wide range of monomers in a large variety of solvents.^{19,23} However, there are also some disadvantages as well. The dithioester groups associated with the chain-ends of RAFT polymers give them color, potential odor and toxicity. Moreover, RAFT agents are not commercially available and must be synthesized.²⁴

1.2.2 Nitroxide Mediated Polymerization (NMP)

Nitroxide mediated radical polymerization (NMP) is one of the most environmentally friendly CRP techniques and has a relatively simple polymerization mechanism since there is no need for a catalyst. As simplified in Figure 1.4, NMP involves a combination of a reactive radical initiator (I^{\bullet}), monomer (M), and a stable nitroxide radical ($\bullet\text{ONR}^1\text{R}^2$), such as 2,2,6,6-tetramethyl-1-piperidinoxyl (TEMPO), for trapping of intermediate radical species. The

reactive radical initiates polymerization while the stable radical mediates the reaction by reacting with propagating radicals to lower their concentration. The nitroxide radical, although unreactive with itself, reacts rapidly with the propagating radical to decrease the concentration of propagating radicals sufficiently that conventional bimolecular termination is negligible. The propagating radical concentration is much lower than that of the dormant species, and this, results in control over molar mass and polydispersity.

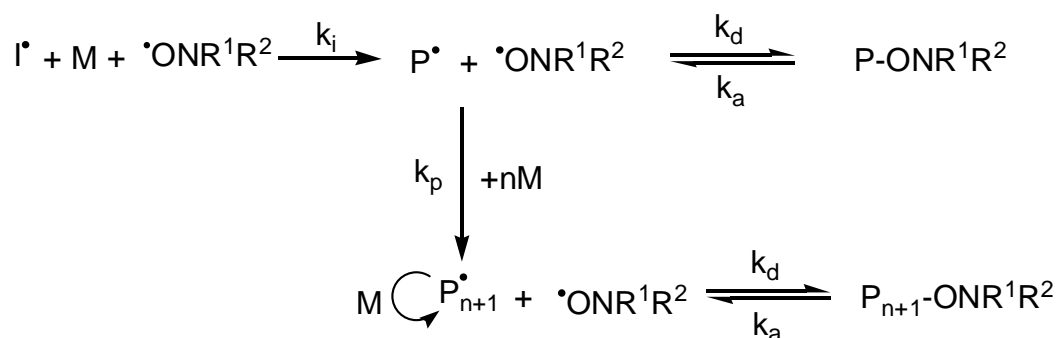


Figure 1.4 Mechanism of nitroxide mediated radical polymerization (NMP)

There are basically two different NMP concepts that have been developed, namely the bimolecular and the unimolecular process, respectively. In the bimolecular process, I^\bullet is generated from a conventional free radical initiator such as AIBN or benzoyl peroxide, whereas in the unimolecular process, the so-called “universal initiator” undergoes homolytic dissociation to provide both I^\bullet and $\cdot\text{ONR}^1\text{R}^2$.^{2,25} The dissociation of a typical universal initiator is shown below in Figure 1.5.

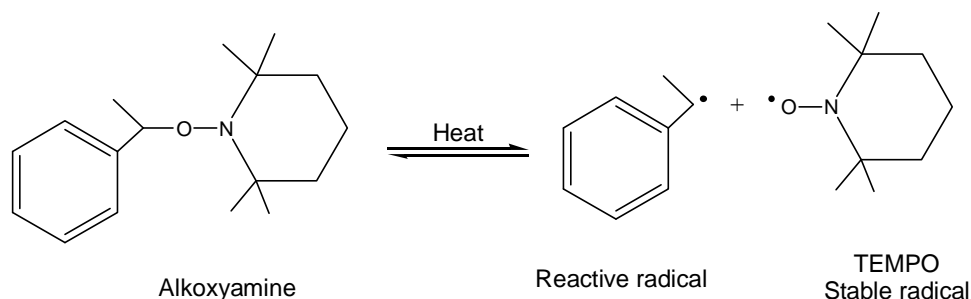


Figure 1.5 Thermal dissociation of alkoxyamine

The problems related to the NMP of monomers other than styrenics with TEMPO have been overcome by the introduction of new groups of nitroxyls such as the phosphonate derivatives, by Gnanou and Tordo^{26,27} and the family of arenes by Hawker.¹ These nitroxyls have been shown to be superior to TEMPO as they allow the controlled polymerization of a variety of monomer families such as acrylates^{28,29} acrylamides,³⁰⁻³³ 1,3-dienes,³⁴ and acrylonitrile³⁵ with shorter reaction times and lower temperatures. Even acrylic acid which was supposed to give side reactions with the nitroxyl can be polymerized using NMP.³⁶ The drawbacks of NMP are the high polymerization temperatures and the long polymerization times as well as the limited range of monomers which can be polymerized. In addition, it is difficult to introduce chain end functionality.³⁷

1.2.3 Atom Transfer Radical Polymerization (ATRP)

ATRP is the most widely used CRP technique due to the simple synthetic procedure and commercial availability of all necessary reagents.³⁷⁻⁴² Furthermore, the ease of the nucleophilic substitution of the terminal halogen of the polymer chains and subsequent modification into other functional groups has indeed promoted ATRP as the most preferred choice for preparing synthetic macromolecular structures intended for post-polymerization functionalization.^{61,62}

The ATRP technique was reported by Sawamoto and Matyjaszewski in 1995.^{43,44} The list of monomers successfully homopolymerized by ATRP is quite extensive and includes various substituted styrenes,⁴⁵ (meth)acrylates,⁴⁶⁻⁴⁸ (meth)acrylamides,^{49,50} vinyl pyridine,⁵¹ acrylonitrile,⁵² vinyl acetate,⁵³ among others. Some nitrogen containing monomers can retard polymerization by displacing the terminal halogen of a growing chain or by participating in transfer.³⁷

ATRP can be conducted over a very broad temperature range of subzero to >130 °C. Reactions have been successful in bulk, organic solvents, CO₂, water (homogeneous and heterogeneous-emulsion, inverse emulsion, miniemulsion, microemulsion, suspension, precipitation) and even in the gas phase and from solid surfaces.³⁷

Essentially, all compounds or macromolecules with halogen atoms activated by α -carbonyl, phenyl, vinyl, or cyano groups can initiate ATRP under appropriate conditions. Weak halogen-heteroatom bond, such as sulfonyl halides, are also good ATRP initiators.³⁷ The catalyst system in ATRP is usually made up of Cu (I) and nitrogen-based ligand complex. Other transition-metal ions complexes of Ru,⁵⁴ Pd,⁵⁵ Ni,⁵⁶ and Fe^{57,58} have also been

successfully used in ATRP. The name is derived from the atom transfer step, which is the key reaction responsible for the uniform growth of the polymeric chains during polymerization. ATRP has its origin from atom transfer radical addition (ATRA) reactions, which target the formation of 1:1 adducts of alkyl halides and alkenes catalyzed by transition metal complexes.⁵⁹ Figure 1.6. shows the generally accepted mechanism for ATRP.

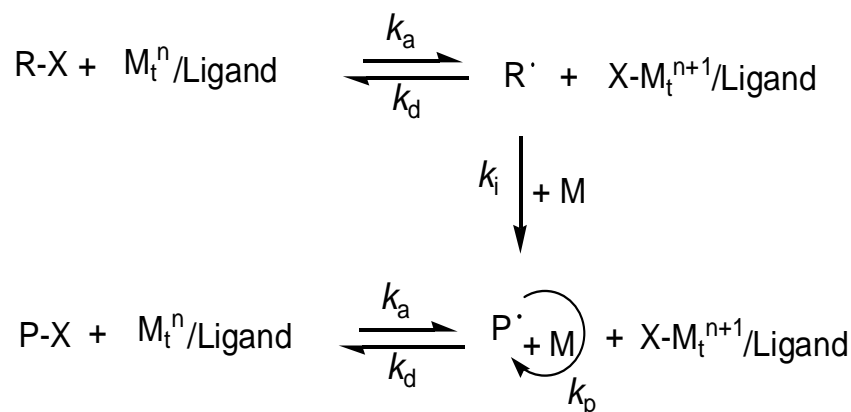


Figure 1.6 General mechanism of atom transfer radical polymerization (ATRP)

The reaction is usually initiated by the activation of the carbon-halogen bond of an appropriate alkyl halide (R-X) in the form of a homolytic cleavage via one-electron oxidation of the metal center ($\text{M}_t^n/\text{Ligand}$) to yield an initiating radical specie ($\text{R}\cdot$) and an oxidized metal compound ($\text{X-M}_t^{n+1}/\text{Ligand}$). The radical reacts with the halogen on the oxidized metal complex to regenerate R-X or adds to the monomer to generate radical oligomeric structures ($\text{P}\cdot$). Depending on the deactivation rate (k_d), after a short period of time the radical is transformed into a dormant oligomeric specie via abstraction of a halogen atom from $\text{X-M}_t^{n+1}/\text{Ligand}$. The carbon-halogen bond of the dormant oligomeric specie is subsequently activated by the metal complex, similar to R-X, to give a radical which can undergo further polymerization. The fast and quantitative initiation and rapid reversible deactivation of propagating radicals, which maintains low radical concentrations and minimize termination through radical coupling, ensures uniform growth of all chains during polymerization.⁶⁰ This is what gives the controlled radical character to the ATRP technique.

1.3 ‘Click’ Chemistry in Macromolecular Synthesis

Nowadays, the synthesis of macromolecules with complex architectures often starts from controlled polymerization processes, with functionalization of the polymer chain-end groups or side chain moieties. The functionalized polymer chains are then coupled to build the desired polymer architecture.⁶³⁻⁷⁴ The coupling reactions are classified as ‘click’ chemistry if they are modular, stereospecific, tolerant to functional groups, wide in scope, result in high yields and generate only safe by-products.^{75,76} This pathway has generated much interest because it is often the only facile means to prepare complex chain topologies or copolymers that contain monomer units not polymerizable by the same method.⁷⁵ Figure 1.7 illustrates the modular approach to synthesis of block, star, and graft copolymers via the ‘click’ coupling method. Well-known reactions that meet these criteria and are applied to macromolecular synthesis include Diels-Alder, thiol-ene, and copper(I) catalyzed Huisgen 1,3-dipolar azide-alkyne cycloaddition (CuAAC).⁷⁵ Among them, the CuAAC ‘click’ reaction proves superior over the others because the two reactants (terminal azide reacting with a terminal alkyne) are of individual low reactivity and as only a catalytic quantity of the metal salt (Cu(I)) is required to accelerate the reaction.⁷

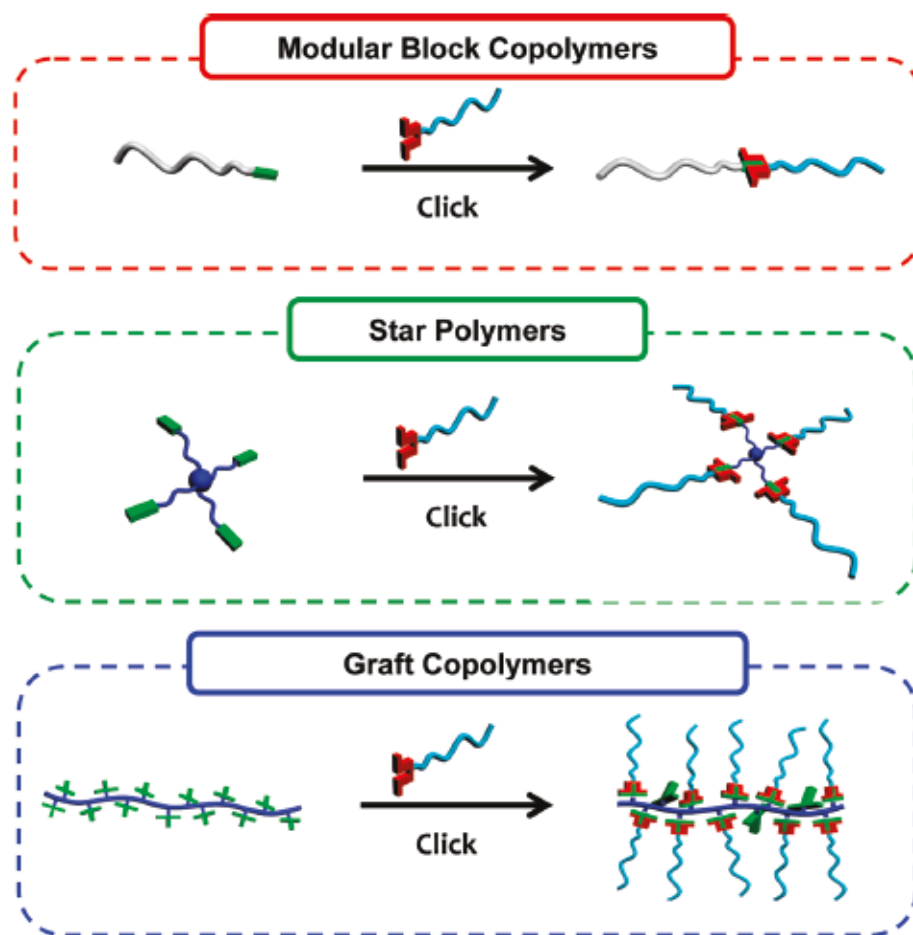


Figure 1.7 Modular approach to synthesizing block, star, and graft copolymer by 'click' chemistry (reprinted from reference 75).

Shortly after its report independently by the Sharpless⁷ and Meldal⁷⁷ groups in 2002, the CuAAC 'click' reaction paved a facile way in polymer synthesis to create macromolecular architectures which were previously difficult or impossible to access. The mechanism of the CuAAC 'click' reaction has been recently explained as a stepwise process beginning with formation of a Cu(I)-acetylide π -complex, followed by azide complexation and cyclization. Subsequent protonation of the triazole-copper derivative and dissociation of the product regenerates the catalyst (Figure 1.8).^{78,79} Different compounds have been utilized as ligands for this process, including pyridines, amines, triazoles, phosphines, and solvents such as water, DMF, DMSO, and acetonitrile.⁸⁰⁻⁸³ Besides Cu(I), other transition metal ions (Ru, Ni, Pd, Pt, and Fe) have been examined as catalysts to broaden the scope of the alkyne-azide cycloaddition reaction.⁸⁰

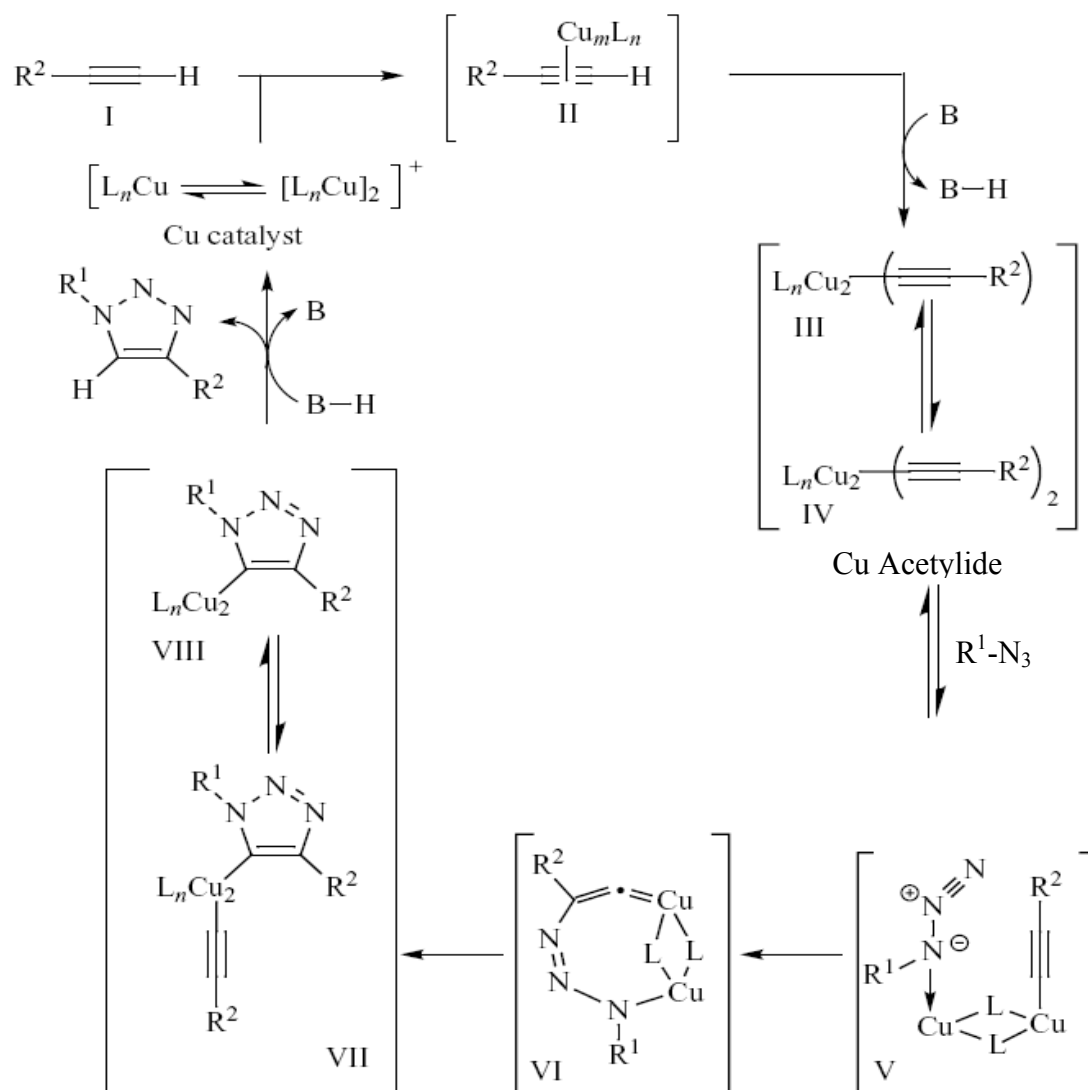


Figure 1.8 Proposed outline of mechanistic pathway in CuAAC 'click' reaction.⁷⁹

However, the potential toxicity of metal catalysts used in the synthesis is a major issue when products are designed for biological applications.^{84,85} Although it is possible to create a wide variety new materials by employing the CuAAC reaction, some Cu ions, at least ppm levels, remains after purification. Therefore, there has been a significant interest, lately, to develop alternative azide-alkyne cycloaddition that do not require any metal catalyst and can still meet the 'click' chemistry criteria.

Though the Huisgen 1,3-dipolar azide-alkyne cycloaddition reaction can proceed without metal catalyst, it however, gives low yield and requires demanding reaction conditions. These features of the uncatalyzed reaction prevent its inclusion in the 'click' chemistry. Bertozzi and coworkers recently showed that using strained cyclooctyne derivatives (instead of the usual linear alkynes) in the uncatalyzed reaction result in high conversions under mild reaction

conditions.⁸⁶⁻⁹² This reaction is called strain-promoted azide-alkyne cycloaddition (SPAAC) reaction. Non-activated cyclooctynes react somewhat slowly with azides, but incorporating electron-withdrawing groups on the ring results in dramatically accelerated rates more typical of ‘click’ reactions. For instance, derivative of cyclooctyne synthesized to decrease the LUMO level of the alkyne functionality via incorporating electron-withdrawing difluoromethylene moiety adjacent to it resulted in reaction rate ~60 times higher.⁸⁶

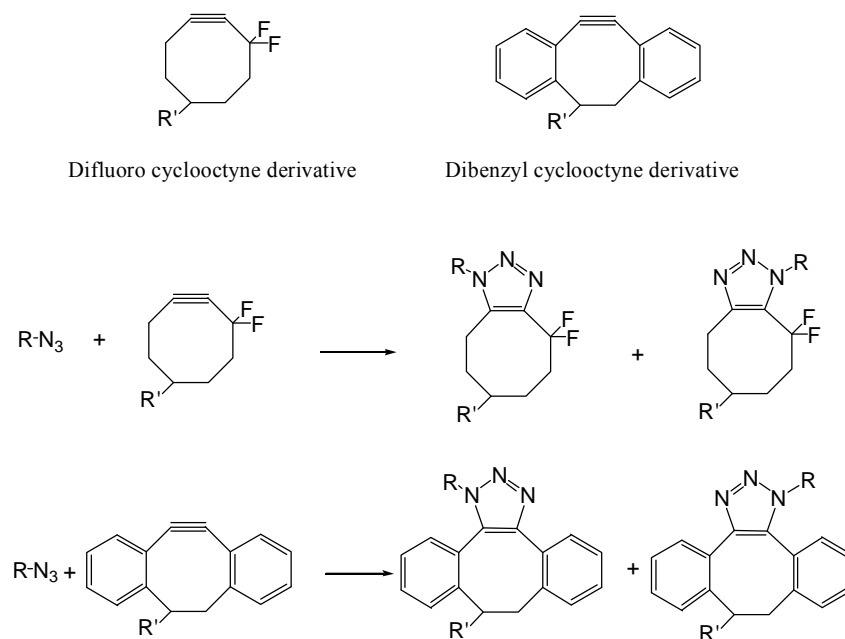


Figure 1.9 Schematic representation of the fluoro and benzyl derivatized cyclooctyne chemical structures and their SPAAC ‘click’ reaction schemes.

Imposing additional ring strain on the cyclooctyne also enhances the rate of the SPAAC reaction. Boons and coworkers by introducing benzyl groups on cyclooctyne were able to increase the rate constant of the reaction by approximately three orders of magnitude greater than that with cyclooctyne.⁹³ The representative chemical structures of the fluoro and benzyl derivatized cyclooctynes, and their SPAAC ‘click’ reaction schemes are shown in Figure 1.9. Due to the biocompatibility and orthogonality of the SPAAC ‘click’ reaction, it has led to its application in labeling and functionalizing biomolecules, even sometimes, in their natural environments.⁹⁴⁻⁹⁷

Although the SPAAC ‘click’ reaction may be advantageous over the CuAAC counterpart where biocompatibility is concerned, it may not be suitable for quantitative structure-property relationships studies in block copolymers. This is because on the nanoscale level, the large coupling units of SPAAC, compared to the 1,2,3-triazole ring of CuAAC, can have significant

influence on the nanostructures formed by the block copolymers. As such in this work, CuAAC reaction is employed as the main coupling reaction in the block copolymers synthesis since the structure-property relationship of the block copolymers is the focus of this research.

1.4 Block Copolymers in Aqueous Medium

In deep analogy to classical low-molecular weight surfactants or amphiphiles, amphiphilic block copolymers may associate reversibly to form micelles when they are dissolved in water. In this respect, a critical micellization concentration (cmc) can be defined and experimentally measured for block copolymer. Compared to low-molar mass amphiphiles, the values of the cmc are much lower in the case of block copolymer. This motivates, e.g., the use of block copolymer micelles as nanocontainers for drug delivery.⁹⁸ In contrast to low-molar mass surfactants, these block copolymer nanocontainers do not easily dissociate into unimers (because of their low cmc) whenever they are diluted in the blood stream and can therefore transport the drugs to a specifically targeted area provided that they are functionalized by suitable moieties for site-recognition.⁹⁹

The micellization properties of amphiphilic block copolymers of AB, ABA, and BAB architectures have been extensively studied and is well understood.¹⁰⁰⁻¹⁰⁶ Regardless of the particular morphology (e.g. sphere, rod, worm-like, flowerlike) such micelles are composed of a single core made up of the non-water soluble lipophilic B blocks and a corona consisting of hydrophilic A blocks (the portion compatible with the aqueous environment) as exemplified in Figure 1.10 for micelles formed by AB, ABA and BAB copolymers.



Figure 1.10 (a) Spherical core corona micelle formed by amphiphilic AB and ABA block copolymers, and (b) spherical core corona flowerlike micelle formed by amphiphilic BAB block polymer.

However, when a second non-water soluble block, C is introduced such as in ABC, CABAC and CAB block copolymers, the partition can be more complex. Consider the case of ABC block copolymer; if the interaction between the B and C blocks is favorable or less repulsive, a single mixed micelle core composed of both blocks is formed. On the contrary, if the interaction between the B and C blocks is strongly repulsive it leads to segregation within the micelle core resulting in a compartmentalized core. In most cases the creation of repulsive interactions which are strong enough to induce segregation within core is achieved through the use of ionic polymers.¹⁰⁸⁻¹¹¹ However, incorporation of fluorinated component into amphiphilic system offers a nonionic route to such compartmentalized core due the strong immiscibility between fluoro- and hydrocarbon-based segments.^{107,112} Thus, a hydrophilic A, a lipophilic B, and a fluorophilic C block (which is neither hydrophilic nor lipophilic) offer strong three-fold philicity, i.e., triphilic system. Different core morphologies ranging from spherical to sphere-on-sphere have been identified for micelles of triphilic block copolymers, as illustrated in Figure 1.11.^{112,114,115}

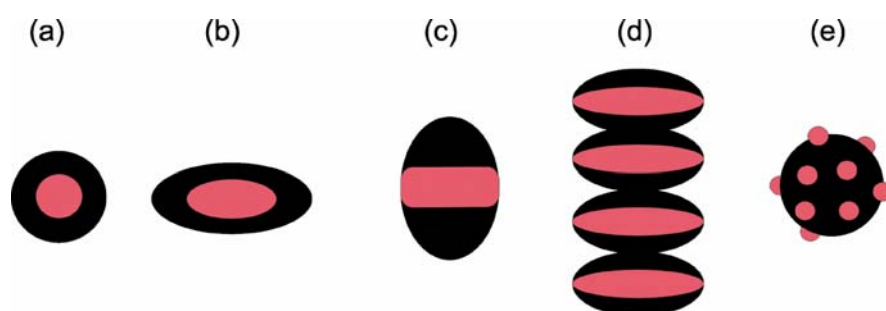


Figure 1.11 Morphologies of micellar cores found for triphilic block copolymer micelles: (a) spherical and (b) disk-like inner-outer cores (c) segmented worm-like (d) “hamburger” and (e) sphere-on-sphere morphology. For clarity, the hydrophilic corona is omitted.

Weberskirch et al.¹¹³ prepared a simple BAC triblock copolymer analogue by end-capping oligomeric poly(*N*-acylethyleneimine) with a hydrocarbon and a fluorocarbon end-group, respectively. The studied telechelics exhibited low cmc's and ¹⁹F NMR relaxation experiments suggested pure fluorocarbon and hydrocarbon phases. The competition between intra- and intermolecular association was controlled by the polymer concentration.

Lodge and coworkers¹¹² prepared a triphilic ABC triblock copolymer by modifying the poly(butadiene) block of poly(ethylene oxide)-*b*-poly(styrene)-*b*-poly(butadiene), PEO-PS-PB, with perfluorohexyl iodide. Remarkably, the micelle core formed by the block copolymer changed from a mixed core to a compartmentalized core after the modification. Moreover, the

modification changed the micelle shape from spherical to oblate elliptical. In another approach, the same researchers synthesized an ABC mikto-arm (μ -arm) star block copolymer based on PEO, poly(ethyl ethylene) (PEE) and poly(perfluoropropylene oxide) (PFO).¹¹⁴ With the three blocks all joined together at the same junction point, the block polymer formed micelles with a segmented worm-like core morphology consisting of distinct lipophilic and fluophilic domains. Interestingly, the researchers demonstrated that micelles with such compartmentalized core are able to selectively store hydro- and fluorocarbon chromophores (dual-storage) and as such hold very great potentials in the application fields of drug delivery, catalysis and nanotechnology.^{115, 116}

Lately, the experimental work on micelles with compartmentalized core has been more and more supported by theoretical simulations. Monte Carlo¹¹⁷ as well as dissipative particle dynamics simulations^{118,119} have been performed to study the influence of the molecular architecture, block length, and polymer concentration on the micelle morphology.

1.5 Motivation and Objectives of this Work

As remarked in the beginning of this chapter, properties of polymers intended for advanced applications have continuously been expanded through block copolymerization. Consequently, novel block copolymers have been created and characterized extensively in the field of polymer synthesis. The most widely studied and industrially applied amphiphilic block copolymer of the type ABA is poly(ethylene oxide)-*b*-poly(propylene oxide)-*b*-poly(ethylene oxide), PEO-PPO-PEO, commonly referred to by the trade name Pluronic® or the generic name Poloxamer. This amphiphilic copolymer has the thermo-responsive PPO block as the lipophilic part and PEO as the hydrophilic block. They find widespread application, partially because of their commercial availability, in investigations dealing with colloids and non-ionic surfactants,^{120,121} drug delivery of poorly water-soluble drugs inside micelles^{122,123} or hydrogels¹²⁴ and cancer therapy.¹²⁵ The proven commercial utility of Poloxamer has led to further research to find analogously novel copolymer architectures and compositions that would broaden the surfactant properties and characteristics. As a result, PG-PPO (PG denotes poly(glycidol)), PEO-PPO and PEO-PBO (PBO denotes poly(butylene oxide)) of di- and triblock chain architectures have been commercialized or prepared on laboratory scales, and extensively investigated.¹²⁶⁻¹³¹

It is in this direction that motivated this research to create novel PPO-based amphiphilic and triphilic block copolymers with poly(glycerol methacrylate), PGMA as the hydrophilic

block and a perfluorocarbon segment as the fluorophilic component. The PGMA block was chosen as the hydrophilic block because of its biocompatibility.¹³² Furthermore, the incorporation of a fluorophilic component into the otherwise amphiphilic block copolymers is expected to cause segregation within the cores of their micelles thereby making them attractive potentials as dual-storage drug delivery vehicles.

The key objectives of this work are:

- Synthesis of series of amphiphilic and triphilic block copolymers based on PPO, PGMA, and perfluorocarbon segments through the use of the ATRP technique and CuAAC ‘click’ reaction.
- Investigation of their micelle-formation in water and the thermodynamics of the micellization process in comparison with and PPO-PEO di- and triblock copolymers.
- Studies on temperature-effect on their micelles/self-assembled structures in water
- Understanding of the structure of their micelles/self-assemblies in relation to the block copolymer architecture and composition.

1.6 References and Notes

1. Förster, S.; Konrad, M. *J. Mater. Chem.* **2003**, *13*, 2671.
2. Ruiz, R.; Kang H. M.; Detcheverry, F. A.; Dobisz, E.; Keercher, D. S.; Albrect, T. R.; de Pablo J. J.; Nealey P. F. *Science* **2008**, *321*, 936.
3. Szwarc, M.; Levy, M.; Milkovich, R. *J. Am. Chem. Soc.* **1956**, *78*, 2656.
4. Kennedy, J.P. *J. Polym. Sci., Part A: Polym. Chem.* **1999**, *37*, 2285.
5. Davis, K. A.; Matyjaszewski K. *Macromolecules* **2001**, *34*, 2101.
6. Web of science search was performed with keywords of “atom transfer radical polymerization” or “nitroxide mediated polymerization” or “reversible addition fragmentation chain transfer” on April 2nd, 2010. Publications for the year 2010 were neglected.
7. Rostovtsev, V. V.; Green L. G.; Fokin V. V.; Sharpless K. B. *Angew. Chem. Int. Ed.* **2002**, *41*, 2596.
8. Kavitha, A. A.; Singha, N. K. *Macromolecules* **2010**, *43*, 3193.
9. Le Droumaguet, B.; Mantovani, G.; Haddleton, D.M.; Velonia, K. *J. Mater. Chem.* **2007**, *17*, 1916.
10. Golas, P.L.; Tsarevsky, N.V.; Summerlin, B.S.; Walker, L.M.; Matyjaszewski, K. *Aust. J. Chem.* **2007**, *60*, 400.
11. Vogt, A. P.; Sumerlin, B. S. *Macromolecules* **2008**, *41*, 7368.
12. Gondi, S. R.; Vogt, A. P.; Sumerlin, B. S. *Macromolecules* **2007**, *40*, 474.
13. Magenau, A. J. D.; Martinez-Castro, N.; Storey, R. F. *Macromolecules* **2009**, *42*, 2353.
14. Ranjan, R.; Brittain, W. J. *Macromol. Rapid Commun.* **2008**, *29*, 1104.
15. Binder, W. H.; Gloger, D.; Weinstabl, H.; Allmaier, G.; Pittenauer, E. *Macromolecules* **2007**, *40*, 3097.
16. Fleischmann, S.; Komber, H.; Voit, B. *Macromolecules* **2008**, *41*, 5255.
17. Chiefari, J.; Chong, Y. K.; Ercole, F.; Krstina, J.; Jeffery, J.; Le, T. P. T.; Mayadunne, R. T. A.; Meijs, G. F.; Moad, C. L.; Moad, G.; Rizzardo, E.; Thang, S. H. *Macromolecules* **1998**, *31*, 5559.
18. Mayadunne, R. T. A.; Rizzardo, E.; Chiefari, J.; Krstina, J.; Moad, G.; Postma, A.; Thang, S. H. *Macromolecules* **2000**, *33*, 243.
19. Moad, G.; Chiefari, J.; Chong, Y. K.; Krstina, J.; Mayadunne, R. T. A.; Postma, A.; Rizzardo, E.; Thang, S. H., *Polym. Int.* **2000**, *49*, 993.

20. Corpart, P.; Charmot D.; Biadatti T.; Zard S. Z.; Michelet D. *Chem. Abstr.* **1998**, *130*, 82018.
21. Chapon, P.; Mignaud, C.; Lizarraga, G.; Destarac M. *Macromol. Rapid Commun.* **2003**, *24*, 87.
22. Barner-Kowollik, C.; Vana, P.; Davis, T. P., The Kinetics of Free-Radical Polymerization. In *Handbook of Radical Polymerization*, Matyjaszewski, K.; Davis, T. P., Eds. John Wiley and Sons, Inc.: Hoboken, 2002; pp 187-261.
23. Moad, G.; Rizzardo, E.; Thang, S. H. *Aust. J. Chem.* **2006**, *59*, 669.
24. Matyjaszewski, K. In *Controlled and Living Polymerizations*; Matyjaszewski, K., Müller A.H.E, Eds.; WILEY-VCH Verlag GmbH & Co. KGaA: Weinheim, 2009 ; pp 103-166.
25. Benoit, D.; Chaplinski, V.; Braslau R.; Hawker C. J. *J. Am. Chem. Soc.* **1999**, *121*, 3904.
26. Benoit, D.; Grimaldi, S.; Robin, S.; Finet, J.-P.; Tordo, P.; Gnanou, Y. *J. Am. Chem. Soc.* **2000**, *122*, 5929.
27. Grimaldi, S.; Finet, J.-P.; Le Moigne, F.; Zeghdaoui, A.; Tordo, P.; Benoit, D.; Fontanille, M.; Gnanou, Y. *Macromolecules* **2000**, *33*, 1141.
28. Farcet, C.; Belleney, J.; Charleux, B.; Pirri, R. *Macromolecules* **2002**, *35*, 4912.
29. Nicolas, J.; Charleux, B.; Guerret, O.; Magnet, S. *Angew. Chem., Int. Ed.* **2004**, *43*, 6186.
30. Schierholz, K.; Givehchi, M.; Fabre, P.; Nallet, F.; Papon, E.; Guerret, O.; Gnanou, Y. *Macromolecules* **2003**, *36*, 5995.
31. Phan, T. N. T.; Bertin D. *Macromolecules* **2008**, *41*, 1886.
32. Gibbons, O.; Carroll, W. M.; Aldabbagh, F.; Yamada, B. *J. Polym. Sci., Part A: Polym. Chem.* **2006**, *44*, 6410.
33. Grassl, B.; Clisson, G.; Khoukh, A.; Billon, L. *Eur. Polym. J.* **2008**, *44*, 50.
34. Benoit, D.; Harth, E.; Fox, P.; Waymouth, R. M.; Hawker, C. J. *Macromolecules* **2000**, *33*, 363.
35. Detrembleur, C.; Sciannamea, V.; Koulic, C.; Claes, M.; Hoebeke, M.; Jérôme, R. *Macromolecules* **2002**, *35*, 7214.
36. Couvreur, L.; Lefay, C.; Belleney, J.; Charleux, B.; Guerret, O.; Magnet, S., *Macromolecules* **2003**, *36*, 8260.
37. Matyjaszewski, K. In *Controlled and Living Polymerizations*; Matyjaszewski, K., Müller A.H.E, Eds.; WILEY-VCH Verlag GmbH & Co. KGaA: Weinheim, 2009; pp 103-166.
38. Matyjaszewski, K.; Xia, J. *Chem. Rev.* **2001**, *101*, 2921.
39. Wang, J.-S.; Matyjaszewski, K. *J. Am. Chem. Soc.* **1995**, *117*, 5614.
40. Tsarevsky, N.V.; Matyjaszewski, K. *Chem. Rev.* **2007**, *107*, 2270.

41. Kamigaito, M.; Ando, T.; Sawamoto, M. *Chem. Rev.* **2001**, *101*, 3689.
42. Patten, T.E.; Matyjaszewski, K. *Acc. Chem. Res.* **1999**, *32*, 895.
43. Kato, M.; Kamigaito, M.; Sawamoto, M.; Higashimura, T. *Macromolecules* **1995**, *28*, 1721.
44. Wang, J. S.; Matyjaszewski, K. *J. Am. Chem. Soc.* **1995**, *117*, 5614-5615.
45. Qiu, J.; Matyjaszewski, K. *Macromolecules* **1997**, *30*, 5643.
46. Wang, J.-L.; Grimaud, T.; Shipp, D.A.; Matyjaszewski, K. *Macromolecules* **1998**, *31*, 1527.
47. Davis, K.A.; Paik, H.-J.; Matyjaszewski, K. *Macromolecules* **1999**, *32*, 1767.
48. Mori, H.; Müller, A.H.E. *Prog. Polym. Sci.* **2003**, *28*, 1403.
49. Teodorescu, M.; Matyjaszewski, K. *Macromolecules* **1999**, *32*, 4826.
50. Neugebauer, D.; Matyjaszewski, K. *Macromolecules* **2003**, *36*, 2598.
51. Tsarevsky, N.V.; Braunecker, W.A.; Brooks, S.J.; Matyjaszewski, K. *Macromolecules* **2006**, *39*, 6817.
52. Matyjaszewski, K.; Jo, S.M.; Paik, H.-J.; Gaynor, S.G. *Macromolecules* **1997**, *30*, 6398.
53. Tang, H.; Radosz, M.; Shen, Y. *AIChE J.* **2009**, *55*, 737.
54. Nishikawa, T.; Ando, T.; Kamigaito, M.; Sawamoto, M. *Macromolecules* **1997**, *30*, 2244.
55. Lecomte, Ph.; Drapier, I.; Dubois, Ph.; Teyssié, Ph.; Jérôme, R. *Macromolecules* **1997**, *30*, 7631.
56. Granel, C.; Dubois, Ph.; Jérôme, R.; Teyssié, Ph. *Macromolecules* **1996**, *29*, 8576.
57. Ando, T.; Kamigaito, M.; Sawamoto, M. *Macromolecules* **1997**, *30*, 4507.
58. Matyjaszewski, K.; Wei, M.; Xia, J.; McDermott, N.E. *Macromolecules* **1997**, *30*, 8161.
59. Curran, D. P. *Synthesis* **1988**, 489.
60. Odian G. *Principles of Polymerization*, 4th Ed.; John Wiley & Sons Inc: Hoboken, New Jersey 2004.
61. Coessens, V.; Nakagawa, Y.; Matyjaszewski, K. *Polym. Bull.* **1998**, *40*, 135.
62. Golas, P. L.; Matyjaszewski K. *QSAR Comb. Sci.* **2007**, *26*, 1116.
63. Tsarevsky, N. V.; Sumerlin, B. S.; Matyjaszewski, K. *Macromolecules* **2005**, *38*, 3558.
64. Golas, P. L.; Matyjaszewski, K. *Chem. Soc. Rev.* **2010**, *39*, 1338.
65. van Camp, W.; Germonpre, V.; Mespouille, L.; Dubois, P.; Goethals, E. J.; Du Prez, F. *E. React. Funct. Polym.* **2007**, *67*, 1168.
66. Kyeremateng, S. O.; Amado, E.; Blume, A.; Kressler, J. *Macromol. Rapid Commun.* **2008**, *29*, 1140.

67. Gao, H.; Matyjaszewski, K. *J. Am. Chem. Soc.* **2007**, *129*, 6633.
68. Durmaz, H.; Dag, A.; Altintas, O.; Erdogan, T.; Hizal, G.; Tunca, U. *Macromolecules* **2007**, *40*, 191.
69. Opsteen, J. A.; van Hest, J. C. M. *Chem. Commun.* **2005**, 57.
70. Opsteen, J. A.; van Hest, J. C. M. *J. Polym. Sci., Part A: Polym. Chem.* **2007**, *45*, 2913.
71. Gao, H.; Matyjaszewski, K. *Macromolecules* **2006**, *39*, 4960.
72. Gao, H.; Min, K.; Matyjaszewski, K. *Macromol. Chem. Phys.* **2007**, *208*, 1370.
73. Gungor, E.; Cote, G.; Erdogan, T.; Durmaz, H.; Demirel, A. L.; Hizal, G.; Tunca, U. J. *Polym. Sci., Part A: Polym. Chem.* **2007**, *45*, 1055.
74. Gungor, E.; Durmaz, H.; Hizal, G.; Tunca, U. J. *Polym. Sci., Part A: Polym. Chem.* **2008**, *46*, 4459.
75. Sumerlin, B. S.; Vogt A. P. *Macromolecules* **2010**, *43*, 1.
76. Becer, C. R.; Hoogenboom, R.; Schubert, U. S. *Angew. Chem. Int. Ed.* **2009**, *48*, 4900.
77. Tornøe, C. W.; Christensen, C.; Meldal M. *J. Org. Chem.* **2002**, *67*, 3057.
78. Bock, V. D.; Hiemstra, H.; Maarseveen, J. H. v., *Eur. J. Org. Chem.* **2006**, 51.
79. Binder, W. H.; Sachsenhofer, R. *Macromol. Rapid Commun.* **2007**, *28*, 15.
80. Golas, P. L.; Tsarevsky N. V.; Sumerlin B. S.; Matyjaszewski K. *Macromolecules* **2006**, *39*, 6451.
81. Chan, T. R.; Hilgraf R.; Sharpless, K. B.; Fokin V. V. *Org. Lett.* **2004**, *6*, 2853.
82. Lewis, W. G.; Magallon, F. G.; Fokin, V. V.; Finn M. G. *J. Am. Chem. Soc.* **2004**, *126*, 9152.
83. Meng, J.-c.; Fokin, V. V.; Finn, M. G. *Tetrahedron Lett.* **2005**, *46*, 4543.
84. Wang, Q.; Chan, T. R.; Hilgraf, R.; Fokin, V. V.; Sharpless, K. B.; Finn, M. G. *J. Am. Chem. Soc.* **2003**, *135*, 3192.
85. Gierlich, J.; Burley, G. A.; Gramlich, P. M. E.; Hammond, D. M.; Carell, T. *Org. Lett.* **2006**, *8*, 3639.
86. Baskin, J. M.; Prescher, J. A.; Laughlin, S. T.; Agard, N. J.; Chang, P. V.; Miller, I. A.; Lo, A.; Codelli, J. A.; Bertozzi, C. R. *Proc. Nat. Acad. Sci. U.S.A.* **2007**, *104*, 16793.
87. Laughlin, S. T.; Baskin, J. M.; Amacher, S. L.; Bertozzi C. R., *Science* **2008**, *320*, 664.
88. Johnson, J. A.; Baskin J. M.; Bertozzi, C. R.; Koberstein J. F.; Turro N. J. *Chem. Commun.* **2008**, 3064.
89. Codelli, J. A.; Baskin, J. M.; Agard, N. J.; Bertozzi, C. R. *J. Am. Chem. Soc.* **2008**, *130*, 11486.
90. Sletten, E. M.; Bertozzi C. R. *Org. Lett.* **2008**, *10*, 3097.

91. Baskin, J. M.; Bertozzi, C. R. *QSAR Comb. Sci.* **2007**, *26*, 1211.
92. Agard, N. J.; Baskin, J. M.; Prescher, J. A.; Lo, A.; Bertozzi, C. R. *ACS Chem. Biol.* **2006**, *1*, 644.
93. Ning, X.; Guo, J.; Wolfert, M. A.; Boons G.-J. *Angew. Chem. Int. Ed.* **2008**, *47*, 2253.
94. Zou, Y.; Yin J. *Bioorg. Med. Chem. Lett.* **2008**, *18*, 5664.
95. Laughlin, S. T.; Bertozzi, C. R. *Proc. Natl. Acad. Sci. U.S.A.* **2009**, *106*, 12.
96. Laughlin, S. T.; Baskin, J. M.; Amacher, S. L.; Bertozzi, C. R. *Science* **2008**, *320*, 664.
97. Neef, A. B.; Schultz, C. *Angew. Chem., Int. Ed.* **2009**, *48*, 1498.
98. Gohy, J.-F. *Adv Polym Sci* **2005**, *190*, 65.
99. Kataoka, K.; Harada, A.; Nagasaki, Y. *Adv Drug Deliv Rev* **2001**, *47*, 113.
100. Dimitrov, P.; Utrata-Wesołek, A.; Rangelov S.; Wałach W.; Trzebicka, B.; Dworak A. *Polymer* **2006**, *47*, 4905.
101. Liu, T.; Zhou, Z.; Wu, C.; Nace, V.M; Chu, B. *J. Phys. Chem. B* **1998**, *102*, 2875.
102. Rakhmatullina, E.; Braun, T.; Chami, M.; Malinova, V.; Meier, W. *Langmuir* **2007**, *23*, 12371.
103. Cau, F.; Lacelle, S. *Macromolecules* **1996**, *29*, 170.
104. Hussain H.; Busse K.; Kressler J. *Macromol. Chem. Phys.* **2003**, *204*, 936.
105. Amado E.; Augsten C.; Mäder K.; Blume A.; Kressler J. *Macromolecules* **2006**, *39*, 9486.
106. Dimitrov, P.; Rangelov, S.; Dworak, A.; Tsvetanov, C.B. *Macromolecules* **2004**, *37*, 1000.
107. (a) Lodge, T. P.; Hillmyer, M. a.; Zhou, Z.; Talmon, Y. *Macromolecules*. **2004**, *37*, 6680-6682. (b) Lodge, T. P. *Macromol. Chem. Phys.* **2003**, *204*, 265.
108. Schacher, F.; Walther, A.; Müller, A.H.E *Langmuir* 2009, *25* 18, 10962.
109. Proch, K.; Ave, C.; Voets, I. K.; Walther, A. *Macromolecules* **2009**, 5605.
110. Shell, R.; Gohy, J.-F; Willet, N.; Varshney, S.; Zhang, J.; Je, R. *Angew. Chem.* **2001**, *113*, **2001**, 3314.
111. Patrickios, C. S.; Lowe, A. B.; Armes, S. P.; Billingham, N. C. *Polymer* **1997**, 617.
112. Zhou Z.; Li Z.; Ren Y.; Hillmyer M. A.; Lodge T.P. *J. Am. Chem. Soc.* **2003**, *125*, 10182.
113. Weberskirch R.; Preuschen J.; Spiess H.W.; Nuyken O. *Macromol. Chem. Phys.* **2000**, *201*, 995.
114. Li, Z.; Kesselman, E.; Talmon, Y.; Hillmyer, M. A.; Lodge, T. P. *Science* **2004**, *306*, 98-101.

115. Lodge T. P.; Rasdal A.; Li Z.; Hillmyer M. A. *J. Am. Chem. Soc.* **2005**, 127, 17608.
116. Ott C.; Hoogenboom R.; Hoepfener S.; Wouters D.; Gohy J.-F.; Schubert U.S. *Soft Matter*, **2009**, 5, 84.
117. Zhu, Y.; Li, R. K. Y.; Jiang, W. *Chem. Phys.* **2006**, 327, 137.
118. Zhao, Y.; Liu, Y.; Lu, Z.; Sun, C. *Polymer* **2008**, 49, 4899.
119. Zhong, C.; Liu, D., *Macromol. Rapid Commun.* **2007**, 28, 292.
120. Alexandridis, P.; Athanassiou, V.; Fukuda, S.; Hatton, T. A., *Langmuir* **1994**, 10, 2604
121. Alexandridis, P.; Holzwarth, J. F.; Hatton, T. A., *Macromolecules* **1994**, 27 (9), 2414
122. Munshi, N.; Rapoport, N.; Pitt, W. G. *Cancer*. **1997**, 118, 13.
123. Chiappetta, D. A.; Sosnik, A. *Eur. J. Pharm. Biopharm.* **2007**, 66, 303.
124. Escobar-Chavez, J.J.; Lopez-Cervantes, M.; Naik A.; Kalia Y.N.; Quintana-Guerrero, D.; Ganem-Quintanar, A. *J.Pharm. Pharmaceut. Sci.* **2006**, 3, 339.
125. Kabanov, A. V.; Batrakova, E. V.; Alakhov, V. Y. *J. Controlled Release* **2002**, 82, 189-212.
126. Halacheva, S.; Rangelov, S.; Garamus, V. M. *Macromolecules* **2007**, 40, 8015.
127. Altinok, H.; Yu, G.-E.; Nixon, S. K.; Gorry, P. A.; Attwood, D.; Booth, C. *Langmuir* **1997**, 13, 5837.
128. Yang, L.; Badells, A. D.; Attwood, D.; Booth, C. *J. Chem. Soc., Faraday Trans.* **1992**, 88, 1447.
129. Deng, Y.; Ding, J.; Stubbersfield, R. B.; Heatley, F.; Price, C.; Booth, C. *Polymer* **1992**, 33, 1963.
130. Booth, C.; Attwood, D. *Macromol. Rapid Commun.* **2000**, 21, 501.
131. Nace, V. M.; Chu, B. *J. Phys. Chem. B* **1997**, 101, 8074.
132. Mequanint, K.; Patel, A.; Bezuidenhout, D. *Biomacromolecules* **2006**, 7, 883.

Chapter 2

Synthesis of Amphiphilic and Triphilic Block Copolymers by ATRP and Copper(I)-Catalyzed Alkyne-Azide Cycloaddition (CuAAC) ‘Click’ Reaction

2.1 Introduction

Several types of amphiphilic block copolymers have been synthesized by living anionic polymerization,¹⁻⁴ NMP,^{5,6} RAFT,^{7,8} or ATRP.⁹⁻¹² Synthesis of copolymer mainly by means of anionic polymerization is rather problematic due to reactivity restrictions of the monomers.¹³ Owing to its monomer versatility and the ease of nucleophilic substitution of a halogen atom from the polymer chain end by the azide functionality, ATRP in combination with CuAAC ‘click’ reaction has in recent years been used to prepare protein-polymer conjugate and block copolymers of different architectures.¹⁴⁻¹⁸ Using the CuAAC ‘click’ reaction¹⁹⁻²² is therefore a powerful tool to attach a third block to conventional amphiphilic AB diblock or ABA triblock polymers.

In the case that AB or ABA block copolymers contain hydrophilic and lipophilic blocks, the addition of a segment containing perfluoro-groups leads to triphilic systems since the additional fluorophilic segment is neither hydrophilic nor lipophilic. This can lead to formation of multicomponent polymeric micelles in solution which mimics the multicompartiment character of biological systems, i.e. eukaryotic cells.²³

Using α,ω -2-bromoisobutanoate poly(propylene oxide) (Br-PPO-Br) and α -azido- ω -2-bromoisobutanoate poly(propylene oxide) (N₃-PPO-Br) as macroinitiators, ATRP is carried out with solketal methacrylate (SMA) to create PSMA_y-PPO_x-PSMA_y and PPO_x-PSMA_y block copolymers, respectively. The halogen terminal groups of the PSMA_y-PPO_x-PSMA_y block copolymers were exchanged with N₃. Through CuAAC ‘click’ reaction of the azido end-groups with an alkyne terminated perfluorinated compound, the polymer chains were end-capped with perfluoroalkyl (F_z) segments, yielding, F_z-PPO_x-PSMA_y and F_z-PSMA_y-PPO_x-PSMA_y-F_z block copolymers. The subscripts *x* and *y* represent the degree of polymerization as determined by ¹H NMR while *z* represents the number of fluorinated carbon atoms in the fluorinated segment. The ketal functions on the SMA units of the block copolymer were then completely hydrolyzed to give water-soluble glycerol monomethacrylate (GMA) units. Thus, yielding, triphilic block copolymer systems. In a similar approach, triphilic F_z-PGMA_y-PPO_x block copolymers were also synthesized by ATRP of SMA with a

perfluoroalkyl initiator followed by ‘click’ reaction with alkyne terminated PPO. In addition, amphiphilic PPO_x-PGMA_y block copolymers are synthesized in a similar fashion starting with 2-bromoisobutanoate poly(propylene oxide) (PPO_x-Br).

2.2 Synthesis of Monomer (Solketal Methacrylate)

Synthesis of the solketal methacrylate monomer was through esterification of isopropylidene glycerol, commonly called soketal, with methacryloyl chloride as shown in the reaction scheme below.²⁴

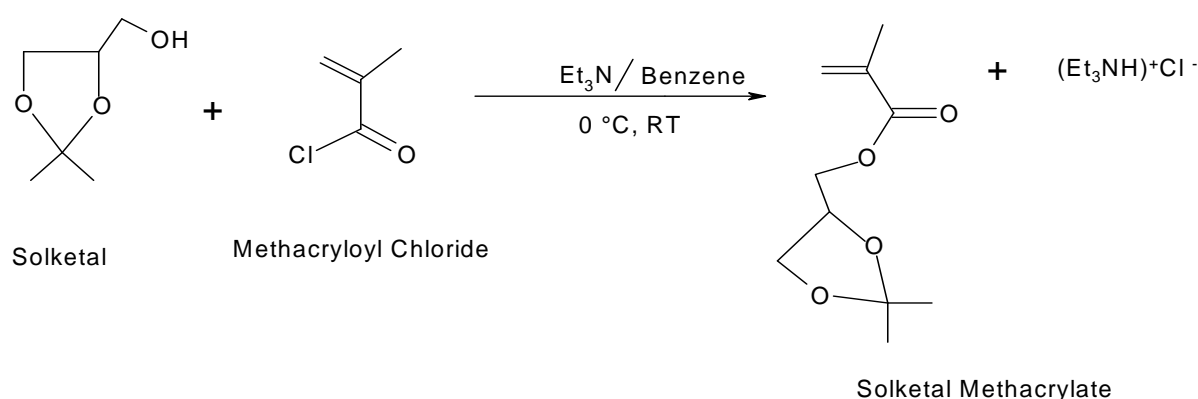


Figure 2.1 Reaction scheme for synthesis of solketal methacrylate monomer.

The ¹H NMR spectrum of the purified product in DMSO-*d*₆ (400 MHz) showed the protons of the methacrylate appearing as; singlet at 1.85 ppm for the three protons of the methyl group, singlets at 6.0 and 5.65 ppm for the trans and cis geminal protons respectively. Signals from the protons of solketal appeared as baseline separated multiplets between 3.65 and 4.30 ppm for the five protons, and two singlets at 1.23 and 1.28 ppm corresponding to the six protons of the two methyl groups. The spectrum is shown in Figure 2.2.

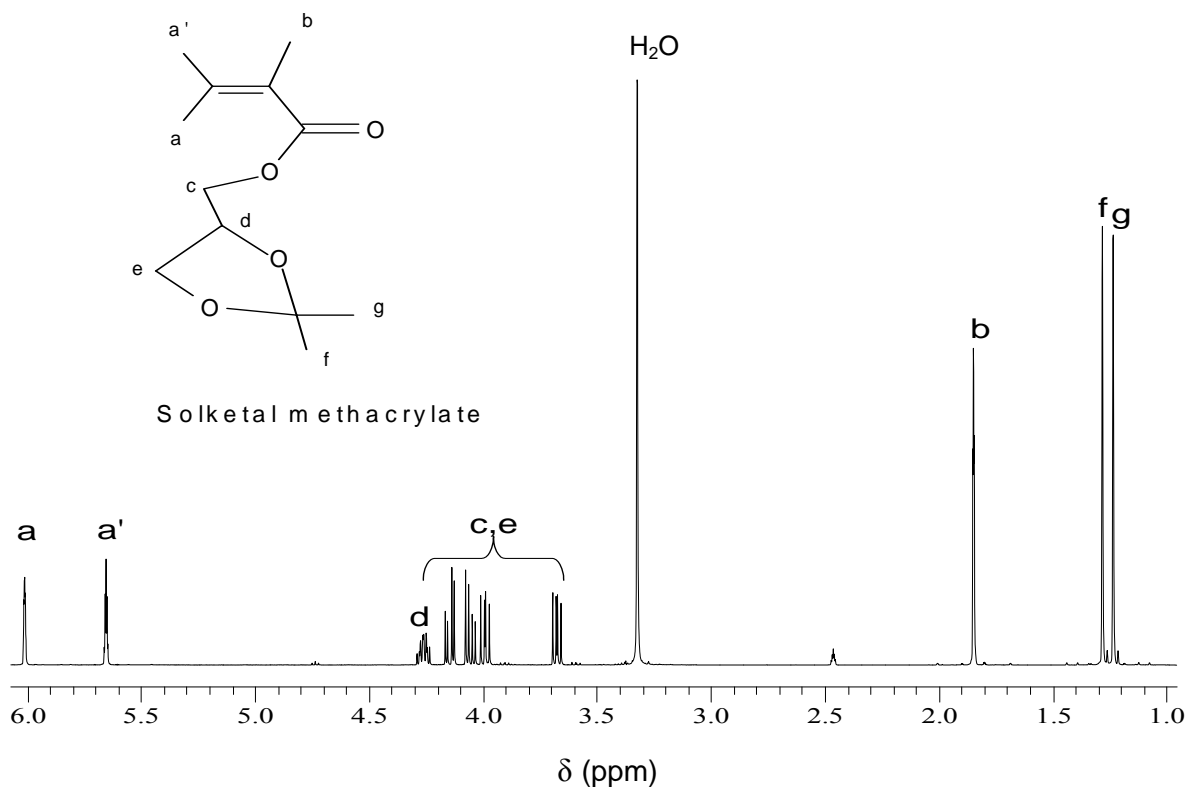


Figure 2.2 ^1H NMR spectrum of solketal methacrylate monomer in $\text{DMSO-}d_6$ at 400 MHz (25 °C)

2.3 ATRP Initiators Synthesis

Heneicosafluoro-1-undecyl 2-bromoisobutanoate (perfluoroalkyl initiator) ($F_{10}\text{-Br}$)

The alcohol, heneicosafluoro-1-undecanol ($\text{C}_{10}\text{F}_{21}\text{CH}_2\text{OH}$), was completely acylated with BIB in THF with pyridine as a base using a molar ratio of $[\text{F}_{10}\text{-OH}]:[\text{BIB}]:[\text{py}]$; 1:2:2. The ^1H NMR spectrum of the purified product showed the BIB methyl protons in addition to the methylene protons of the original perfluoroalkyl segment.

α,ω -2-Bromoisobutanoate poly(propylene oxide) (difunctional macroinitiator) (Br-PPO-Br)

The difunctional macroinitiator was prepared by complete acylation of dihydroxy-terminated PPO (HO-PPO-OH) with 2-bromoisobutyryl bromide (BIB) in the presence triethylamine (Et_3N) as a base and benzene as solvent, using a molar ratio of $[\text{PPO}]:[\text{BIB}]:[\text{Et}_3\text{N}]$; 1:4:4. The reaction was carried out for 24 h at room temperature.²⁵ After thorough purification of the product, the peak corresponding to the protons of BIB, in addition to the usual PPO proton peaks, could be observed in the ^1H NMR spectrum.

Bromoisobutanoate poly(propylene oxide) (monofunctional macroinitiator) (PPO-Br)

Similar to the synthesis of the difunctional macroinitiator, monohydroxy-terminated PPO (PPO-OH) was completely acylated with BIB under the same conditions.

 α -Azido- ω -2-bromoisobutanoate poly(propylene oxide) (heterofunctional macroinitiator) (N_3 -PPO-Br)

Similar to the preparation of the difunctional macroinitiator, the heterofunctional macroinitiator was prepared by first partial acylation of dihydroxy-terminated PPO (HO-PPO-OH) in a molar ratio [PPO]:[BIB]:[Et₃N]; 1:1.3:1.3. Thin layer chromatography (TLC) showed the product did not contain unacylated PPO. Based on this knowledge, it was estimated from analysis of the ¹H-NMR spectrum that the product contains about 15 mol-% of completely acylated PPO; i.e., 85 mol-% of the PPO is end-capped with a free OH group. The terminal Br group of the chains was then replaced with N₃ through azidation reaction with NaN₃ according to a literature method.²⁶ The terminal free OH of the PPO chains were further acylated with BIB using the same method as mentioned above but replacing Et₃N with pyridine, to afford 85 mol-% monofunctional macroinitiator (N₃-PPO-Br) and 15 mol-% α,ω -diazido-terminated poly(propylene oxide) (N₃-PPO-N₃).

In the TLC performed with toluene/THF (6:4 v/v), the partially acylated products registered an untailed single spot with *R_f* value of 0.80 vs. a *R_f* value of 0.56 for pure HO-PPO-OH. A mixture of both gave two untailed consecutive spots at the mentioned *R_f* values. This revealed that the partially acylated products did not contain HO-PPO-OH. Analysis of the ¹H-NMR spectrum of the azidated product showed complete reaction. The peak corresponding to 6H protons of the methyl groups attached to the α -carbon (with respect to the Br) shifted from 1.90 to 1.43 ppm as Br was replaced by a less electronegative N₃ group. The ¹H-NMR spectrum evolution and that of the product after final acylation with BIB are shown in Figure 2.3. Resonance peaks at 1.43 and 1.90 ppm in the final product confirm the presence of two kinds of methyl protons found in the vicinity of N₃ and Br group, respectively. Notice that the peak labeled 'b' in Figure 2.3 is slightly larger than 'c' because the product still contains 15 mol-% N₃-PPO-N₃.

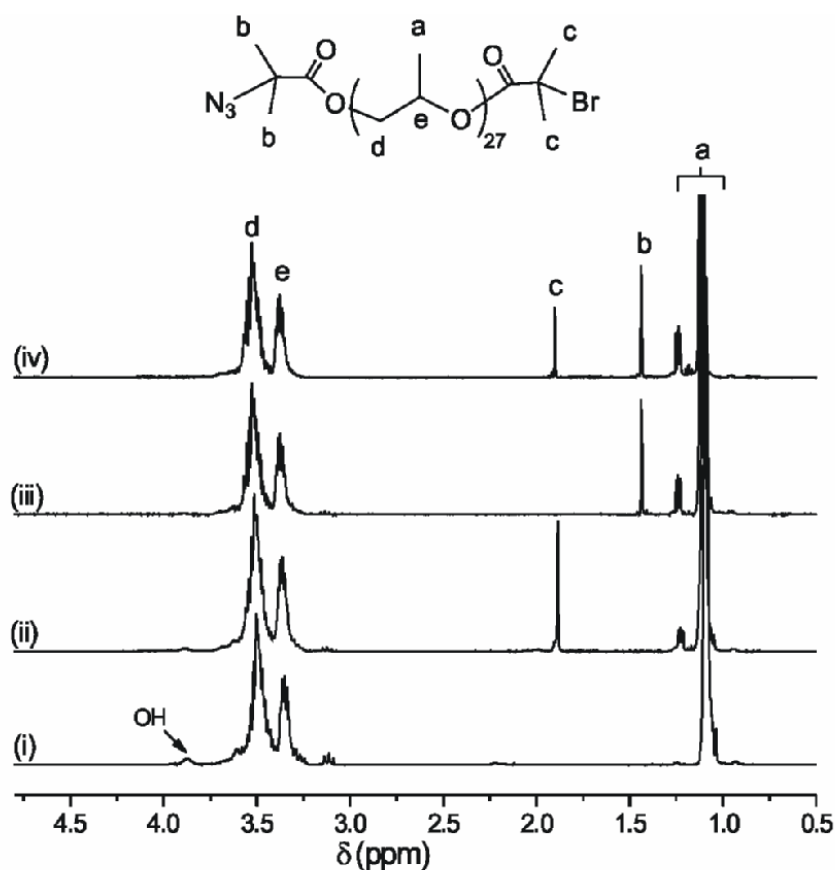


Figure 2.3 ^1H NMR spectra in CDCl_3 (400MHz): (i) Pure PPO, (ii) PPO after partial acylation with BIB, (iii) partially acylated PPO after replacement of terminal Br with N_3 , (iv) subsequent acylation of product (iii) with BIB.

2.4 Synthesis of Alkyne-End Functionalized Compounds

Poly(propylene oxide) hex-5-ynoate (PPO-C \equiv H)

This product was synthesized by esterifying PPO-OH with hex-5-ynoic anhydride in the presence of DMAP, pyridine, and anhydrous dichloromethane as solvent. The ^1H NMR spectrum of the purified product showed resonance signals that could be clearly assigned to the terminal alkyne moiety in addition to signals from the PPO polymer.

Nonadecafluoro-1-decyl hex-5-ynoate (F $_9$ C \equiv H)

The compound was prepared by esterifying nonadecafluoro-1-decanol with hex-5-ynoic anhydride using THF as a solvent in the presence of pyridine and DMAP. The completion of the reaction and purity of the product were confirmed by ^1H and ^{19}F NMR spectroscopy.

2.5 Synthesis of Polymers by ATRP

*N*₃-PPO₂₇-PSMA_y block copolymers

The N₃-PPO₂₇-PSMA_y block copolymers were prepared from the heterofunctional macroinitiators, N₃-PPO-Br, via the ATRP technique using CuBr as catalyst, bpy as ligand and anisole as solvent with a [initiator]₀: [catalyst]₀: [ligand]₀ ratio of 1:1:3. The reaction scheme is presented in Figure 2.4. Two block copolymers were prepared with this macroinitiator.

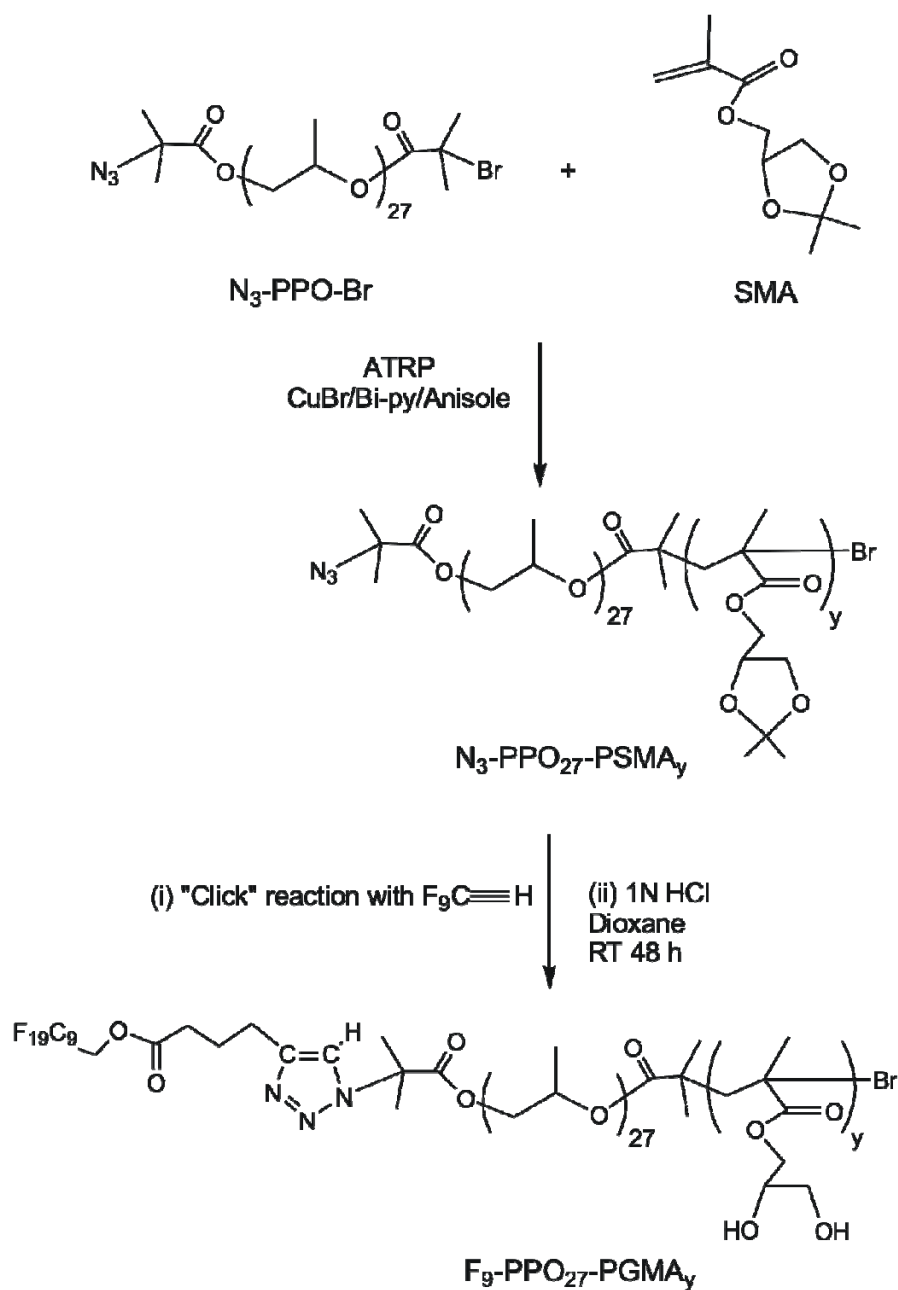


Figure 2.4 Synthetic route to triphilic F₉-PPO₂₇-PGMA_y block copolymers.

The first block copolymer was prepared with [initiator]₀: [monomer]₀ ratio of 1:25 and polymerization was carried out at 40 °C. The second block copolymer was prepared with [initiator]₀: [monomer]₀ of 1:10 and polymerization was carried out 60 °C. In both cases the 15 mol-% inactive N₃-PPO-N₃ contained in the heterofunctional macroinitiator was taken into account. Polymerization reactions were allowed to proceed for 20 h. The synthesized polymers were purified by column chromatography followed by precipitation into *n*-hexane. Note the PPO-based macroinitiators are soluble in hexane; therefore, the inactive N₃-PPO-N₃ was isolated from the diblock copolymers during the precipitation process. Entries 1 and 2 in Table 2.1 give the molar masses and polydispersity indices (M_w/M_n) obtained from NMR and SEC for the two synthesized copolymers.

Table 2.1 Molar Mass and Polydispersity Indices of Synthesized Polymers Determined from NMR and SEC

Entry	Polymer	SEC ^f	
		M_n (g mol ⁻¹)	M_w/M_n
1 ^a	N ₃ -PPO ₂₇ -PSMA ₉₄	20500 ^d	1.36
2 ^c	N ₃ -PPO ₂₇ -PSMA ₄₄	10500 ^d	1.23
3 ^a	N ₃ -PSMA ₄₂ -PPO ₂₇ -PSMA ₄₂ -N ₃	18600 ^d	1.50
4 ^c	N ₃ -PSMA ₂₄ -PPO ₂₇ -PSMA ₂₄ -N ₃	11200 ^d	1.21
5 ^a	PPO ₃₄ -PSMA ₆₆	15200 ^d	1.40
6 ^c	PPO ₃₄ -PSMA ₃₇	9400 ^d	1.25
7 ^b	F ₁₀ -PSMA ₆₆ -N ₃	13900 ^e	1.29
8 ^b	F ₁₀ -PSMA ₈₅ -N ₃	17700 ^e	1.20

^{a,b,c}) Polymerization carried at 40, 50, and 60 °C, respectively; ^d) Calculated from ¹H NMR spectroscopy ^e) Calculated from ¹⁹F NMR spectroscopy; ^f) Obtained from measurements in THF with poly(styrene) calibration standards before azidation reactions

The tolerance of azido-functionalized initiators towards ATRP has been demonstrated in literature.^{27,28} Compared to the theoretical molar mass expected based on monomer conversion $M_{n(\text{theo})}$, an initiation efficiency f , of 0.25 was determined [$f = M_{n(\text{theo})} / M_{n(\text{NMR})}$]. The low f of α -azido-terminated initiators has been reported in literature,^{28,29} although the reason is unclear. It was with this fore knowledge that a molar ratio of [initiator]₀: [CuBr]₀: [bpy]₀ of 1:1:3 and an initial temperature of 40 °C was employed in the first polymerization with the to improve f . On the other hand, the data reveal that polymerization carried out with the same

catalyst-ligand ratio at 60 °C yields a block copolymer with a lower polydispersity. The respective f value determined was 0.13. It can therefore be surmised that increasing temperature leads to better controlled polymerization,²⁹ however, it also leads to enhancement of possible side reaction involving the N₃ group which results in relatively low initiator efficiency.³⁰

N₃-PSMA_y-PPO₂₇-PSMA_y-N₃ block copolymers

Using the difunctional macroinitiator, Br-PPO-Br, ATRP was carried out with SMA to yield PSMA_y-PPO₂₇-PSMA_y block copolymers as schematically illustrated in Figure 2.5. The same experimental and purification procedures used during the polymerization of SMA with the heterofunctional macroinitiator were applied, except, the [initiator]₀:[CuBr]₀:[ligand]₀ ratio used in this case was 1:1:2. The ratio of the monomer to initiator was varied depending on the desired degree of polymerization. Likewise, two polymerization reactions were carried out at 40 and 60 °C, respectively, for 90 min each. The relatively short polymerization time was employed to maintain a high degree of bromine chain-end functionality.³¹ After purifying the polymers, substitution reaction of the bromine chain-end functionality with azido functionality was performed in DMF with NaN₃ for the 24 h. Detailed experimental procedure for this reaction is reported in literature.²⁶ Entries 3 and 4 in Table 2.1 give the molar masses and polydispersity indices (M_w/M_n) obtained from ¹H NMR and SEC for the two synthesized block copolymers. As can be seen from the Table 2.1 increasing temperature to 60 °C yields a block copolymer with a lower polydispersity index, similar to the polymerization with the heterofunctional macroinitiator. Moreover, the initiation efficiency f calculated (based on monomer conversion) increased from 0.43 (at 40 °C) to 0.60 (at 60 °C). This indicates that for the difunctional macroinitiator, increasing temperature leads to an increase in initiation efficiency and better control over the polymerization reaction.²⁹

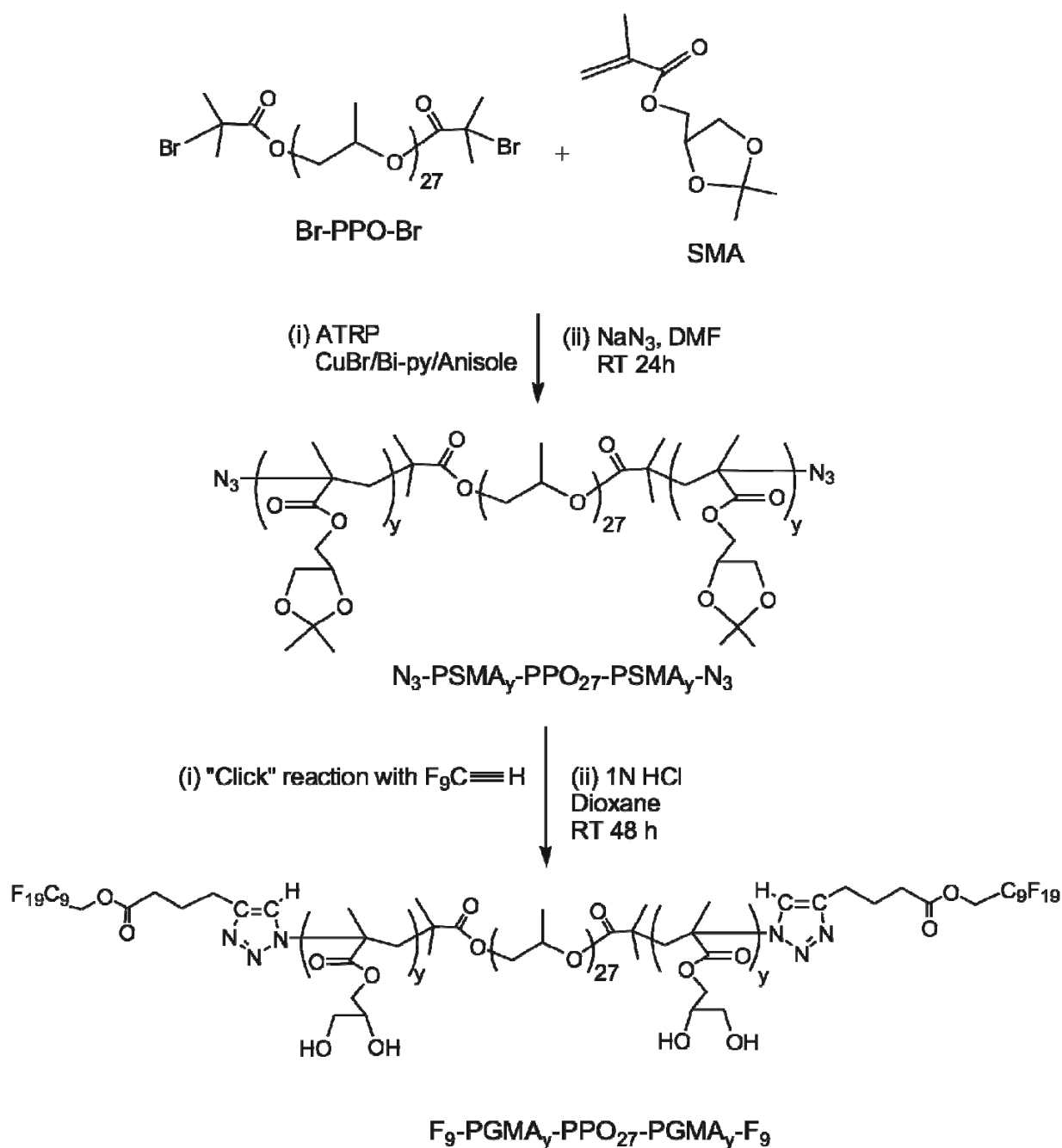


Figure 2.5 Synthetic route to triphilic F₉-PGMA_y-PPO₂₇-PGMA_y-F₉ block copolymers.

PPO₃₄-PSMA_y block copolymers

The ATRP of SMA with the monofunctional macroinitiator, PPO-Br, afforded PPO₃₄-PSMA_y block copolymers as depicted in Figure 2.6. Typical experimental procedures and polymerization temperatures were the same as in the case with the difunctional macroinitiator. However, the polymerization reactions were carried out for 20 h because the degree

of bromine chain-end functionality was unimportant as no post-polymerization reactions were carried out on the block copolymers. Two PPO₃₄-PSMA_y block copolymers were synthesized, as indicated in Table 2.1. The usual improvement in polydispersity and f with increasing temperature, from 0.47 at 40°C to 0.84 at 60 °C, was also observed for this set of block copolymers as well.

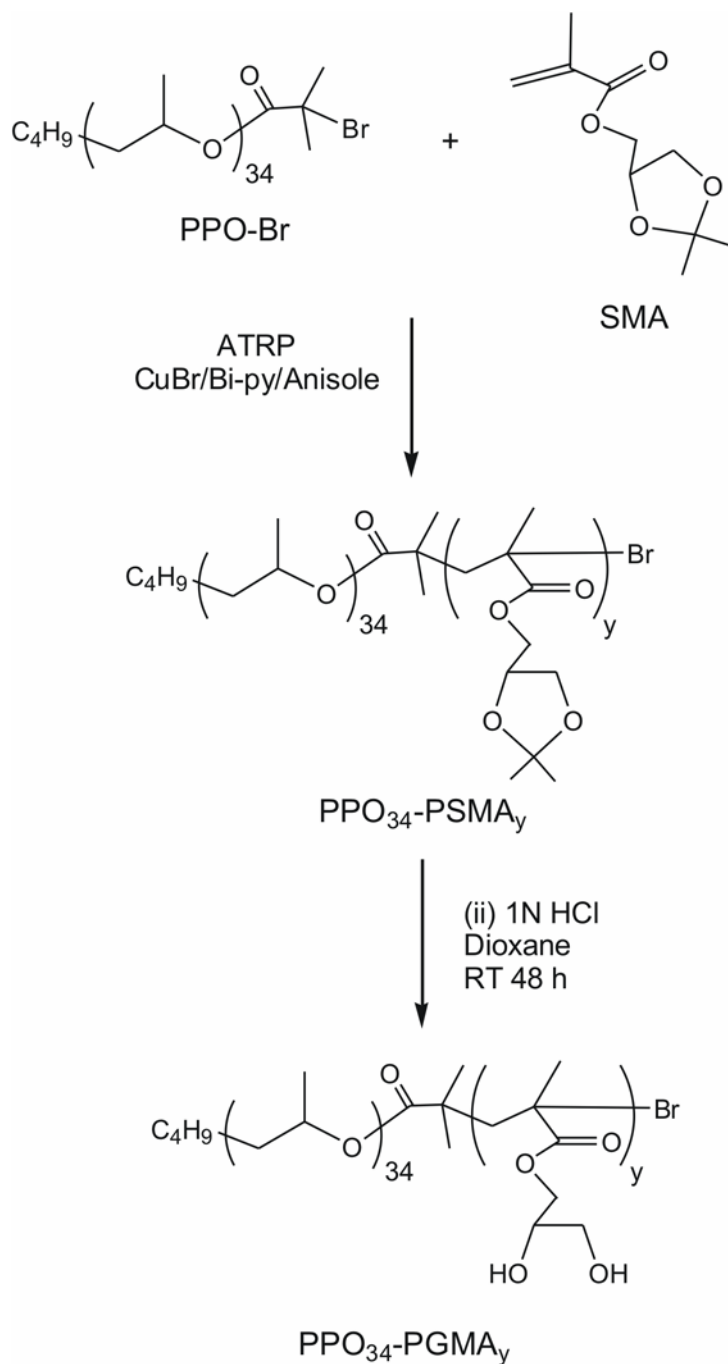


Figure 2.6 Synthetic route to amphiphilic PPO₃₄-PGMA_y block copolymers.

F₁₀-PSMAy-N₃ polymers

During the ATRP of SMA with the perfluoroalkyl initiator, F₁₀-Br, significant changes were made with regard to the metal halide and solvent used for the system. Since the F₁₀-Br is insoluble in the solvent (anisole) used in the other polymerizations, α,α,α -trifluorotoluene (TFT) was used instead. In addition, the usual metal halide, CuBr, was replaced with CuCl because the initial polymer prepared using CuBr showed very low bromine chain-end functionality even though polymerization was carried for short period (40 mins) to achieve low conversion. On the other hand, using the mixed halide system of F₁₀-Br/CuCl resulted in polymers with 80-90% halogen chain-end functionality (estimated from post-polymerization ‘click’ reactions discussed in detail in Chapter 7). It therefore seems that the F₁₀-Br/CuBr system leads to higher proportion of “dead chains” probably due to high propagation rate during the polymerization reaction. Besides, studies by Matyjaszewski et al. have shown that such mixed halide systems have faster initiation and slower propagation due to the dominant and stronger C–Cl bonds formed at the ends of the polymer chains.³²

The usual bpy was used as the complexing ligand for the CuCl catalyst with ratio of [initiator]₀: [CuBr]₀: [bpy]₀ as 1:1:2. Polymerization reactions were carried out for 40 min at 50 °C. However, a low initiation efficiency, *f*, value of about 0.18 was determined for the polymerization. The low *f* value can be attributed to the low solubility of the perfluoro-initiator in SMA. Nevertheless, the polymers obtained showed narrow polydispersity indices.

After polymer purification, substitution reaction of the halogen chain-end functionality with azido functionality was performed in DMF with NaN₃ for the 24 h. Detailed experimental procedure for this reaction is reported in literature.²⁶ Two polymers were synthesized as given in Table 2.1, entries 7 and 8. An interesting characteristic of the F₁₀-PSMAy-N₃ polymers is the apparent discrepancy between the *M_n* values obtained from NMR (¹⁹F) and SEC. This discrepancy is presumably due to the presence of the high fluorine containing F₁₀ moiety at the polymer chain end which can reduce the hydrodynamic volume of polymer chains or cause specific interaction with the column. Similar observations have been made for fluorine containing polymers by other authors.^{33,34}

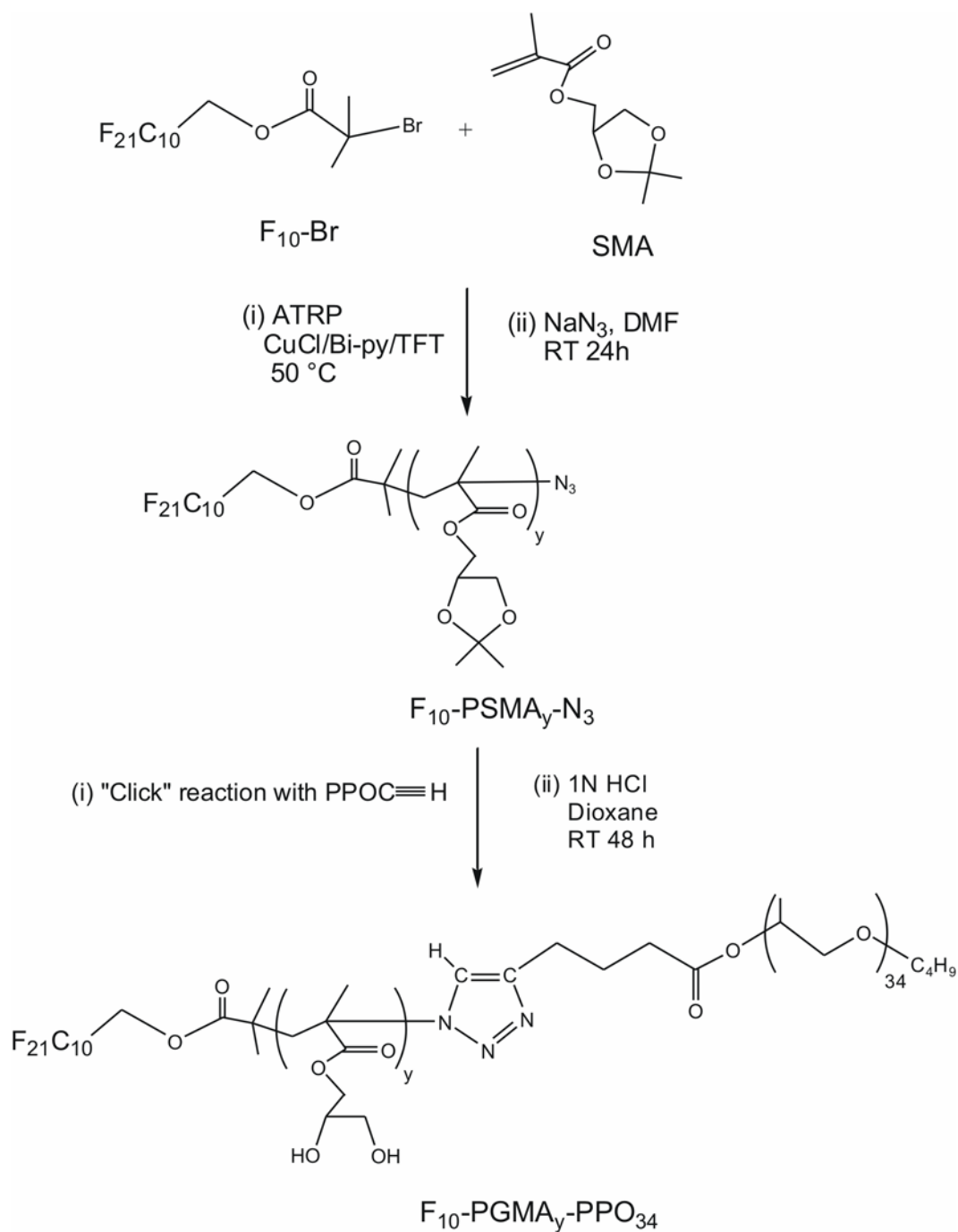


Figure 2.7 Synthetic route to triphilic $F_{10}\text{-PGMA}_y\text{-PPO}_{34}$ block copolymers

2.6 Copper(I)-Catalyzed Alkyne-Azide Cycloaddition (CuAAC) ‘Click’ Reactions

The PPO-based azido-terminated block copolymers given Table 2.1, with the exception of N_3 -PPO₂₇-PSMA₄₄, were clicked with nonadecafluoro-1-decyl hex-5-ynoate ($F_9C\equiv H$) through the copper(I)-catalyzed alkyne-azide cycloaddition reaction (CuAAC) in THF at 50°C using DIPEA as the main ligand and TBTA co-ligand. Investigations have shown that addition of small quantities of the polytriazole ligand, TBTA, stabilizes the Cu(I) species and help drive the reaction to completion.³⁵ Thus, N_3 -PPO₂₇-PSMA_y and N_3 -PSMA_y-PPO₂₇-PSMA_y- N_3 block copolymers afforded F_9 -PPO₂₇-PSMA_y and F_9 -PSMA_y-PPO₂₇-PSMA_y- F_9 block copolymers, respectively, after the ‘click’ reactions as given Table 2.2. Figures 2.3 and 2.4 show the respective schemes for the reactions. Under the same experimental conditions, the F_{10} -PSMA_y- N_3 block copolymers were also clicked with hex-5-ynoate poly(propylene oxide) (PPOC \equiv H) to give F_{10} -PSMA_y-PPO₃₄ block copolymers as schematized in Figure 2.6. The excess unreacted $F_9C\equiv H$ and PPOC \equiv H were removed during precipitation of the polymers in excess *n*-hexane. Complete disappearance of the azide band in FT-IR of the products confirmed quantitative conversion of the azido-end groups during the ‘click’ reaction. This was further corroborated by ¹⁹F and ¹H NMR spectroscopy results. Furthermore, the SEC results of the clicked copolymers also showed increase in M_n values.

Table 2.2. Molar Mass and Polydispersity indices of Block Copolymers Determined from NMR and SEC after ‘Click’ Reactions

Block copolymer	NMR	SEC ^c	
	M_n (g mol ⁻¹)	M_n (g mol ⁻¹)	M_w/M_n
F_9 -PPO ₂₇ -PSMA ₉₄	21100 ^a	26000	1.36
F_9 -PSMA ₂₄ -PPO ₂₇ -PSMA ₂₄ - F_9	12400 ^a	14100	1.20
F_9 -PSMA ₄₂ -PPO ₂₇ -PSMA ₄₂ - F_9	19800 ^a	22900	1.50
F_{10} -PSMA ₆₆ -PPO ₃₄	15900 ^b	7500	1.29
F_{10} -PSMA ₈₅ -PPO ₃₄	19700 ^b	8500	1.40

^a) Calculated from ¹H NMR spectroscopy; ^b) Calculated from ¹⁹F NMR spectroscopy

^c) Obtained from measurements in THF with poly(styrene) calibration standards

2.7 Acidic Hydrolysis of Block Copolymers

The acetonide rings of the water-insoluble PSMA blocks of all the synthesized block copolymers were completely hydrolyzed in 1,4-dioxane for 24 h to give water-soluble poly(glycerol monomethacrylate) (PGMA). Thus, all the block copolymers synthesized were rendered water-soluble after this final reaction step as depicted in Figures 2.4, 2.5, 2.6 and 2.7. The ^1H NMR spectra of the block copolymers showed the complete disappearance of the 6H protons (1.17 -1.39 ppm) corresponding to the two pendant methyl groups on the SMA unit upon complete hydrolysis. The OH functional groups formed appeared at 4.69 and 4.95 ppm on the spectra. A typical ^1H NMR spectrum before and after acid hydrolysis is shown in Figure 2.8 for one of the block copolymers. The water-soluble block polymers synthesized can be categorized into amphiphilic and triphilic block copolymers as listed in Table 2.3 and 2.4, respectively.

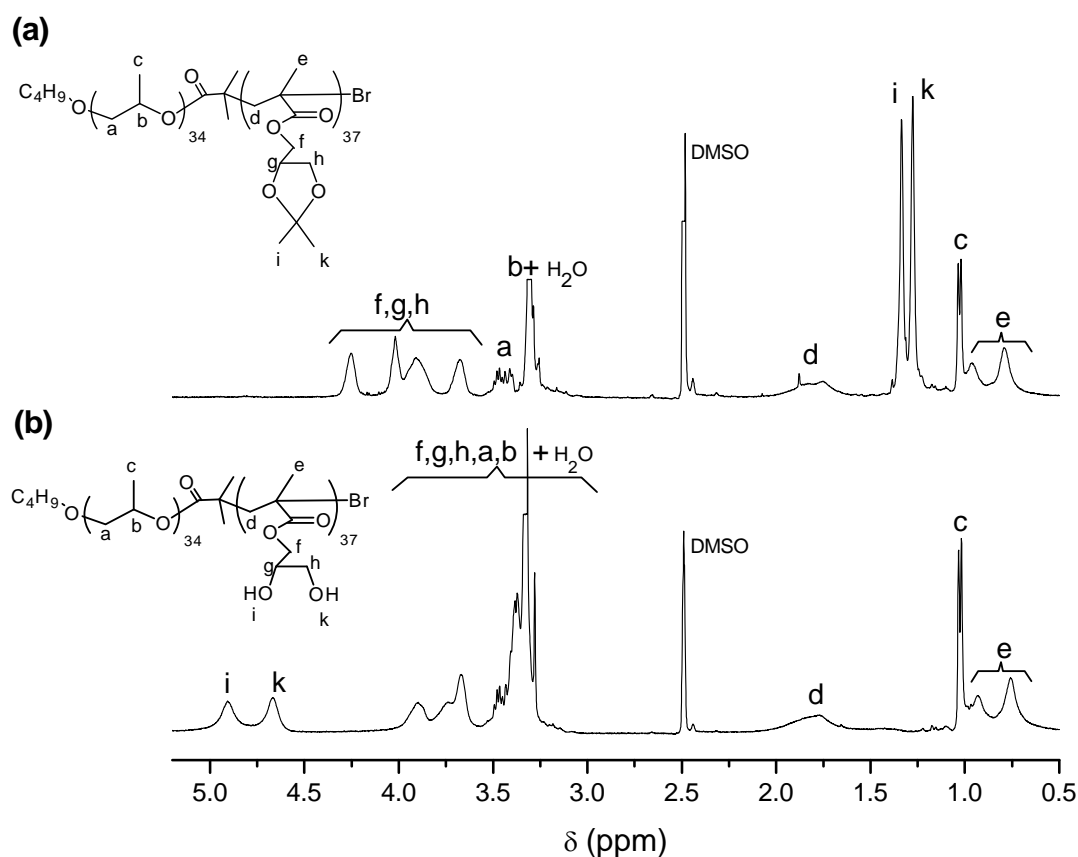


Figure 2.8 ^1H NMR spectrum of $\text{PPO}_{34}\text{-PSMA}_{37}$ obtained in $\text{DMSO-}d_6$ at 400 MHz (a) and spectrum of the polymer after acid hydrolysis to yield $\text{PPO}_{34}\text{-PGMA}_{37}$ (b).

Table 2.3. Molar Mass and Polydispersity Indices of Triphilic Block Copolymers Synthesized by ATRP and ‘Click’ Reaction

Triphilic block copolymer	Analogous block architecture	NMR	SEC ^c
		M_n (g mol ⁻¹)	M_w/M_n
F ₉ -PPO ₂₇ -PGMA ₉₄	CBA	17400 ^a	1.36
F ₉ -PGMA ₂₄ -PPO ₂₇ -PGMA ₂₄ -F ₉	CABAC	10500 ^a	1.20
F ₉ -PGMA ₄₂ -PPO ₂₇ -PGMA ₄₂ -F ₉	CABAC	16500 ^a	1.50
F ₁₀ -PGMA ₆₆ -PPO ₃₄	CAB	13300 ^b	1.29
F ₁₀ -PGMA ₈₅ -PPO ₃₄	CAB	16300 ^b	1.40

^a) Calculated from ¹H NMR spectroscopy; ^b) Calculated from ¹⁹F NMR spectroscopy; ^c) Obtained from measurements of unhydrolyzed polymers in THF with poly(styrene) calibration standards

Table 2.4. Molar Mass and Polydispersity Indices of Amphiphilic Block Copolymers Synthesized by ATRP

Amphiphilic block copolymer (BA block architecture)	¹ H NMR	SEC ^a
	M_n (g mol ⁻¹)	M_w/M_n
N ₃ -PPO ₂₇ -PGMA ₄₄	8800	1.23
PPO ₃₄ -PGMA ₃₇	7900	1.25
PPO ₃₄ -PGMA ₆₆	12600	1.40

^a) Obtained from measurements of unhydrolyzed polymers in THF with poly(styrene) calibration standards

The detailed experimental procedure for the monomer, ATRP initiators, alkyne-end functionalized compounds, polymer syntheses, and ‘click’ reactions are described in chapter 7. Their ¹H and ¹⁹F NMR, SEC chromatograms, as well as FT-IR spectra are presented in the appendix.

2.8 Conclusions

Water-soluble triphilic perfluoroalkyl end-capped block copolymers based on lipophilic PPO and hydrophilic PGMA have been synthesized by ATRP combined with ‘click’ reaction and characterized. The non-fluoro counterpart, i.e., amphiphilic block copolymers have also been synthesized by ATRP and characterized as well. Well-defined block polymers were obtained as evidenced by their generally low polydispersities ($1.2 \leq M_w/M_n \leq 1.5$).

2.9 References

1. Zhang, H.; Ruckenstein, E. *Macromolecules* **2000**, *33*, 4738.
2. Lambert, O.; Dumas P.; Hurtrez, G.; Riess G. *Macromol. Rapid Commun.* **1997**, *18*, 343.
3. Feldthusen, J.; Iván, B.; Müller, A.H. E. *Macromolecules* **1998**, *31*, 578.
4. Hillmyer, M. A.; Bates, F. S. *Macromolecules* **1996**, *29*, 6994.
5. Hawker, C. J.; Bosman, A. W.; Harth, E.; Copolymers, D. R. *Chem. Rev.* **2001**, *101*, 3661.
6. Schierholz, K.; Givehchi, M.; Fabre, P.; Nallet, F.; Papon, E.; Guerret, O.; Gnanou, Y. *Macromolecules* **2003**, *36*, 5995.
7. Garnier, S.; Laschewsky, A. *Colloid Polym. Sci.* **2006**, *284*, 1243.
8. Mertoglu, M.; Garnier, S.; Laschewsky, A.; Skrabania, K.; Storsberg, J. *Polymer* **2005**, *46*, 7726.
9. Mühlebach, A.; Gaynor, S. G.; Matyjaszewski, K. *Macromolecules* **1998**, *31*, 6046.
10. Evena, M.; Haddleton, D. M.; Kukulj, D. *Eur. Polym. J.* **2003**, *39*, 633.
11. Narrainen, A. P.; Pascual S.; Haddleton D. M. *J. Polym. Sci., Part A: Polym. Chem.* **2002**, *40*, 439.
12. Davis, K. A.; Matyjaszewski, K. *Macromolecules* **2000**, *33*, 4039.
13. Davis, K. A.; Matyjaszewski K. *Macromolecules* **2001**, *34*, 2101.
14. Opsteen, J.A.; van Hest, J.C.M. *Chem. Commun.* **2005**, 57.
15. Golas, P.L.; Tsarevsky, N.V.; Summerlin, B.S.; Walker, L.M.; Matyjaszewski K. *Aust. J. Chem.* **2007**, *60*, 400.
16. Le Droumaguet, B.; Mantovani G.; Haddleton, D.M.; Velonia, K *J. Mater. Chem.* **2007**, *17*, 1916.
17. Altintas, O.; Yankul, B.; Hizal, G.; Tunca, U. *J. Polym. Sci., Part A: Polym. Chem.* **2006**, *44*, 6458.
18. Tsarevsky, N.V.; Summerlin, B.S.; Matyjaszewski, K. *Macromolecules* **2005**, *38*, 3558.
19. Opsteen, J. A.; van Hest, J.C.M. *J. Polym. Sci., Part A: Polym. Chem.* **2007**, *45*, 2913.
20. Altintas, O.; Hizal, G.; Tunca, U. *J. Polym. Sci., Part A: Polym. Chem.* **2006**, *44*, 5699.
21. Durmaz, H.; Dag A.; Altintas, O.; Erdogan, T.; Hizal, G.; Tunca, U. *Macromolecules* **2007**, *40*, 191.
22. Binder, W. H.; Sachsenhofer, R. *Macromol. Rapid Commun.* **2007**, *28*, 15.

23. Weberskirch, R.; Preuschen, J.; Spiess, H. W.; Nuyken, O. *Macromol. Chem. Phys.* **2000**, *201*, 995.
24. Kyeremateng, S. O.; Amado, E.; Kressler J. *Eur. Polym. J.* **2007**, *43*, 3380.
25. Liu, S.; Armes, S.P. *J. Am. Chem. Soc.* **2001**, *123*, 9910.
26. Coessens, V.; Nakagawa, Y.; Matyjaszewski, K. *Polym. Bull.* **1998**, *40*, 135.
27. Mespouille, L.; Vachaudes, M.; Suriano, F.; Gerbaux, P.; Coulembier, O.; Degee, P.; Flammang, R.; Dubois P. *Macromol. Rapid Commun.* **2007**, *28*, 2151.
28. Mantovani, G.; Ladmiral, V.; Tao, L.; Haddleton, D. *Chem. Commun.* **2005**, 2089.
29. Matyjaszewski, K.; Xia, J. *Chem. Rev.* **2001**, *101*, 2921.
30. Kyeremateng, S. O.; Amado, E.; Blume, A.; Kressler J. *Macromol. Rapid Commun.* **2008**, *29*, 1140.
31. Lutz, J.-F.; Matyjaszewski, K. *J. Polym. Sci., Part A: Polym. Chem.* **2005**, *43*, 897.
32. Matyjaszewski, K.; Wang, J.; Grimaud, T; Shipp, D. *Macromolecules* **1998**, *31*, 1527.
33. Hussain, H.; Budde, H.; Höring, S.; Busse, K.; Kressler J. *Macromol. Chem. Phys.* **2002**, *203*, 2103.
34. Radhakrishnan, K.; Switek K. A.; Hillmyer M.A. *J. Polym. Sci., Part A: Polym. Chem.* **2004**, *42*, 853-861.
35. Chan, T. R.; Hilgraf, R.; Sharpless, K. B.; Fokin, V. V. *Org. Lett.* **2004**, *6*, 2853.

Chapter 3

Aggregation Behavior of Amphiphilic PPO/PGMA and PPO/PEO Block Copolymers in Water

3.1 Introduction

In the unique case of a water-soluble diblock copolymer in which one block is permanently hydrophilic while the other block's hydrophobicity depends on a stimulus, the copolymer character can be tuned to be either double-hydrophilic or amphiphilic, depending on the absence or presence of the stimulus.¹ Selective dehydration of the responsive block under the influence of the stimulus leads to reversible self-assembly into aggregates such as polymeric micelles, vesicles, or higher-order morphologies. Thus, variety of drugs, genes, and proteins can be incorporated into the hydrophobic parts of the aggregates and released upon the aggregates disassembly triggered by the absence of the stimulus.^{2,3,4,5}

While a variety of stimuli including pH^{6,7} and light^{8,9} have been employed to induce self-assembly in solution, temperature-stimulus responsive polymers are among the most widely studied category, as sensitivity is relatively easy to introduce and potential *in vitro* and *in vivo* applications can also be monitored easily.¹ The members of this category mostly possess lower critical solution temperature (LCST) phase behavior in aqueous solution. Thus, below the LCST the polymer chains are hydrated and behave as hydrophilic entities. Conversely, at temperature above the LCST they become dehydrated (insoluble) and as such behave as hydrophobic entities.¹⁰ Such LCST behaving polymers include *N*-alkyl-substituted polyacrylamides,¹¹⁻¹⁸ alkyl substituted celluloses,^{19,20} poly(vinyl methyl ether) (PVME),²⁰ poly(*N*-vinyl caprolactam) (PVCL),²¹ poly(propylene oxide) (PPO) and poly(ethylene oxide) (PEO).²² Amongst them, the block copolymer system based on PPO and PEO is the most intensely researched due to the commercial availability of the symmetric triblock copolymer, PEO-PPO-PEO, under the generic name Ploxamers and the trade name Pluronic® (BASF) or Synperonics® (ICI).²³ Although, both the homopolymers of PPO and PEO exhibit LCST behaviors in solution, the phase separation temperature of PEO is relatively very high (usually close to 100°C) compared to 10-20 °C for the PPO block.^{22,24} Hence for most parts of the

behavior of the block copolymer in water, PPO and PEO behave as the temperature-responsive and hydrophilic blocks, respectively.

The thermoresponsiveness of Poloxamers and their eventual self-assembly into micelles in aqueous solution has been well investigated by a broad range of techniques including ^1H NMR spectroscopy,²⁵⁻²⁸ dynamic light scattering (DLS),²⁹⁻³¹ static light scattering (SLS),³²⁻³⁴ Fourier transform infrared spectroscopy (FT-IR),^{35,36} differential scanning calorimetry (DSC),³⁷⁻³⁹ high sensitivity differential scanning calorimetry (HSDSC),^{40,41} and small angle neutron scattering (SANS).⁴²⁻⁴⁵ The diblock copolymer, PPO-PEO, has also received some attention^{46,47} as well as the triblock copolymer of reversed architecture, PPO-PEO-PPO.^{48,49} It is generally accepted that the dehydration of the PPO block at room and elevated temperatures is responsible for the micelle formation in PPO-PEO block copolymer systems in water.^{50,51} The micelles consist of a hydrophobic PPO core surrounded by a hydrated PEO corona.⁴³ Thus, these block copolymers form micelles in aqueous solutions (at a given concentration) above a certain critical micellization temperature (cmt).

There have been efforts, although few, to substitute the PEO block with other hydrophilic polymers, thus, creating amphiphilic PPO-based block copolymers analogous to Poloxamers and PPO-PEO diblock copolymer. Such hydrophilic polymers include poly(glycerol monomethacrylate) (PGMA),^{52,53} poly(glycidol) (PG),⁵⁴ and poly(ethyl ethylene phosphate) (PEEP).⁵⁵ However, in all these articles no attempts were made to investigate the comparative influence of the PEO block replacement on the aggregation behavior in aqueous solution. In this chapter, comparative analyses of the aggregation behaviors are made between the synthesized PPO₂₇-PGMA₄₄ block copolymer and two other commercial block copolymers, P9184 (PPO₂₉-PEO₄₅) and Pluronic-F68 (PEO₇₆-PPO₃₀-PEO₇₆). The PPO block content in all these three samples is nearly the same ($\sim 1700 \text{ g mol}^{-1}$) and the degree of polymerization hydrophilic block is similar in the case of the diblock copolymers. Pluronic-F68, which contains relatively high PEO content, is chosen because it will better help elucidate the behavior of the PEO blocks during the aggregation process.

To understand the influence of the different hydrophilic blocks .i.e., PEO and PGMA, on the aggregation process, temperature-dependent DLS and ^1H NMR measurements are carried out. In addition, the influence of the different hydrophilic blocks on the micellization parameters is investigated by temperature-dependent surface tension measurement and isothermal titration calorimetry. Finally, temperature-dependent SANS measurements are used to elucidate the structure of the PPO core of PPO₂₇-PGMA₄₄ micelles and the results are compared to those of PPO-PEO block copolymers reported in literature.

3.2. Experimental Part

3.2.1 Materials

P9184 ($M_n = 3800 \text{ g mol}^{-1}$, PDI = 1.2) and Pluronic-F68 ($M_n = 8400 \text{ g mol}^{-1}$, PDI = 1.2) purchased from Polymer Source Inc. (Dorval, Canada) and Sigma-Aldrich, respectively, were used without further purification. PPO₂₇-PGMA₄₄ ($M_n = 8800 \text{ g mol}^{-1}$, PDI = 1.2) and PGMA homopolymer ($M_n = 6400 \text{ g mol}^{-1}$, PDI = 1.3) were synthesized by ATRP as discussed in the Chapter 2. Deuterated water (D₂O, 99.9%) and deuterated dimethyl sulfoxide (DMSO-*d*₆, 99.9%) were purchased from Sigma-Aldrich.

3.2.2 Characterization

3.2.2.1 Dynamic Light Scattering (DLS)

DLS measurements of aqueous solutions of the block copolymers were performed using an ALV-NIBS/HPPS automatic goniometer from ALV-Laser (Langen, Germany), in the scattering angle range of 30° to 130°. The light source was a neodymium:YAG DPSS-200 laser ($\lambda = 532 \text{ nm}$) with a power output of 200 mW. Intensity time correlation functions were measured with an ALV-5000E multiple- τ digital correlator. The CONTIN algorithm was applied to obtain distribution functions from the obtained autocorrelation function. The apparent diffusion coefficient, D_{app} , is related to the reciprocal of the characteristic decay rate, Γ and the scattering vector, q as $D_{app} = \Gamma/q^2$ [where $q = (4\pi n_o/\lambda)\sin(\theta/2)$, with n_o = refractive index of the medium, λ = wavelength of the light, θ = scattering angle]. The corresponding apparent hydrodynamic radii, R_h , were obtained via the Stokes-Einstein equation $R_h = kT/(6\pi\eta D_{app})$, where k is the Boltzmann constant and η is the viscosity of the solvent, water in this case, corrected at the absolute temperature T . Aqueous solution of the samples block copolymers were prepared by dissolution in bidistilled water and stirred overnight. The solutions were filtered directly into the light scattering cells through a 0.45 μm pore size filter. For each temperature, the sample was equilibrated at the given temperature for 1 h prior to measurement.

3.2.2.2 ^1H NMR Spectroscopy

Spectra were recorded from 25 to 60 °C in D_2O and at 25 °C in $\text{DMSO-}d_6$ using Varian Magnetic Resonance equipment with Gemini 2000 spectrometers operating at 200 MHz and 400 MHz, respectively. The solutions were prepared by dissolution of appropriate amounts of polymer in solvent followed with slight agitation. The temperature-dependent shift of the residual HDO resonance signal was corrected for each temperature in accordance with earlier studies by Gottlieb et al.⁵⁶

3.2.2.3 Small Angle Neutron Scattering (SANS)

Appropriate amounts of polymer were dissolved in D_2O at room temperature and stirred overnight to give 0.6 wt% solutions. The solutions were filtered through a 0.45 μm pore size filter into 1 or 2 mm thick quartz containers. The use of D_2O as solvent instead of H_2O provides better contrast. Experiments were carried out using SANS II diffractometer at the Swiss Spallation Neutron Source SINQ, Paul Scherrer Institute. The wavelength of the neutron beam was 0.53 nm and the experiments were performed at two different samples to detector distances of 2 and 6 m to cover a q -range of 0.1 to 2.5 nm^{-1} . The scattered neutrons were detected using a two-dimensional 128 x 128 pixels detector (64 cm diameter). In all the measurements the temperature was kept constant at 15, 20, and 40 °C. The measured SANS data have been corrected and normalized to a cross-sectional unit, using standard procedures.

3.2.2.4 Surface Tension

The surface tension (γ) of the aqueous solutions of the samples at different polymer concentrations was measured by the Wilhelmy plate method using the automated DCAT11 tensiometer (DataPhysics Instruments GmbH, Filderstadt, Germany). Stock solutions were prepared by dissolution of the polymer in bidistilled water, stirred overnight at room temperature and passed through 0.45 μm pore-size PTFE filters before usage. Measurements were carried out in the temperature range of 20-40 °C by circulating thermostated water accurate to ± 0.1 °C through the jacketed vessel containing the measuring solution.

3.2.2.5 Isothermal Titration Calorimetry (ITC)

A Microcal VP-ITC system (Microcal, Inc., Northampton, MA) was used for this measurement. Aqueous solutions of the samples were prepared by dissolution of polymer in bidistilled water with stirring overnight. The solutions were then passed through 0.45 μm pore-size PTFE filters. Under computer control, aliquots of 10 μL were injected over regular time interval (10 min.) into the sample cell, which initially contained 1.8 mL of bidistilled water. The heat change upon injection of the aliquots was recorded, from which a plot of the heat per mole of injection against solution concentration was generated. Blank experiment performed by injecting water into water was carried out and used as a reference data which was subtracted from the experimental data to establish a good baseline correction.

3.3 Results and Discussion

3.3.1 Temperature-Dependent DLS Studies

In order to understand the influence of the PGMA or PEO on the aggregation behavior of the respective block copolymers, temperature-dependent DLS measurements were carried out on aqueous solutions of PPO₂₇-PGMA₄₄ and Pluronic-F68 at temperatures close to their cmt. Figure 3.1 shows the R_h peak distributions obtained for 1.4 g/L aqueous solution of PPO₂₇-PGMA₄₄ at 5, 15 and 25 °C. It can be seen that at 5 °C the intensity of the distribution is dominated by scattering from large species of ca. 60 nm in size.

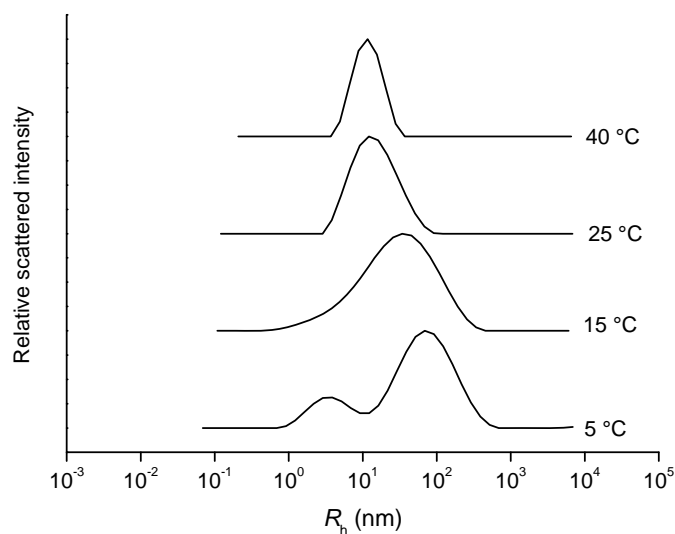


Figure 3.1 DLS data obtained at $\theta = 90^\circ$ for hydrodynamic radii (R_h) distributions as a function of temperature for 1.4 g/L aqueous solution of PPO₂₇-PGMA₄₄.

Such large species have also dominated DLS results reported by Cai et al.⁵⁷ for aqueous solutions of PPO-PGMA di- and “Y-shaped” triblock copolymers at temperatures below their cmc’s. These large species are the result of unimer-clustering due to the strong tendency of the hydroxyl groups of the PGMA blocks to partially self-associate through hydrogen-bonding (H-bonding).^{58,59} The peak with R_h at 3.4 nm corresponds to “free” unimer species. On increasing temperature to 15 °C, the unimer peak diminishes and the distribution transforms into a broad monodal peak with $R_h = 27$ nm. These changes signify the beginning of the concerted transition of block copolymer chains into micelles as the PPO blocks become dehydrated and hydrophobic. At 25°C, only a single narrow peak distribution with R_h of 14 nm is obtained in solution. This distribution corresponds to micelles which are composed of hydrophobic PPO core stabilized by hydrophilic PGMA chains which serve as coronae. With increasing temperature to 40 °C the micelle R_h reduces 11.5 nm which can be attributed to continued dehydration of the PPO core.

Figure 3.2 shows the R_h peak distributions obtained for 100 g/L aqueous solution of Pluronic-F68 at 35, 45 and 55 °C. At 35 °C the intensity of the distribution is dominated by scattering from unimers with R_h of 2.3 nm, which is in excellent agreement with the results obtained by Zhou et al.⁶⁰ for the same block copolymer. A relatively small contribution to the distribution comes from large species of $R_h \sim 55$ nm, which is attributed to hydrophobic impurities usually present in commercially available Pluronic.³⁰ Increasing temperature to 45 °C leads to transition of the unimers into a broad micelle peak distribution with R_h of 5.9 nm.

Further increasing of the temperature to 55 °C narrowed the distribution while the R_h value stayed the same. Thus from Figures 3.1 and 3.2, it can be tentatively concluded that prior to micelle formation, hydrogen bonding plays a significant role in the behavior of the block copolymer when the PEO block is replaced with PGMA.

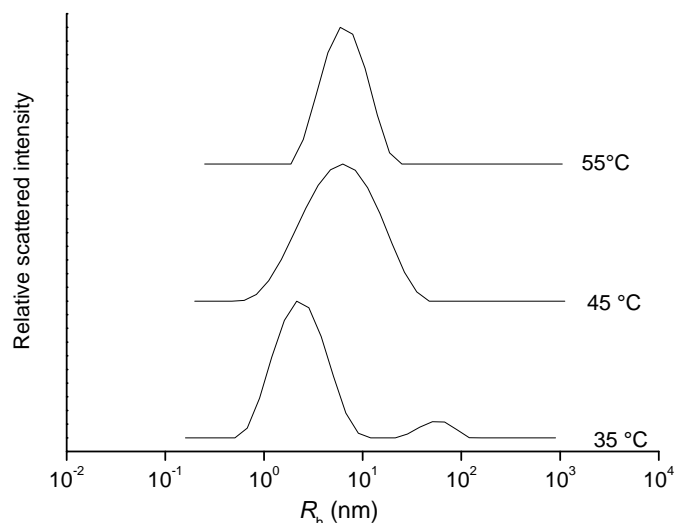


Figure 3.2 DLS data obtained at $\theta = 90^\circ$ for hydrodynamic radii (R_h) distributions as a function of temperature for 100 g/L aqueous solution of Pluronic-F68.

3.3.2 Temperature-Dependent ^1H NMR Studies

NMR spectroscopy is a powerful tool for investigating mobility of polymer chains in solution. In order to investigate and understand the influence of the different hydrophilic blocks on micelle formation, temperature-dependent ^1H NMR studies in D_2O were carried out. To start with, the ^1H NMR spectrum of $\text{PPO}_{27}\text{-PGMA}_{44}$ in $\text{DMSO-}d_6$, a non-selective solvent for both PPO and PGMA blocks, is shown in Figure 3.2a with the methyl protons of the PPO (PPO-CH_3) and PGMA (PGMA-CH_3) blocks identified. The peak at 0.76 ppm corresponds to the high content syndiotactic rr triads PGMA methyl protons (rr-PGMA- CH_3), while the peak at 0.93 ppm corresponds to the heterotactic rm triads (rm-PGMA- CH_3) of the same protons.⁶¹ The usual splitting of the PPO methyl protons peak at 1.02 ppm is due to J coupling of the methyl group to the methine group and can be noticed clearly in the spectrum.²⁵

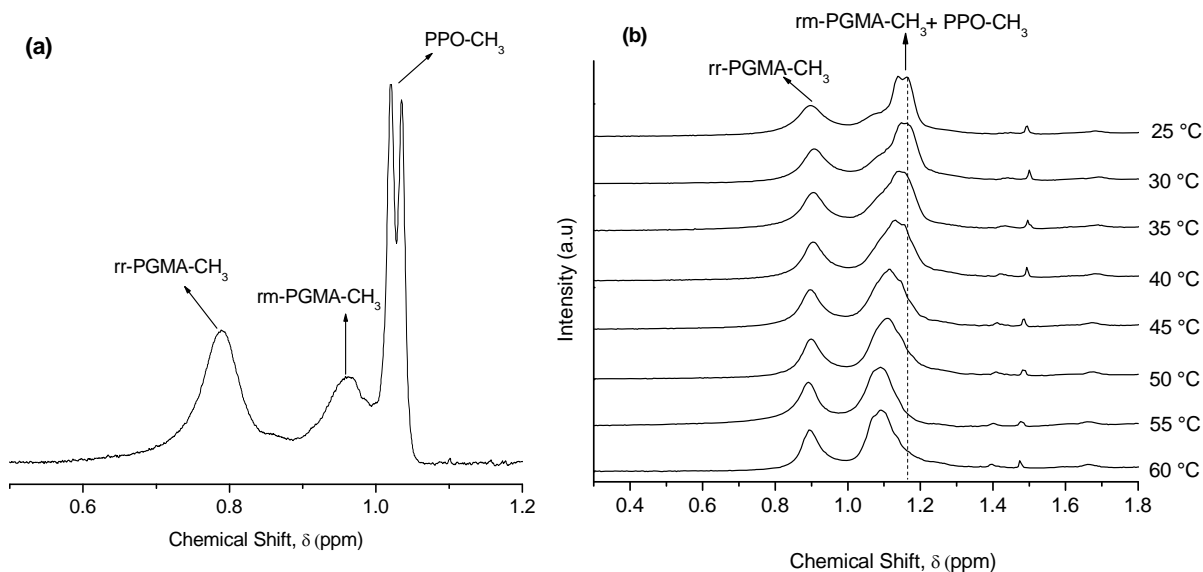


Figure 3.3 ^1H NMR spectra of $\text{PPO}_{27}\text{-PGMA}_{44}$ showing the PGMA- CH_3 and PPO- CH_3 signals (a) at 400 MHz in $\text{DMSO-}d_6$ at 25 °C and, (b) at 200 MHz in 7 g/L D_2O at different temperatures. The dashed line in (b) represents the position of the PPO methyl protons at 25 °C.

Figure 3.3b compares the systematic changes in the ^1H NMR spectra with temperature for the PPO- CH_3 and PGMA- CH_3 resonance signals of $\text{PPO}_{27}\text{-PGMA}_{44}$ in D_2O . In Figure 3.3b it is clearly evident that the PPO- CH_3 resonance signal intensity at 25 °C is highly attenuated relative to the rr-PGMA- CH_3 signal and overlaps with the rm-PGMA- CH_3 signal to give a broad peak at ~ 1.17 ppm. Also, the usual splitting of the PPO- CH_3 resonance signal has completely disappeared and the signal broadened as well. Attenuation, broadening and disappearance of the splitting of the PPO- CH_3 signal is due to the reduced mobility of the PPO block.^{25,62} These significant changes in the PPO- CH_3 resonance signal of $\text{PPO}_{27}\text{-PGMA}_{44}$ in D_2O indicate a change in the chemical environment of the methyl protons and signify that the PPO block is already in the relatively hydrophobic microenvironment of a micelle core.^{25,28} A clear observation in the ^1H NMR spectra of the block copolymer in Figure 3.3b is the shifting of the resonance signal of the PPO- CH_3 upfield with increasing temperature while the rr-PGMA- CH_3 resonance signals remains at relatively the same position. Eventually, the PPO- CH_3 signal completely overlaps with the rm-PGMA- CH_3 signal, resulting in a broader intense single peak at 1.07 ppm at 60 °C. The upfield shift is due to the change in magnetic susceptibility around the PPO- CH_3 protons owing to the deshielding effect caused by removal of water molecules around the protons.²⁸ Thus, with increasing temperature the PPO core becomes increasingly dehydrated and hydrophobic.^{36,38} The fact that the PPO- CH_3 signal is still very pronounced at 60 °C although it is in the micelle

core signifies that the core contains significant amount of trapped-water which is not easily removed. Similar ^1H NMR spectra observations regarding partially hydrated PPO cores of PPO-PGMA block copolymer micelles in aqueous solution at high temperatures has also been reported by Save et al.⁵²

Careful examination of the rr-PGMA- CH_3 resonance peak at ~ 0.91 ppm (25°C) in Figure 3.3b shows a gradual narrowing of the peak-width with increasing temperature. The spectra of the PGMA homopolymer in D_2O also revealed the same trend as can be seen in Figure 3.4. This suggests that the mobility of PGMA chains in aqueous solution increases with temperature. The behavior can be attributed to H-bonding weakening between the partially self-associated OH groups of the GMA units with increasing temperature resulting in increasing solubility and mobility of the PGMA blocks in the aqueous medium.

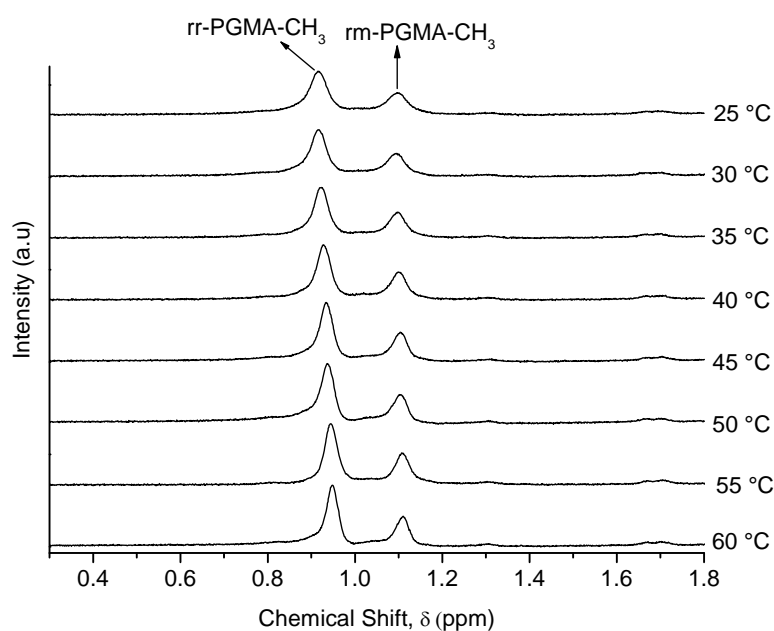


Figure 3.4 ^1H NMR spectra of PGMA homopolymer in D_2O at 200 MHz showing the PGMA- CH_3 signals at different temperatures

Figure 3.5 shows the local spectra of the methyl (PPO-CH_3) and the methylene protons ($\text{PEO-(CH}_2)_2$) of the PPO and PEO blocks, respectively, for 100 g/L Pluronic-F68 in D_2O at different temperatures. For easier comparison the PPO-CH_3 signal intensity relative to the PEO has been increased. Also the signal of the PPO methine protons which is usual found at 3.57 ppm is strongly diminished due to the relatively high PEO-content of the copolymer and as such can not be noticed in the spectra presented in Figure 3.5. At 25°C , the usual splitting

of the PPO-CH₃ resonance peak due to J coupling of the methyl protons to the methine protons can be noticed clearly in the spectrum.²⁵ At higher temperatures, precisely above 40 °C, the splitting disappears completely and the peak width of the signal broadened. The peak position also shifts upfield suddenly by ~0.02 ppm at 45 °C and continues to shift further upfield with increasing temperature. These changes in the peak shape and width, and the sudden chemical shift to the upfield reflect the transfer of the PPO blocks into the microenvironment of a micelle core. Thus, temperature-induced micellization of the block copolymer occurs above 40 °C which is in line with the DLS results. The PEO-(CH₂)₂ resonance peak meanwhile shows a slight peak-width broadening with increasing temperature which becomes very pronounced above 40 °C when micelles are formed. This signifies that mobility of the PEO chains reduces slightly with temperature and becomes very significant on micellization. The slight reduction in mobility prior to micellization can be attributed to slight dehydration of PEO with temperature since it is an LCST-capable polymer. On the other hand, the very significant reduction in mobility after micellization is due to the close packing of the PEO chains in the micellar coronae.

It can be concluded from Figures 3.3b, 3.4, and 3.5 that with increasing temperature PGMA and PEO interact with water in opposite manners. While the former increases in solubility the latter seems to interact less effectively with water.

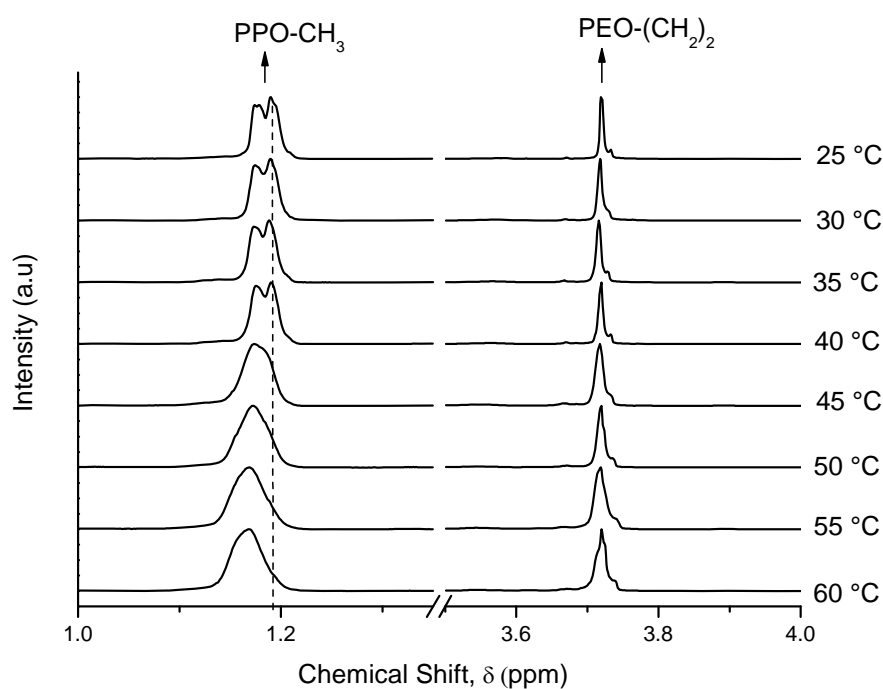


Figure 3.5 ^1H NMR spectra at 200 MHz of 100 g/L of Pluronic-F68 in D_2O at different temperatures, showing the PPO- CH_3 and PEO- $(\text{CH}_2)_2$ signals. The dashed line represents the position of the PPO methyl protons at 25 °C. Note that the PPO- CH_3 signal intensity in the region of 1.0-1.3 ppm has been increased relative to the PEO- $(\text{CH}_2)_2$ signal for clarity sake.

3.3.3 Temperature-Dependent Surface Tension Measurements

Critical micellization concentration determination. The critical micellization concentration (cmc) is a fundamental parameter in characterizing the micellization properties of a given copolymer-solvent system.²³ The cmc is defined as the copolymer concentration above which the formation of micelles becomes increasingly important. Surface tension measurement over a wide range of concentration is one of the several methods used for determination of cmc. Therefore, surface tension measurements were carried out on aqueous solutions of P9184 and PPO₂₇-PGMA₄₄ in order to obtain information on their cmc. The surface tensions γ of aqueous solutions of the block copolymers were measured as a function of polymer concentrations at 20, 25 30 and 40 °C. Plotting γ versus copolymer concentration yields the cmc indicated by intersection of the extrapolation of the two linear regimes where the curves show abrupt change in slope as indicated in Figures 3.6 and 3.7 for P9184 and PPO₂₇-PGMA₄₄, respectively, at 25 and 40 °C.

Interestingly, at 25 °C the cmc value of PPO₂₇-PGMA₄₄ (1.2×10^{-5} M) is about 20 times smaller than P9184 (2.5×10^{-4} M). This suggests that substitution of the PEO blocks with the hydroxyl-bearing PGMA blocks facilitates formation of micelles. A similar trend was also observed when the PEO block was replaced by a hydroxyl-bearing poly(glycidol)(PG) as in PG-PPO-PG triblock copolymers.⁵⁴ Intuitively, one will expect a higher hydrophilic character for the PGMA and PG blocks compared to the PEO block due the presence of the hydroxyl groups on the former. This expected higher hydrophilic character should in turn be reflected in higher cmc values since cmc is known to increase with hydrophilicity⁵¹ However, the contrary is observed because of the partial self-association through hydrogen bonding in these hydroxyl-bearing blocks.^{58,59,63} The self-association leads to lesser interactions with water molecules,⁶⁴ i.e., lower hydrophilicity compared to PEO. Thus, the hydrogen bonding effect in the PGMA- and PG-based block copolymers gives them the unexpected lesser hydrophilic character; hence, lower cmc's than their PEO-based counterparts.

It can also be noted that the cmc of PPO₂₇-PGMA₄₄ is less sensitive to temperature compared to P9184 as the former decreased by a factor of only 1.2 from 25 to 40 °C while the latter decreased by a factor of 10 at the same temperature range. The strong decrease in the cmc of P9184 copolymer with temperature is not usual as the cmc's of Poloxamers are known to decrease by a factor of 10 for ~10 °C increase in temperature.⁶⁵ According to literature, this strong decrease in cmc with increasing temperature for PPO-PEO block copolymer systems in water is attributable to increasing dehydration and consequently hydrophobicity of the PPO block.²³ In addition, one can also argue from the temperature-dependent ¹H NMR discussion that the PEO block to a lesser extent also contributes to the increasing hydrophobicity as slight dehydration with increasing temperature was observed for the PEO block as well. Since cmc is known to decrease with increase hydrophobicity,⁵¹ P9184 therefore shows significantly reduced cmc at 40 °C.

On the other hand, increasing temperature results in increasing solubility and weakening of hydrogen bonding among the PGMA blocks as observed in the in the temperature-dependent ¹H NMR measurements. It implies that in the case of PPO₂₇-PGMA₄₄ the increasing hydrophobicity of the PPO block with temperature is counterbalanced largely by the increasing hydrophilicity of the PGMA block with temperature. Hence, the cmc of PPO₂₇-PGMA₄₄ shows lower sensitivity to temperature increase compared to P9184. It may also explain why the γ values reached above cmc for PPO₂₇-PGMA₄₄ at 25 and 40 °C are very close (Figure 3.7) contrary to the case of P9184 (Figure 3.6), as the latter exhibits overall increase in hydrophobicity with temperature.

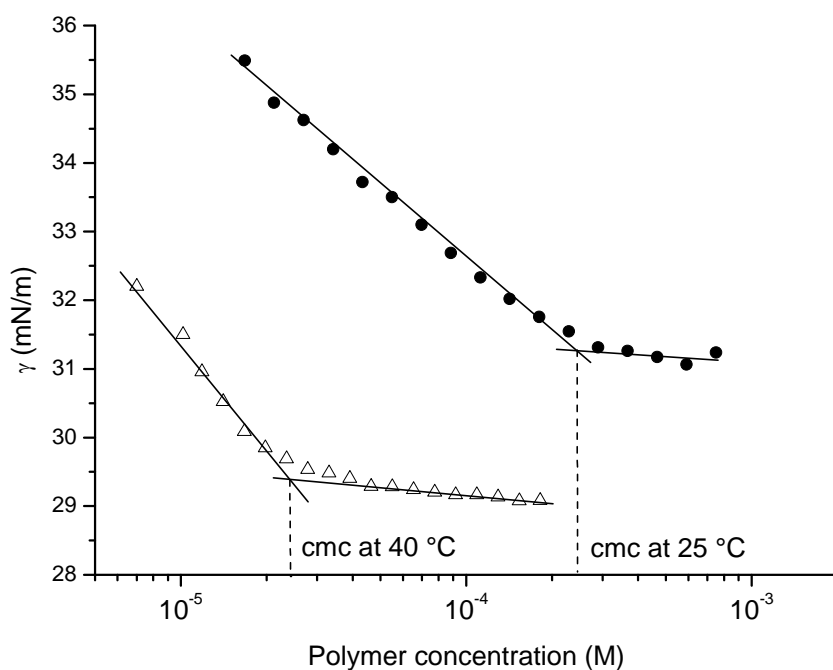


Figure 3.6 Critical micellization concentration (cmc) determination from surface tension measurements as a function of concentration at 25(●) and 40 °C(Δ) for aqueous solution of P9184.

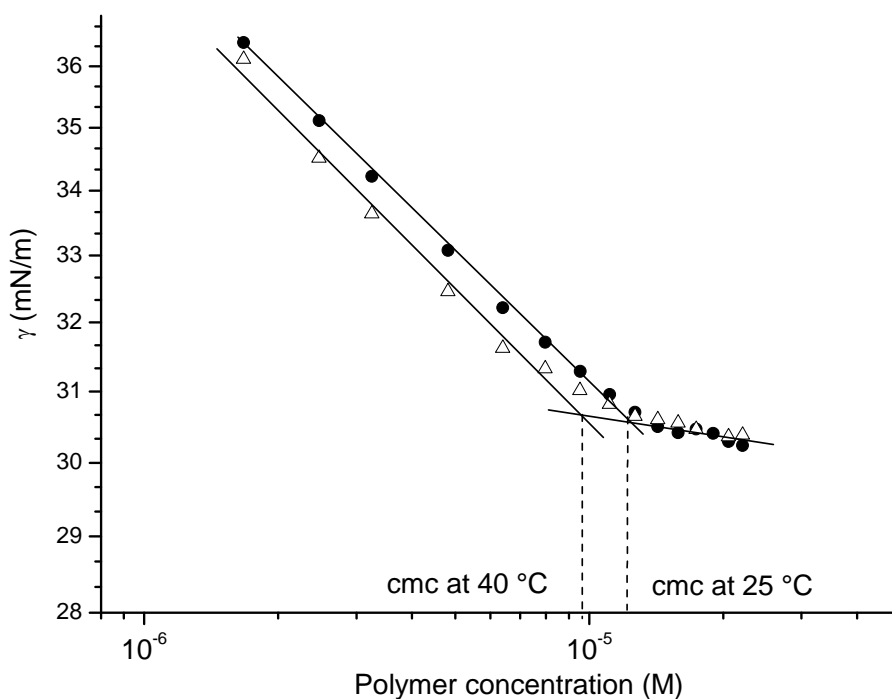


Figure 3.7 Critical micellization concentration (cmc) determination from surface tension measurements as a function of concentration at 25(●) and 40 °C(Δ) for aqueous solution of PPO₂₇-PGMA₄₄.

Thermodynamics of micellization. For a micellization process with significant association number the use of the relation below to calculate the standard free energy of micellization, $\Delta G_{\text{mic}}^{\circ}$ based on the cmc values is tolerable within experimental error.⁶⁶

$$\Delta G_{\text{mic}}^{\circ} = RT \cdot \ln(X_{\text{cmc}}) \quad (1)$$

Where R is the molar gas constant, T the thermodynamic temperature and X_{cmc} is the cmc in mole fraction at temperature T . The obtained $\Delta G_{\text{mic}}^{\circ}$ values are plotted as a function of temperature for P9184 and PPO₂₇-PGMA₄₄ in Figure 3.8. The $\Delta G_{\text{mic}}^{\circ}$ values are negative and they increase in magnitude with temperature for both both copolymers. This indicates that for both copolymers, micelle formation is a spontaneous process which increases with temperature. However, it is comparatively more spontaneous for PPO₂₇-PGMA₄₄ than P9184, especially at lower temperatures, which doesn't come as surprise since the former micellizes at lower concentrations than the latter. The standard enthalpy of micellization, $\Delta H_{\text{mic}}^{\circ}$, and the standard entropy of micellization, $\Delta S_{\text{mic}}^{\circ}$, can be estimated from the intercepts and the slopes, respectively, of the linear fits of the $\Delta G_{\text{mic}}^{\circ}$ vs T plot in Figure 3.8 according to eq 2.⁶⁷

$$\Delta H_{\text{mic}}^{\circ} = \Delta G_{\text{mic}}^{\circ} - T\Delta S_{\text{mic}}^{\circ} \quad (2)$$

Table 1 lists $\Delta H_{\text{mic}}^{\circ}$ and $\Delta S_{\text{mic}}^{\circ}$ estimated for the two block copolymers by this method. Similar to other PPO-based block copolymers, $\Delta H_{\text{mic}}^{\circ}$ which represents of the overall enthalpy change associated with the micellization process is positive.^{54,55} This indicates that the micellization process is an enthalpy disfavored process. However, the overall entropy gain due to the structural change of water on removal of the hydrophobic-like PO units is the driving force for the process.²³

It is interesting to note from Table 1 the relatively large values of $\Delta H_{\text{mic}}^{\circ}$ and $\Delta S_{\text{mic}}^{\circ}$ for P9184 compared to PPO₂₇-PGMA₄₄. The $\Delta H_{\text{mic}}^{\circ}$ of P9184 is more than 100 kJ mol⁻¹ K⁻¹ larger than PPO₂₇-PGMA₄₄. Even though it is generally accepted that most of the contribution to $\Delta H_{\text{mic}}^{\circ}$ comes from the endothermic transfer enthalpy, ΔH_t , associated with dehydration and transfer of the PO units into the micelle core,²³ the extra two PO units of P9184 compared to PPO₂₇-PGMA₄₄ definitely cannot account for this large difference. It has been shown by similar temperature-dependent cmc measurements on PPO-PEO diblock copolymers that the contribution to $\Delta H_{\text{mic}}^{\circ}$ per PO unit is about 3-6 kJ mol⁻¹.⁶⁸ Certainly, the large difference in

$\Delta H^\circ_{\text{mic}}$ between the two diblock copolymers is mainly the result of the different hydrophilic block components. It is obvious that upon micellization ΔH_t is similar for the two copolymers. When P9184 copolymer chains form micelles most of the contribution to $\Delta H^\circ_{\text{mic}}$ comes from ΔH_t because the PEO block interacts effectively with water both in the unimer-state and as a coronal component of the formed micelle. However, the situation is different when PPO₂₇-PGMA₄₄ copolymer chains form micelles. As mentioned earlier, the self-association through H-bonding between the OH groups of the PGMA blocks (which leads to formation of unimer-clusters as discussed in the DLS section) results in fewer OH groups available for interactions with water. Therefore, when PPO₂₇-PGMA₄₄ forms micelles most of the hydrogen bonds between the OH groups are broken and more OH groups of the PGMA blocks become available for hydration. Since in terms of magnitude, the endothermic enthalpy associated with breaking of alkyl-OH---HO-alkyl interactions is less than the exothermic enthalpy associated with formation of alkyl-OH---HOH (hydration),^{69,70} there is a net exothermic heat change associated with this process. This net exothermic effect offsets the magnitude of ΔH_t which leads to relatively lower $\Delta H^\circ_{\text{mic}}$ for PPO₂₇-PGMA₄₄ micellization compared to P9184 micellization. It also explains the comparatively lower $\Delta S^\circ_{\text{mic}}$ associated PPO₂₇-PGMA₄₄ micellization. Thus, the entropic gain by the water molecules on removal of the hydrophobic-like PO units upon micellization is offset by their entropic loss associated with hydration of the OH groups of the GMA units which now become available.

Table 1. Standard Enthalpy ($\Delta H^\circ_{\text{mic}}$) and Standard Entropy ($\Delta S^\circ_{\text{mic}}$) of Micellization Estimated from Standard Free Energy of Micellization ($\Delta G^\circ_{\text{mic}}$) Versus Thermodynamic Temperature (T) Plot

block copolymer	$\Delta H^\circ_{\text{mic}}$ (kJ mol ⁻¹)	$\Delta S^\circ_{\text{mic}}$ (kJ mol ⁻¹ K ⁻¹)
P9184	119.88	0.51
PPO ₂₇ -PGMA ₄₄	13.18	0.17

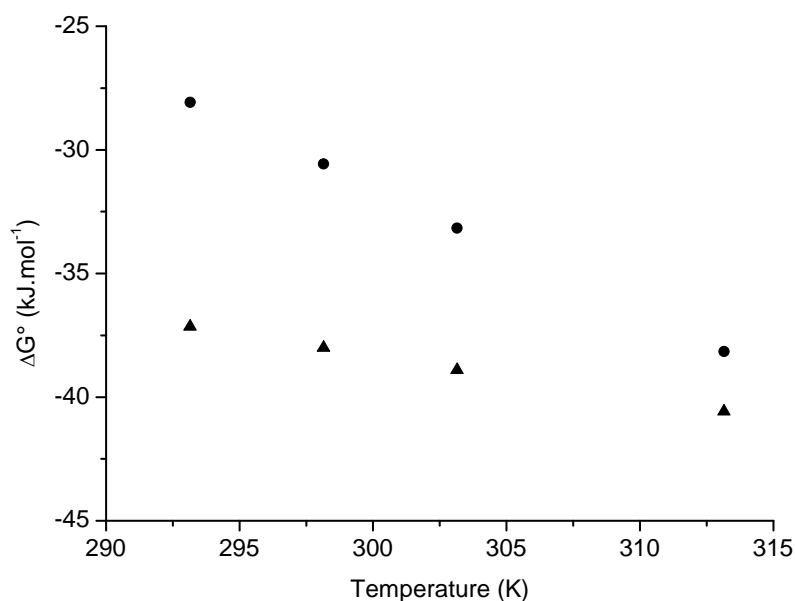


Figure 3.8 Plot of micellization free energy, $\Delta G^\circ_{\text{mic}}$, as a function of thermodynamic temperature for P9184 (●) and PPO₂₇-PGMA₄₄ (▲).

3.3.4 Isothermal Titration Calorimetry Studies

ITC directly measures the heat effects accompanying association or dissociation between molecular entities.^{71a} In determining the thermodynamic parameters of micellization ITC has an advantage that $\Delta H^\circ_{\text{mic}}$ can be directly determined in addition to cmc. Therefore, ITC measurements are performed at 40 °C for P9184 and PPO₂₇-PGMA₄₄. Small aliquots (10 μL) of stock solution of copolymers at a concentration well above the cmc were injected into a known volume of water (1.8 mL) held in the titration cell of the calorimeter. Upon initial injection into the cell, the exothermic heat change associated with dilution of the polymeric micelles and demicellization is automatically registered as a negative peak. The magnitude of the peak decreases sharply with successive injections. However, when the concentration in the titration cell exceeds cmc, only the heat change associated with micellar solution dilution is measured, and remains nearly constant.

Figures 3.9 and 3.10 show the titration curves and the heat per injection as a function polymer concentration obtained for P9184 and PPO₂₇-PGMA₄₄, respectively. The intercept of the linear fits to the demicellization range (extrapolated to zero concentration) and the micellar solution dilution range is taken as the cmc.^{71b} The cmc values determined by this method are 1.7×10^{-4} and 9.8×10^{-6} M for P9184 and PPO₂₇-PGMA₄₄, respectively.

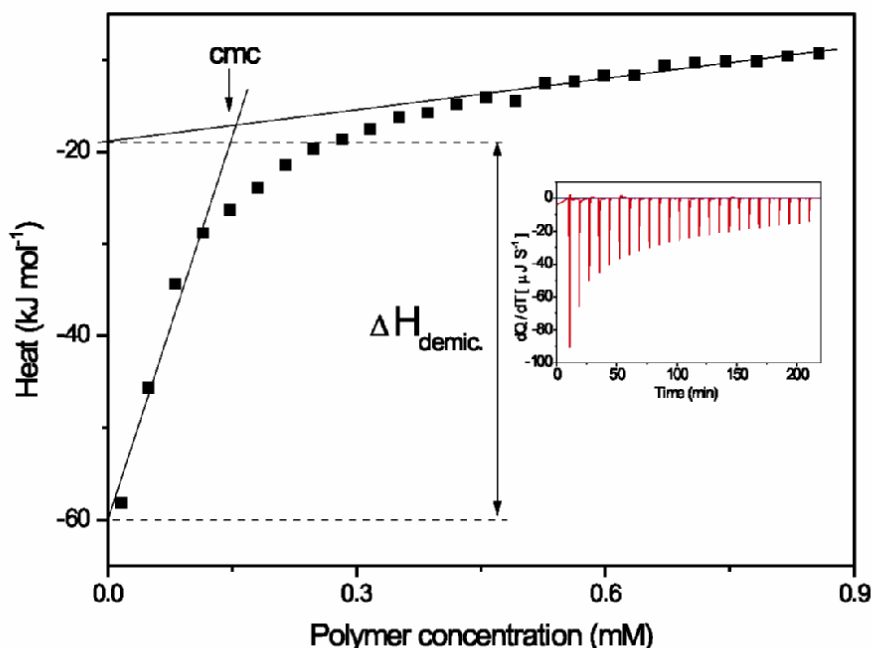


Figure 3.9 Titration curve (inset) observed from injecting P9184 ($10 \mu\text{L}$ aliquots) of 4.67 mmol L^{-1} into water at $40 \text{ }^\circ\text{C}$ (baseline corrected). The integrated heat per injection (normalized with respect to the injected number of moles of polymer) as a function of the total concentration of polymer in the sample cell. The approximated enthalpy for demicellization, ΔH_{demic} ($-41.0 \text{ kJ mol}^{-1}$), is indicated by the double arrow. The critical micellization concentration, cmc, is estimated to be $1.7 \times 10^{-4} \text{ M}$ and indicated by the arrow.

Once again the marked difference in the cmc values of the two block copolymers observed in the surface tension measurement is reflected in the ITC measurements as well. Likewise, the explanation outlined above for this difference applies equally as well under this instance too. As illustrated in Figures 3.9 and 3.10, the enthalpy of demicellization, $\Delta H_{\text{demic}}^{\circ}$, is determined according to a method described by Raju et al.^{71b} Thus, the enthalpy of micellization, $\Delta H_{\text{mic}}^{\circ}$ (which is the same in magnitude as $\Delta H_{\text{demic}}^{\circ}$ but opposite in sign) determined for are P9184 and PPO₂₇-PGMA₄₄ are 41.0 and 19.2 kJ mol^{-1} , respectively. Substituting the ITC cmc values into in eq 1 give $\Delta G_{\text{mic}}^{\circ}$ of -33.1 and $-40.5 \text{ kJ mol}^{-1}$ which are in turn substituted into eq 2 together with $\Delta H_{\text{mic}}^{\circ}$ values to give $\Delta S_{\text{mic}}^{\circ}$ values of 0.24 and 0.19 kJ mol^{-1} for P9184 and PPO₂₇-PGMA₄₄, respectively. The $\Delta H_{\text{mic}}^{\circ}$ and $\Delta S_{\text{mic}}^{\circ}$ obtained from the ITC measurements are different in magnitude (but not in sign) to those estimated from the temperature-dependent cmc measurement. In fact, micellization parameters determined from ITC are always found

to be significantly different in magnitude compared that estimated from temperature-dependent cmc measurement.^{47,72}

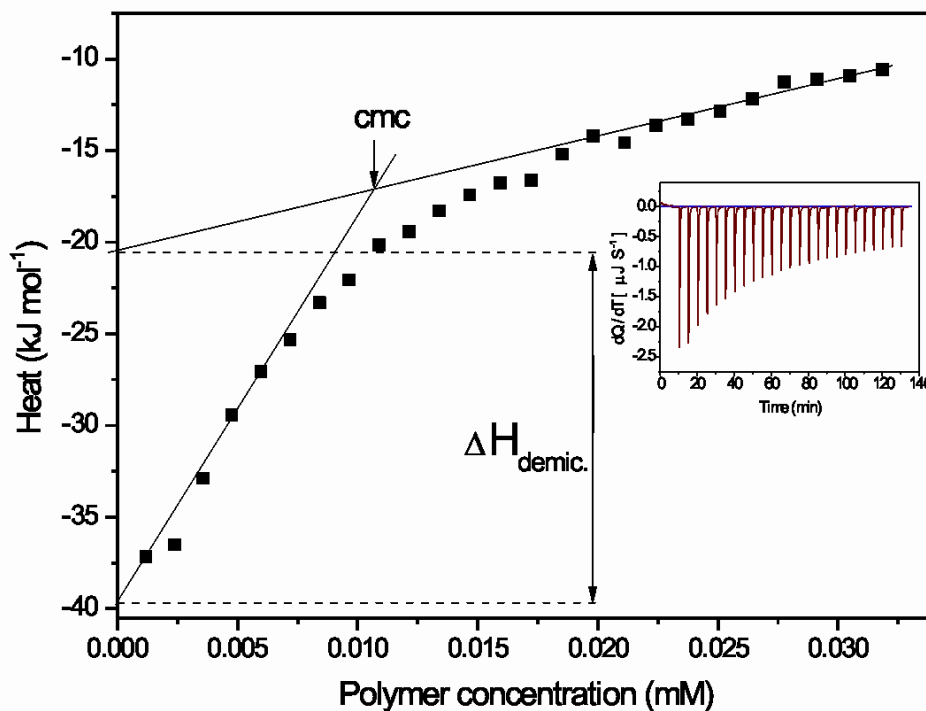


Figure 3.10 Titration curve (inset) observed from injecting PPO₂₇-PGMA₄₄ (10 μL aliquots) of 0.17 mmol L⁻¹ into water at 40 °C (baseline corrected). The integrated heat per injection (normalized with respect to the injected number of moles of polymer) as a function of the total concentration of polymer in the sample cell. The approximated enthalpy for demicellization, ΔH_{demic} (-19.2 kJ mol⁻¹), is indicated by the double arrow. The critical micellization concentration, cmc, is estimated to be 9.8×10^{-6} M and indicated by the arrow.

This is because micellization parameters from ITC relate to real condition whereas that from temperature-dependent cmc measurements relate to hypothetical standard conditions.⁷² Even so, the micellization parameters obtained from the ITC measurements reflect the same trend as those estimated from the temperature-dependent cmc measurements. Thus, the real micellization parameters obtained from ITC measurements corroborate the influence of the hydrophilic block on the micellization behavior of the two diblock copolymers as discussed above.

3.3.5 Temperature-Dependent SANS Studies

To obtain further information about the structural features of micelles formed by PPO₂₇-PGMA₄₄, we employed SANS measurements at 15, 20 and 40°C, for 0.6 wt% D₂O solutions of the copolymer. As with the chosen concentration micelle-micelle interactions should be negligible,²² the obtained SANS profiles reflect mainly the micelle form factor. It was observed that the scattering profile is dominated by contribution from the PPO core. The outer hydrated PGMA shell gives a small contribution at low q -values but due to the limited q -range of our measurement and the low scattering intensity from this part, it is treated as background and not discussed within this investigation. A hard sphere model is not able to describe the PPO core due to a dehydration gradient from outer to inner part of the core. Therefore, the fitting model consists of a radially decreasing PPO density, following a $r^{-\alpha}$ power law, with a maximum outer core radius r_0 . Typical values for the exponent are $\alpha = 2$ in case of stretched chains or $\alpha = 4/3$ for Gaussian coils. To prevent the unphysical infinite density in the limit $r \rightarrow 0$, the center of the core was set to neat PPO scattering length density of $0.347 \times 10^{-14} \text{ cm } \text{\AA}^{-3}$.⁷³ The radial size of this center part, r_1 is slightly varied (approx. 10%, log-normal distribution) to remove sharp fringes and is typically in the range of 1 - 2 nm for all fitted curves. The r_0 and α values are also varied during the fitting procedure.

Figure 3.11 shows the SANS profiles of PPO₂₇-PGMA₄₄ obtained at various temperatures together with their corresponding best fitting curves. The curves show the typical scattering profile of a spherical particle. Table 2 lists the obtained r_0 and α values after the fitting process.

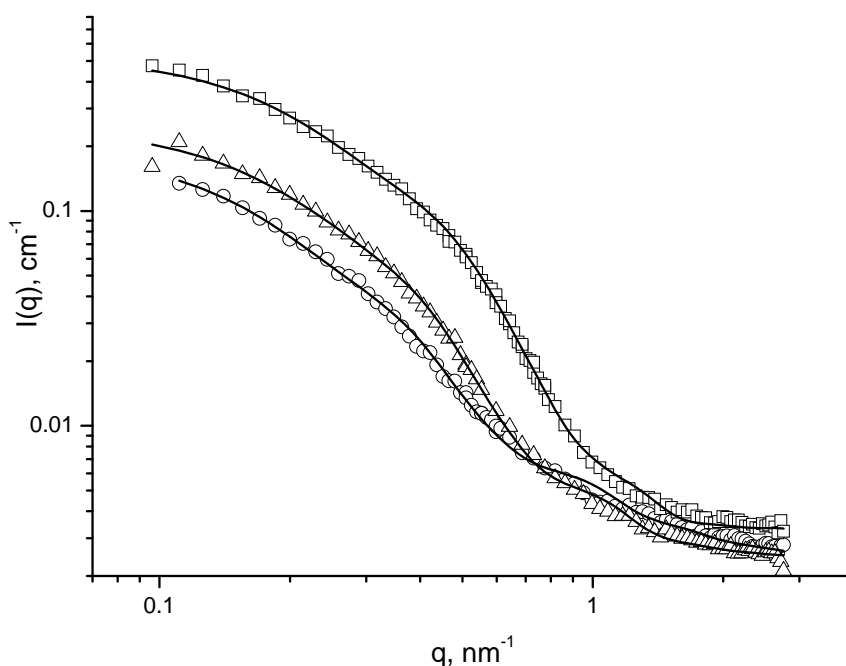


Figure 3.11 SANS profiles of 0.6 wt% D₂O solution of PPO₂₇-PGMA₄₄ at 15(○), 20(Δ) and 40 °C(□). The solid curves represent the fits using the $r^{-\alpha}$ model and the parameters from obtained the fits are given in Table 2.

Table 2: Fitting Parameters Obtained from the $r^{-\alpha}$ Model for 0.6 wt% D₂O Solution of PPO₂₇-PGMA₄₄ at 15, 20 and 40 °C

Sample	Temperature (°C)	α	Core radius r_0 (nm)
PPO ₂₇ -PGMA ₄₄	15	2.2	7.7
	20	2.0	6.8
	40	2.2	6.5

It can be seen from Table 2 that the exponent α remains at approximately 2, indicating that the PPO blocks in the outer, hydrated part of the core are in stretched-chain configuration pointing out to the attached PGMA block. Increasing temperature from 15 to 20 °C leads to a decrease of the core radius from 7.7 to 6.8 nm as given in Table 2. At 40 °C, the core radius decreases to about 85 % of its initial value at 15 °C. This observed effect of temperature on the PPO core corroborates the decreasing of PPO₂₇-PGMA₄₄ micelles size with increasing temperature, as observed in DLS measurement. Furthermore, the effect is also in agreement

with the dehydration of the PPO blocks within the micelle core with increasing temperature, as observed in the ^1H NMR temperature-dependent measurements.

Our SANS results agree with other researchers results on PPO-PEO block copolymer systems in two ways. First, the PPO-PEO block copolymer systems form core-shell micelles composed of spherical PPO core and hydrated PEO shell.⁷⁴⁻⁷⁶ Second, the PPO core of the micelles is not composed of only PPO but contains significant amount water.⁷⁴⁻⁷⁶ However, the obtained PPO core size of the PPO₂₇-PGMA₄₄ micelles is significantly larger than the ~4 nm core size reported for micelles of PPO-PEO block copolymers with comparable PPO block length.⁷⁴⁻⁷⁶ One can argue that the larger PPO core size of the PGMA-based copolymer may be due to the fact that it has very low cmc and cmt compared to the PEO-based copolymers and as such the PPO blocks of the former are relatively more hydrated when they form the micelle core. Hence, more water will be trapped within the PPO core of the PGMA-based copolymer than their PEO-based counterpart.

3.4 Conclusions

Comparative analysis has been performed on the micellization behavior of PPO₂₇-PGMA₄₄, P9184 (PPO₂₉-PEO₄₅) and Pluronic-F68 (PEO₇₆-PPO₃₀-PEO₇₆) block copolymers in aqueous solution. It is found that replacing the hydrophilic PEO block with PGMA influences very significantly the micellization process but not the final shape of the micelle formed as evidenced by SANS measurements. Typically, the replacement leads to comparatively lower cmc, $\Delta G^\circ_{\text{mic}}$, $\Delta H^\circ_{\text{mic}}$, and $\Delta S^\circ_{\text{mic}}$ of the micellization process. It also leads to larger PPO core size of the PPO₂₇-PGMA₄₄ formed micelles as determined from the SANS measurements. These significant differences stem from the partial self-association through H-bonding which occurs among the PGMA blocks. The self-association effect leads to lesser interactions with water molecules giving PGMA a lesser hydrophilic character than PEO. Consequently, the effect results in comparatively lower cmc, $\Delta G^\circ_{\text{mic}}$, $\Delta H^\circ_{\text{mic}}$, and $\Delta S^\circ_{\text{mic}}$ for the micellization of PPO₂₇-PGMA₄₄ in water.

3.5 References

1. De, P.; Gondi, S. R.; Sumerlin, B. S. *Biomacromolecules* **2008**, *9*, 1064.
2. Jule, E.; Nagasaki, Y.; Kataoka, K. *Bioconjugate Chem.* **2003**, *14*, 177.
3. Chung, J. E.; Yokoyama, M.; Okano, T. *J. Controlled Release* **2000**, *65*, 93.
4. Jeong, B.; Gutowska, A. *Trends Biotechnol.* **2002**, *20*, 305.
5. Schmaljohann, D. *Adv. Drug Delivery Rev.* **2006**, *58*, 1655.
6. Liu, C.; Hillmyer, M. a.; Lodge, T. P. *Langmuir* **2009**, *25*, 13718.
7. Dai, S.; Ravi, P.; Tam, K. C.; Mao, B. W.; Gan, L. H. *Langmuir*. **2003**, *19*, 5175.
8. Wang, G.; Tong, X.; Zhao, Y. *Macromolecules* **2004**, *37*, 8911.
9. Yoshida, T.; Kanaoka, S.; Aoshima, S. *J. Polym. Sci., Part A: Polym. Chem.* **2005**, *43*, 5337.
10. Xu, J.; Ge, Z.; Zhu, Z.; Luo, S.; Liu, H.; Liu, S. *Macromolecules* **2006**, *39*, 8178.
11. Laukkanen, A.; Valtola, L.; Winnik, F. M.; Tenhu, H. *Macromolecules* **2004**, *37*, 2268.
12. Hirotsu, S. *J Chem Phys* **1988**, *88*, 427.
13. Zhang, Y.; Furyk, S.; Bergbreiter, D. E.; Cremer, P.S. *J. Am. Chem. Soc.* **2005**, *127*, 4505.
14. Baltes, T.; Garret-Flaudy, F.; Freitag, R. *J Polym. Sci., A: Polym. Chem.* **1999**, *37*, 2977.
15. Diab, C.; Akiyama, Y.; Kataok, K.; Winnik, F. M. *Macromolecules* **2004**, *37*, 2556.
16. Cho, C. S.; Jung J. H.; Sung, Y. K.; Lee, Y. M.; *Macromol Rapid Commun* **1994**, *15*, 727.
17. Schild, H.G. *Prog. Polym. Sci.* **1992**, *17*, 163.
18. Liu, H. Y.; Zhu, X. X.; *Polymer* **1999**, *40*, 6985.
19. Schild, H. G.; Tirrel, D. A. *J. Phys. Chem.* **1990**, *94*, 4352.
20. Persson, J. Johansson, H. Galaev, I. Mattiasson, B. Tjerneld, F. *Bioseparation* **2000**, *9*, 105.
21. de Las Heras Alarcon, C.; Pennadam, S.; Alexander, C. *Chem.Soc.Rev.* **2005**, *34*, 276.
22. Alexandridis, P.; Yang, L. *Macromolecules* **2000**, *33*, 5574.
23. Chu B.; Zukang Z. In *Nonionic Surfactants, Polyoxyalkylene Block Copolymers*; Nace, V.M., Ed.; Marcel Dekker, Inc.: New York, NY, 1996; pp 67-144.
24. Li, C.; Buurma, N. J.; Haq, I.; Turner, C.; Armes, S. P.; Castelletto, V.; Hamley, I. W.; Lewis, A. L. *Langmuir* **2005**, *21*, 11026.

25. Cau F.; Lacelle S. *Macromolecules* **1996**, *29*, 170.
26. Malmsten, M.; Lindman, B. *Macromolecules* **1992**, *25*, 5446.
27. Ma, J.; Guo, C.; Tang, Y.; Wang, J.; Zheng L.; Liang, X.; Chen, S.; Liu, H. *J. Colloid Interface Sci.* **2006**, *299*, 953.
28. Ma J-h.; Guo C.; Tang Y-l.; Liu H-z. *Langmuir* **2007**, *23*, 9596.
29. Zhou, Z.; Chu, B. *Macromolecules* **1988**, *21*, 2548.
30. Almgren, M.; Brown, W.; Hvidt, S. *Colloid Polym. Sci.* **1995**, *273*, 2.
31. Alexandridis, P.; Nivaggioli, T.; Hatton T. A. *Langmuir* **1995**, *11*, 1468.
32. Brown, W.; Schillen, K.; Almgren, M.; Hvidt, S.; Bahadur, P. *J. Phys. Chem.* **1991**, *95*, 1850.
33. Nolan, S. L.; Phillips, R. J.; Cotts, P. M.; Dungan, S. R. *J. Colloid Interface Sci.* **1997**, *302*, 291.
34. Liu, Y.; Chen, S.; Huang, J. S. *Macromolecules* **1998**, *31*, 6226.
35. Su, Y.L.; Wang, J.; Liu H. Z. *J. Phys. Chem. B* **2002**, *106*, 11823.
36. Guo, C.; Liu, H.Z.; Chen, J.Y. *Colloid Polym. Sci.* **1999**, *277*, 376.
37. Wanka G.; Hoffmann H.; Ulbricht W. *Macromolecules* **1994**, *27*, 4145.
38. Hvidt S.; Trandum C.; Batsberg W. *J. Colloid Interface Sci.* **2002**, *250*, 243.
39. Barba, A. A.; Amore, M.; Grassi, M.; Chirico, S.; Lamberti, G.; Titomanlio, G.; Ponte, V.; Farmaceutiche, S.; Chimica, I. *J. Appl. Polym. Sci.* **2009**, *114*, 688.
40. Mitchard, N. M.; Beezer, a. E.; Mitchell, J. C.; Armstrong, J. K.; Chowdhry, B. Z.; Leharne, S.; Buckton, G. *J. Phys. Chem.* **1992**, *96*, 9507.
41. Beezer, A. E.; Loh W.; Mitchell, J. C.; Royall, P. G.; Smith, D. O.; Tute M. S.; Armstrong, J. K.; Chowdhry, B. Z.; Leharne, S. A; Eagland, D.; Crowtherg, N. J. *Langmuir* **1994**, *10*, 4001.
42. Ganguly, R.; Choudhury, N.; Aswal, V. K.; Hassan, P. A. *J. Phys. Chem. B.* **2009**, *113*, 668.
43. Yang, L.; Alexandridis, P.; Steytler, D. C.; Kositza, M. J.; Holzwarth, J. F. *Langmuir.* **2000**, *16*, 8555.
44. Liu, Y.; Chen, S.; Huang, J. S. *Macromolecules.* **1998**, *31*, 2236.
45. Mata, J. P.; Majhi, P. R.; Guo, C.; Liu, H. Z.; Bahadur, P. *J. Colloid Interface Sci.* **2005**, *292*, 548.
46. Rangelov, S.; Petrov, P.; Berlinova, I.; Tsvetanov, Ch. *Polym. Bull.* **2004**, *52*, 155.
47. Taboada, P.; Mosquera, V.; Attwood, D.; Yang, Z.; Booth, C. *Phys. Chem. Chem. Phys.* **2003**, *5*, 2625.

48. Alexandridis, P.; Athanassiou, V.; Fukuda, S.; Hatton, T.A. *Langmuir* **1994**, *10*, 2604.
49. Zhou, Z.; Chu, B. *Macromolecules* **1994**, *27*, 2025.
50. Wanka G.; Hoffmann H.; Ulbricht W. *Colloid Polym. Sci.* **1990**, *268*, 101.
51. Alexandridis P.; Holzwarth J. F.; Hatton T. A. *Macromolecules* **1994**, *27*, 2414.
52. Save, M.; Weaver, J. V.; Armes, S. P.; McKenna, P. *Macromolecules* **2002**, *35*, 1152.
53. Amado E.; Augsten C.; Mäder K.; Blume A.; Kressler J. *Macromolecules* **2006**, *39*, 9486.
54. Halacheva, S.; Rangelov, S.; Tsvetanov, C. *Macromolecules*. **2006**, *39*, 6845.
55. Wang, Y.; Xia, H.; Yang, X.; Wang, J. *J. Polym. Sci., Part A: Polym. Chem.* **2009**, *47*, 6168.
56. Gottlieb H.E.; Kotlyar V.; Nudelman A. *J. Org. Chem.* **1997**, *62*, 7512
57. Cai, Y.; Tang, Y.; Armes, S. P. *Macromolecules*. **2004**, *37*, 9728.
58. Kyeremateng S.O.; Amado E.; Kressler J. *Euro. Polym. J.* **2007**, *43*, 3380.
59. Kyeremateng S.O., Henze T., Busse K., Kressler J. *Macromolecules* **2010**, *43*, 2502.
60. Zhou, Z.; Chu, B. *J. Colloid Interface Sci.* **1988**, *126*, 171.
61. Carriere P.; Grohens Y.; Spevacek J.; Schultz J. *Langmuir* **2000**, *16*, 5051.
62. Riess G. *Prog. Polym. Sci.*, **2003**, *28*, 1107.
63. Rangelov S., Almgren M., Halacheva S., C. Tsvetanov *J. Phys. Chem. C* **2007**, *111*, 13185.
64. Wang C.; Yu B.; Knudsen B.; Harmon J.; Moussy F.; Moussy Y. *Biomacromolecules* **2008**, *9*, 561.
65. Desai, P. R.; Jain, N. J.; Bahadur, P. *Colloids Surf., A* **2002**, *197*, 19.
66. Yang Y-W.; Deng N.-J., Yu G.-E.; Zhou Z. K.; Attwood D.; Booth C. *Langmuir* **1995**, *11*, 4703.
67. Hunter, R. J. *Foundations of Colloid Science*; Oxford University Press: New York, 1987; Vol. 1.
68. Altinok, H. *Colloids and Surfaces B: Biointerfaces*. **1999**, *16*, 73.
69. Solomonov B.N.; Novikov V.B.; Varfolomeev M.A.; Klimovitskii A.E. *J. Phys. Org. Chem.* **2005**, *18*, 1132.
70. Graziano G. *Phys. Chem. Chem. Phys.* **1999**, *1*, 3567.
71. (a) Okhrimenko O.; Jelesarov L. *J. Mol. Recongnit.* **2008**, *21*, 1. (b) Raju, B. B.; Winnik, F. M.; Morishima, Y. *Langmuir*. **2001**, *17*, 4416.
72. Taboada, P.; Velasquez, G.; Barbosa, S.; Yang, Z.; Nixon, S. K.; Zhou, Z.; Heatley, F.; Ashford, M.; Mosquera, V.; Attwood, D.; Booth, C. *Langmuir* **2006**, *22*, 7465.

73. Mortensen, K.; Pedersen, J. S. *Macromolecules* **1993**, *26*, 805.
74. Pedersen, J.S; Gertsenberg, M.C *Colloids Surf., A* **2003**, *213*, 175.
75. Goldmints I.; Yu G.-E.; Booth C.; Smith K. A.; Hatton T. A. *Langmuir* **1999**, *15*, 1651.
76. Goldmints I.; v. Gottberg F.K.; Smith K.A.; Hatton T.A *Langmuir* **1997**, *13*, 3659.

Chapter 4

Effect of Hydrophilic Block Length-A on the Aggregation Behavior of Triphilic CABAC Pentablock Copolymer Analogues in Water

4.1 Introduction

In the recent decade the combination of three mutually incompatible fluorophilic, lipophilic, and hydrophilic blocks (i.e., triphilic) in polymer synthesis has generated much interest because of the intriguing structures formed in bulk and in solution.^{1-7,9,11-15} The micelle structures formed in aqueous media by these copolymers have mostly a phase-separated core due to the immiscibility between the hydrophobic blocks (fluorophilic and lipophilic) resulting in a multicompartment micelle.¹ Their final morphology depends sensitively on the block copolymer architecture, composition, number of segments, and segment lengths.^{1,8} Recently, Lodge et al.⁹ demonstrated that micelles with hydrocarbon/fluorocarbon phase-separated cores are able to selectively store hydro- and fluorocarbon chromophores. Such micelles hold very great potentials in the application fields of drug delivery, catalysis, and nanotechnology.¹⁰

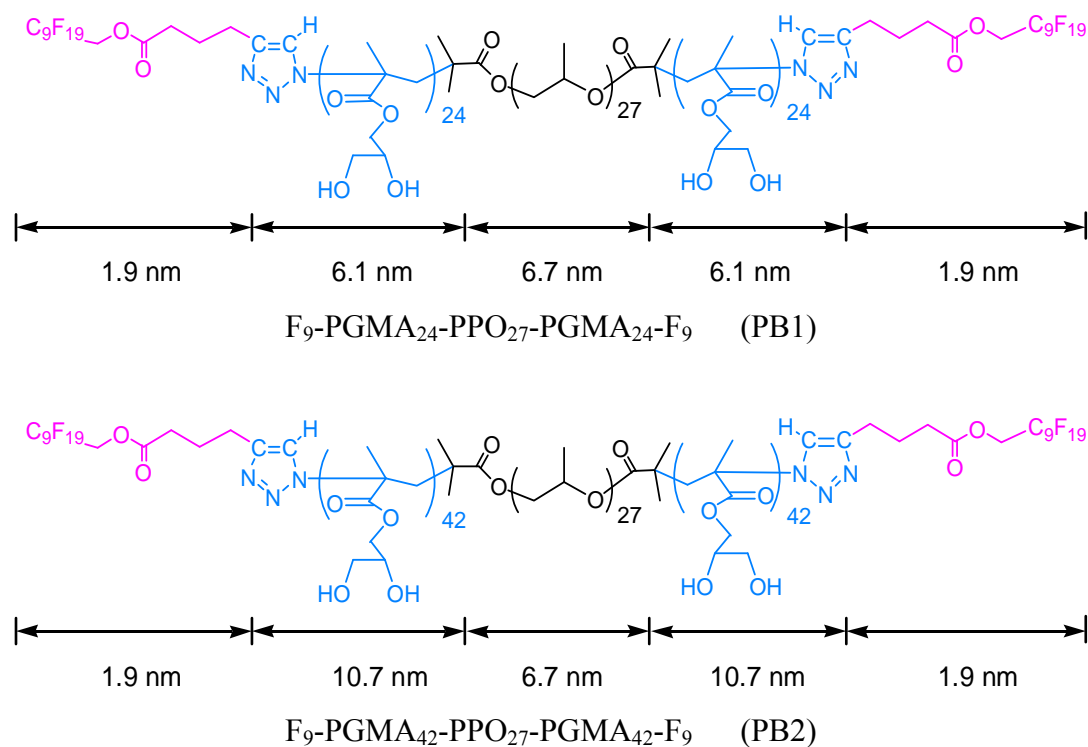
In fact, multicompartment micelles formed by hydrophilic-lipophilic-fluorophilic ABC triblock copolymers of linear^{2,11,12} and miktoarm¹ architectures are well documented in the literature. Typically, Li and co-workers have made an in-depth characterization of the diverse morphologies of multicompartment micelles formed by varying the composition of μ -[poly(ethylene)][(poly(ethylene oxide))][poly(perfluoropropylene oxide)] miktoarm block copolymers.¹ Multicompartment micelles formed by triblock copolymers with linear and hyperbranched star architectures where the lipophilic and the fluorophilic blocks are separated by the hydrophilic block, i.e., BAC, are also reported.^{5,6,13} However, there are only a few studies reporting on the multicompartment micelle structures formed by linear symmetric triphilic pentablock copolymer systems. One of them by Thünemann et al.³ employs poly(ethylene oxide), poly(γ -benzyl-L-glutamate), and poly(perfluoroether), and the other by He et al.¹⁵ is achieved by end modifying Pluronic 127 with poly(octafluoropentyl methacrylate). In the former, the micelle structure in water is investigated whereas in the latter the effect of the perfluoro block content on the micelle size in water is studied.

This chapter discusses the effect of varying the hydrophilic block length on the aggregation behavior in water for the two CABAC pentablock copolymer analogues synthesized in chapter two, i.e., F₉-PGMA₂₄-PPO₂₇-PGMA₂₄-F₉ and F₉-PGMA₄₂-PPO₂₇-PGMA₄₂-F₉. Surface tension measurements are employed to determine the critical micelle concentration (cmc) of the block copolymers in water. By combining NMR (¹H and ¹⁹F) spectroscopy and dynamic light scattering (DLS) techniques, the influence of the hydrophilic block length on the micelle structures formed in aqueous solution is investigated. Furthermore, the hydrophilic block length influence is also assessed in terms of structures formed on solid supports (after evaporation of water) by atomic force microscopy (AFM) and transmission electron microscopy (TEM) investigations. Finally, tetrafluorobenzene uptake-capabilities of the micelles formed by the triphilic block copolymers are assessed in comparison with those formed by the amphiphilic diblock copolymer.

4.2. Experimental Part

4.2.1 Materials

Deuterated water (D₂O, 99.9 %), deuterated dimethyl sulfoxide (DMSO-*d*₆, 99.9 %), and tetrafluorobenzene (TFB, 99 %) were purchased from Sigma-Aldrich. The two block copolymers, F₉-PGMA₂₄-PPO₂₇-PGMA₂₄-F₉ and F₉-PGMA₄₂-PPO₂₇-PGMA₄₂-F₉, hereafter referred to as PB1 and PB2, were synthesized by ATRP and CuAAC ‘click’ reaction as already detailed in Chapter 2. PB1 and PB2 have molar masses of 10500 and 16200 g/mol, respectively, as calculated from ¹H NMR spectroscopy. Their polydispersities obtained from size exclusion chromatography (SEC) are 1.2 and 1.5, respectively. Scheme 1 illustrates the chemical structures of the two copolymers and the contour lengths of their constituent blocks. Assuming fully extended all-trans conformations between the carbon-carbon bonds, the contour lengths are determined using 2.54 Å for GMA monomer units and for two successive carbon-carbon bonds in the F₉ segments. The PPO contour length calculations are usually based on monomer unit length dimensions between 2.5 and 3.6 Å.^{16b,17c} Since the PPO block length is always fixed, we use here as an example the value of 2.5 Å.

Scheme 1 Chemical Structure of the PBs Showing the Contour Lengths of the Individual Blocks

4.2.2 Characterization

4.2.2.1 NMR Spectroscopy

¹H and ¹⁹F NMR spectra were recorded from 25 to 60 °C in D₂O and at 25 °C in DMSO-*d*₆ using Varian magnetic resonance equipment with Gemini 2000 spectrometers operating at 200 and 400 MHz for measurements in D₂O and DMSO-*d*₆, respectively. Polymer solutions of concentration 7 g/L were employed. The solutions were prepared by dissolution of appropriate amounts of polymer in solvent followed with slight agitation.

4.2.2.2 Surface Tension Measurement

The surface tension (γ) of the aqueous solutions of the samples at different polymer concentrations was measured by the Wilhelmy plate method using the automated DCAT11 tensiometer (Data Physics Instruments GmbH, Filderstadt, Germany). Stock solutions of 2.5

g/L were prepared by dissolution of the polymer in bidistilled water, stirred overnight at room temperature, and filtered through 0.45 μm pore-size PTFE before usage. The tensiometer works by automatically injecting predetermined volumes of the stock solution into a thermostated glass vessel containing initially only distilled water. Following each injection, the surface tension is then measured after 10 min of stirring and a 3 h waiting period. Measurements were carried out at 25 $^{\circ}\text{C}$ by circulating thermostated water accurate to 0.1 $^{\circ}\text{C}$.

4.2.2.3 Dynamic Light Scattering (DLS)

DLS measurements of aqueous solutions of the block copolymers were performed using an ALV-NIBS/HPPS automatic goniometer from ALV- Laser (Langen, Germany) in the scattering angle range of 30 $^{\circ}$ -130 $^{\circ}$. The light source was a neodymium:YAG DPSS-200 laser ($\lambda=532$ nm) with a power output of 200 mW. Intensity time correlation functions were measured with an ALV-5000E multiple- τ digital correlator. The CONTIN algorithm was applied to obtain distribution functions from the obtained autocorrelation function. In case of bimodal distributions, the g^1 autocorrelation function was fitted with two exponential decay functions to obtain an average effective diffusion constant of the two species. The diffusion constant, D_{app} , is related to the reciprocal of the characteristic decay time, Γ , and the scattering vector, q , as $D_{\text{app}} = \Gamma/q^2$ [where $q = (4\pi n_0/\lambda) \sin(\theta/2)$, with n_0 = refractive index of the medium, λ = wavelength of the light, and θ = scattering angle]. The corresponding apparent hydrodynamic radii, R_h , were obtained via the Stokes-Einstein equation $R_h = kT/(6\pi\eta D_{\text{app}})$, where k is the Boltzmann constant and η is the viscosity of the solvent, water in this case, corrected at the absolute temperature T . Stock solutions of 5.6 g/L were prepared by dissolution of polymers in bidistilled water and stirred overnight. Lower concentrations were prepared by gradual dilution. The solutions were filtered directly into the light scattering cells through a 0.45 μm pore size filter.

4.2.2.4 Tetrafluorobenzene (TFB) Solubilization Experiments

In solubilization experiments, 5 mg/mL D_2O solutions of PB1, PB2, and the diblock copolymer PPO₂₇-PGMA₄₄ were prepared by stirring for 24 h. The polymer solutions were then transferred into clean NMR tubes and 30 μL of TFB was added followed by strong agitation of the mixture for 1 h. Then the tubes were kept still in the dark for at least 3 weeks to allow the excess TFB to phase separate to the bottom of the tube. Carefully, 0.8 mL of the

clear top aqueous solutions were removed and analyzed by ^1H NMR spectroscopy. The amounts of solubilized TFB were then calculated from the integral of the characteristic 2H-benzyl signal of TFB at 7.01 ppm in comparison to the signal of the backbone methylene group of the hydrophilic PGMA block at 1.86 ppm.

4.2.2.5 Atomic Force Microscopy (AFM)

AFM images were obtained on a NANOWIZARD I (JPK Instruments, Berlin) operated in tapping mode with silicon cantilevers at a scan rate of 1 Hz. The cantilevers (Arrow, NanoWorld, Neuchâtel) had a resonance frequency of ~ 285 kHz and a force constant of ~ 42 N/m.

4.2.2.6 Transmission Electron Microscopy (TEM)

The TEM images were obtained from a JEOL 100CX microscope, operating at an acceleration voltage of 100 kV. Samples were prepared by drop-coating 0.014 g/L aqueous solutions of polymers on carbon-coated copper grids and allowed to dry under ambient conditions.

4.3 Results and Discussion

4.3.1 Surface Tension Measurements

The surface tensions, γ , of aqueous solutions of the block copolymers are measured as a function of polymer concentrations at 25 °C. Plotting γ vs polymer concentration ($\log C$) yields the critical micellization concentration (cmc) indicated by intersection of the extrapolation of the two linear regimes where the curves show abrupt change in slope as indicated in Figure 4.1.

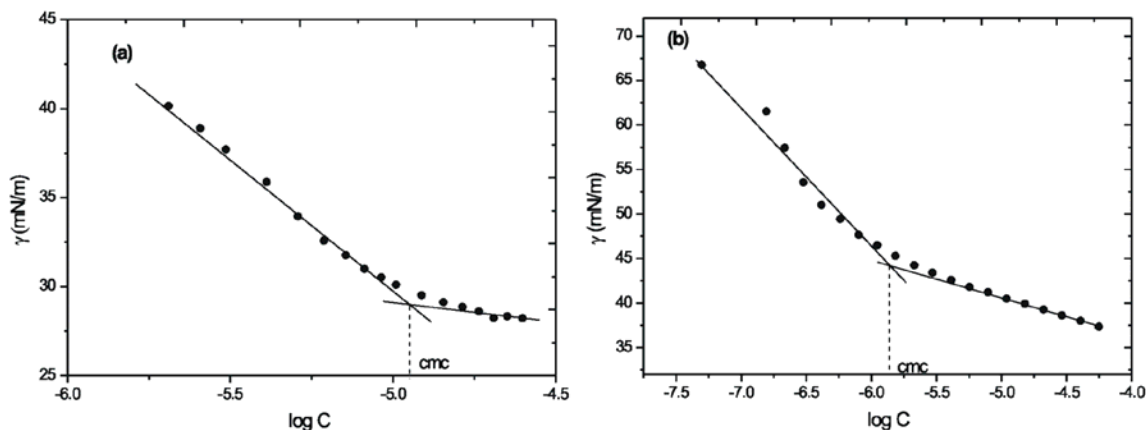


Figure 4.1 Critical micellization concentration (cmc) determination of (a) PB1 and (b) PB2 from surface tension measurements as a function of concentration at 25 °C.

The values obtained by this method at 25 °C for PB1 and PB2 are 9.5 and 2.5 μM , respectively. Unambiguously, the increase of hydrophobicity by shorten of the hydrophilic PGMA block is evidenced by lower values of the surface tension at any given bulk concentration when comparing PB1 with PB2. However, the relatively higher surface activity of PB1 compared to PB2 is not directly translated into a lower cmc value as would be expected from the literature.¹⁷ Moreover, the PB2 curve shows a slight continuous decrease in surface tension values even at concentrations larger than cmc. This significant difference in the surface tension behavior of the two block copolymers with increasing polymer concentration is probably a result of their different micellization mechanism as a function of concentration as discussed in section 4.3.4. Nevertheless, the inability of PB2 to attain constant γ after cmc is not unusual for triphilic systems containing PPO as the lipophilic component.¹⁵

4.3.2 DLS Studies

Concentration-Dependent Measurements. DLS studies of aqueous solutions of PGMA homopolymer revealed high affinity of the PGMA chains to cluster,¹⁶ similar to other hydroxyl group bearing polymers,^{18,19} via formation of intermolecular hydrogen bonds between the pendant hydroxyl groups. A similar phenomenon also occurs with the block copolymers under investigation. At 25 °C and concentrations below cmc, most of the block copolymer chains associate to form unimer-cluster in solution with $R_h \sim 67$ nm as can be seen in Figure 4.2a for PB2.

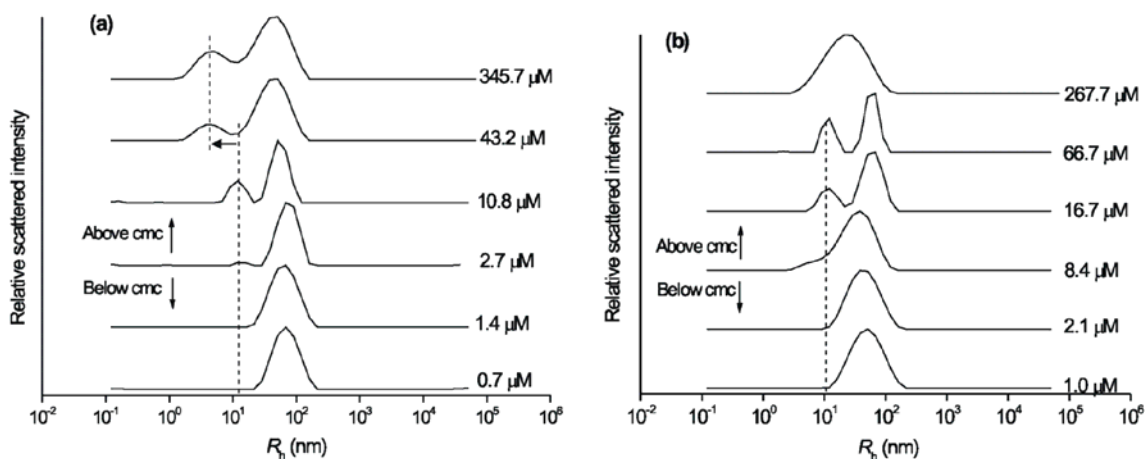


Figure 4.2 DLS data obtained at $\theta = 90^\circ$ for hydrodynamic radii (R_h) distributions as a function of concentration for aqueous solutions of (a) PB2 and (b) PB1 at 25°C .

On gradual increase of the concentration, some of the block copolymer chains are transferred from the unimer-clusters to form the regular micelles at concentrations around cmc as observed in Figure 4.2a. In order to confirm that the signals detected really originated from translational diffusion processes, an angular dependent measurement of the decay rates (Γ) between 30° and 130° shown in Figure 4.3 is performed for the $10.8\ \mu\text{M}$ PB2 aqueous solution.

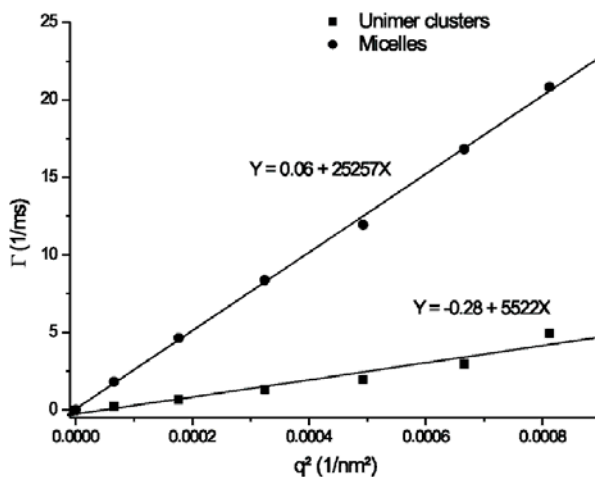


Figure 4.3 Relaxation rate (Γ) as a function of the square of the magnitude of the scattering vector (q^2) at 25°C for $10.8\ \mu\text{M}$ aqueous solutions of PB2.

The linear relationships obtained between Γ and the square of the scattering vector, q^2 , confirm that the observed peaks are due to diffusive processes. Further increase in the concentration of the PB2 solution above $10.8\ \mu\text{M}$ leads to an increase in the intensity of the

micelle peak until 43.2 μM , when the peak distribution suddenly shift as seen in Figure 4.2a. The new distribution generated at concentrations of 43.2 μM and above has two species with R_h of 5 and 40 nm. The specie with R_h of 5 nm corresponds to single chains of PB2, and the unusual existence, at least in this particular case, of “free” unimers in solution only at concentrations above cmc is a good proof of the association model of micellization. According to this model, micelles are in equilibrium with single chains above cmc.^{20,21} For comparison purpose, the R_h of the single chain can be estimated from the Einstein relation which relates the intrinsic viscosity to polymer volume fraction in solution according to the following expression:²²

$$R_h = \left(\frac{3M_n[\eta]}{10\pi N_A} \right)^{1/3} \quad (1)$$

Where M_n , $[\eta]$, and N_A are the molar mass of the polymer, intrinsic viscosity of polymer solution, and Avogadro’s number, respectively. The experimental value of $[\eta]$ for PB2 in water is not available. However, the PGMA block makes up 81 wt % of the block copolymer composition; hence, the $[\eta]$ value of 50 mL/g for PGMA in water at 25 °C can be used as a good approximation.²³ The estimated R_h from eq 1 gives 5 nm, which agrees well with the DLS determined unimer size at 25 °C. It is known that copolymers with BAB architecture upon micellization in a solvent which is selective of the middle block have a tendency to form “flowerlike” micelles and aggregates of micelles through bridging of the middle block at high concentrations.^{24,25} Analogously, the block copolymers under investigation can be viewed as having such architecture since the hydrophilic PGMA block is located between two hydrophobic entities (PPO and F₉) and therefore capable of forming such “flowerlike” micelles and aggregate of micelles. It is therefore reasonable to assume that the sudden change in the R_h distribution at concentrations of 43.2 μM and above and the peak distribution with $R_h \sim 40$ nm generated are most likely due to the formation of such aggregate of micelles. However, it cannot be excluded that this distribution also contains some unimer-cluster which cannot be distinguished from the aggregate of micelles.

Similar to the PB2 solution, PB1 solutions below cmc also contain mostly unimer-clusters with R_h of ~ 43 nm as shown in Figure 4.2b. At a concentration close to the cmc, the micelle peak appears as a shoulder on the unimer-cluster peak and continues to increase in intensity with concentration as seen Figure 4.2b. Increasing the polymer concentration to 268 μM and above, the unimer-cluster peak diminishes, and mostly micelles with R_h of 18.7 nm are found

in the solution as depicted in Figure 4.2b. In Figure 4.4, the normalized DLS intensity correlation functions, $g^{(1)}(\tau)$, at $\theta = 90^\circ$ and the corresponding relative amplitudes of the micelle and unimer-cluster peaks obtained from the exponential fitting of the correlation functions for the two species are shown for concentrations above cmc.

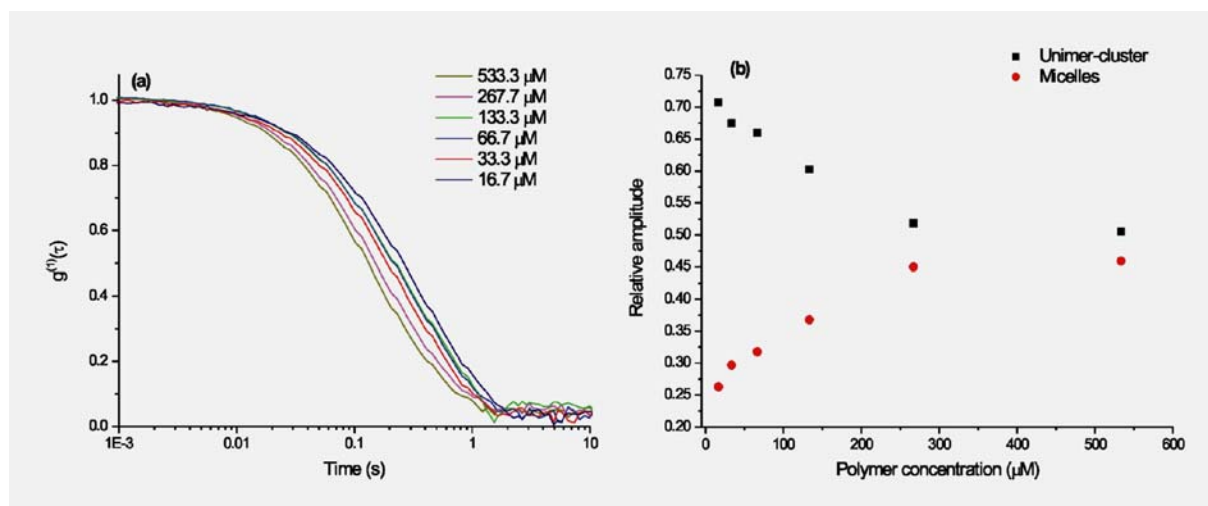


Figure 4.4 Normalized DLS intensity correlation functions $g^{(1)}(\tau)$ at $\theta = 90^\circ$ measured for different concentrations of PB1 aqueous solutions at 25 $^\circ\text{C}$ (a) and the corresponding relative amplitude of micelle and unimer-cluster peaks obtained from exponential fitting of the correlation functions for two decay modes (b).

From this figure, the relative amplitude of the micelle species steadily increases from about 0.25 at 16.7 μM to almost 0.5 at 533 μM . It should be emphasized here that, although the unimer-cluster and micelle peaks have comparable amplitudes at this highest concentration, the weight concentration of the unimer-cluster will be small. The ratio of the weight concentrations is given by the relative amplitudes divided by the relative molar masses M_u/M_m .²⁵ Using the R_h values of the unimer-cluster and micelle peaks, eq 1 can be applied for an approximate estimation of M_m/M_u , which is close to 1/72, and the relative weight concentrations C_u/C_m will thus be about 0.7×10^{-2} . This suggests that at 533 μM the unimer-clusters species in solution constitutes only ~ 0.7 wt % of the total polymer chains in solution and is of marginal interest. It is also worth mentioning that species with unimer dimensions are not observed in the DLS measurements of PB1 solutions under the given experimental conditions. This lack of unimer or molecular exchange between individual micelles is often referred to as nonergodicity.²⁷ Furthermore, it seems that the micelles of PB1 do not form aggregates of micelles at high solution concentrations which is contrary to micelles of PB2. Formation of such aggregates of micelles is most likely hindered in PB1 micelles because the

contour length of the PGMA block is short and therefore incapable of serving as a bridge between individual micelles as discussed below.

Temperature-Dependent Measurements. Systematic changes in the behavior of the aqueous solutions of the block copolymers with respect to temperature are also investigated in terms of R_h . Figure 4.5 shows the variation of R_h with temperature for aggregates formed by both block copolymers at a concentration of 5.6 g/L (533 μ M for PB1 and 346 μ M for PB2), which is above their cmc values at 25 °C.

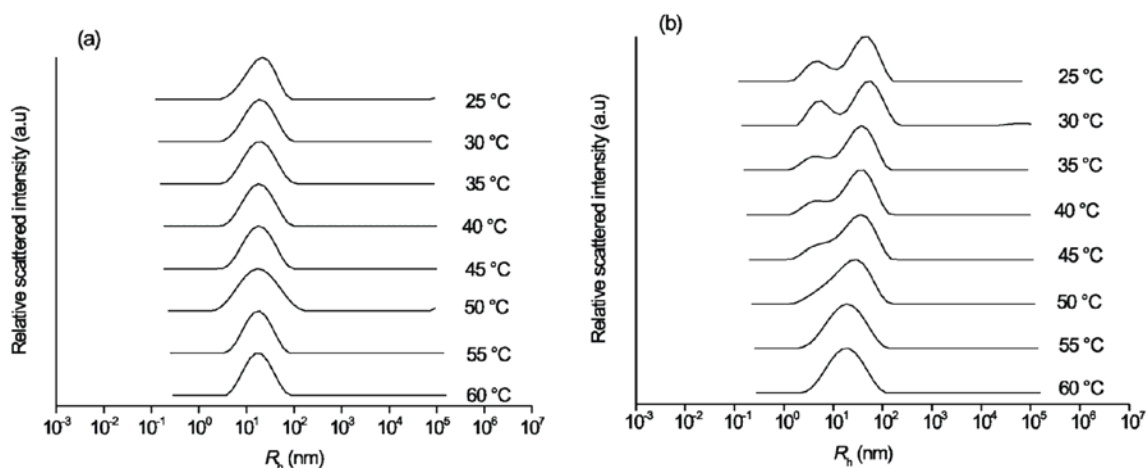


Figure 4.5 DLS data obtained at $\theta = 90^\circ$ for hydrodynamic radii (R_h) distributions as a function of temperature for (a) 533 and (b) 346 μ M aqueous solutions of PB1 and PB2, respectively.

At 25 °C, PB2 forms mainly aggregate of micelles and unimers in solution with R_h of 40 and 5 nm, respectively, as mentioned above. The R_h value of the aggregate of micelles steadily decreases until 40 °C and then drops to 22 nm at 45 °C. In addition, the single chain peak at 5 nm also starts to disappear at 45 °C as evidenced in Figure 4.5b. A further decrease in the R_h value of the aggregate of micelles to a typical micelle size of ~ 17 nm occurs above 50 °C as seen in Figure 4.5b. In summary, high temperature causes the aggregates of micelles to disintegrate into single micelles, and simultaneously all unimers are incorporated into the single micelles.

In contrast, at 25 °C PB1 forms only micelles in solution with R_h of 18.7 nm, which decrease only slightly to 17 nm at 60 °C as seen in Figure 4.5a. The slight decrease in the R_h value of the micelles on increasing temperature can be attributed to slight dehydration of the PPO blocks of the micelle.^{28,29} At any given temperature, the R_h values for the PB1 micelles are constant for scattering angle range of 30° - 130° , indicating the micelles are spherical in structure.

4.3.3 NMR Spectroscopy Studies

^{19}F NMR. Considering, the particular sequence of the block copolymers architecture, fluorophilic-hydrophilic-lipophilic-hydrophilic-fluorophilic, the hydrophilic blocks are expected to loop to shield the hydrophobic blocks (fluorophilic and lipophilic) from the aqueous environment when micelles are formed. To ascertain whether the F_9 segments are located within the core or corona of the micelle structures formed, ^{19}F NMR measurements were carried at 25 and 50 °C on 7 g/L aqueous solutions of the block copolymers. In Figure 4.6 the ^{19}F NMR spectra of PB1 solution with the corresponding resonance signals assignment is shown.

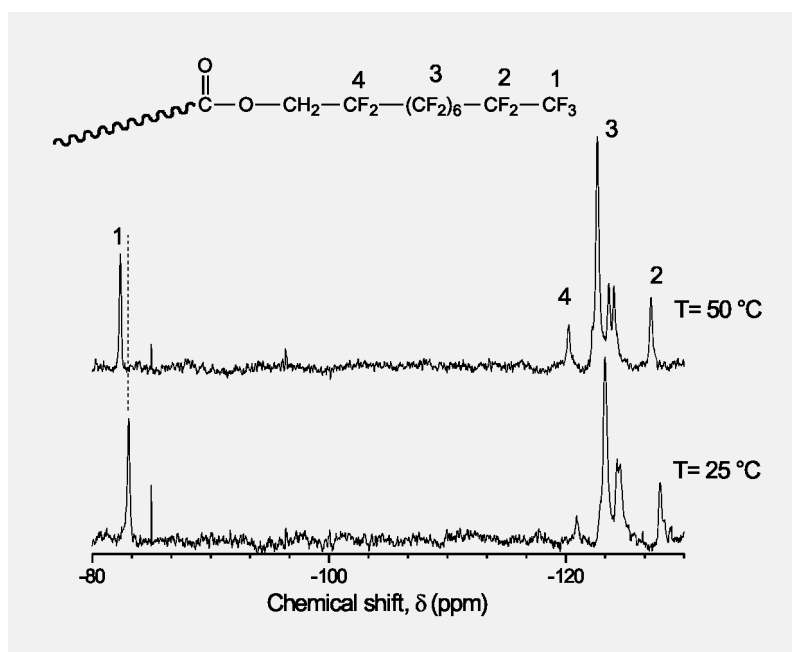


Figure 4.6 ^{19}F NMR spectra of 7 g/L PB1 in D_2O obtained at 200 MHz for 25 and 50 °C.

At 25 °C high-resolution ^{19}F resonance signals can be observed, an indication that the mobility of the fluorine moieties is not restricted. Thus, the F_9 segments do not contribute to the formation of the cores of the micelles. Increasing the temperature to 50 °C recorded a better signal resolution. Especially, the signal from the CF_2 unit (labeled 4 in Figure 4.6) closest to the hydrophilic block becomes very prominent. Additionally, the temperature increase caused an increase in the chemical shift of the resonance signals by ~ 0.7 ppm. In the literature, such increases in chemical shift and signal resolution have been attributed to increasing mobility of the fluorocarbon moieties.^{30,31} Thus, the increase in mobility may be

due to breaking of H-bonding between the coronal PGMA chains which consequently leads to increase in mobility the F₉ segments since they are located at the ends of the PGMA blocks.

PB2 on the contrary did not register any ¹⁹F signal when measurements are carried out under identical experimental conditions. Thus, suggesting that the perfluoro F₉ segments in this case are part of the micelle core.

¹H NMR. NMR spectroscopy is a powerful tool for investigating mobility of polymer chains in solution. Figure 4.7 shows the ¹H NMR spectra of the methyl protons of the PPO (PPO-CH₃) and the PGMA (PGMA-CH₃) blocks of PB1 and PB2 at 25 °C in DMSO-*d*₆, a nonselective solvent for both blocks as well as the fluorophilic segment. The peak at 0.76 ppm corresponds to the high content syndiotactic rr triads PGMA methyl protons (rr-PGMA-CH₃), while the peak at 0.93 ppm corresponds to the heterotactic rm triads (rm-PGMA-CH₃) of the same protons.³² Analysis of the syndiotactic sequence content gives 66%, which is similar to values obtained for poly(methyl methacrylate) (PMMA) prepared by radical polymerization.^{33,34}

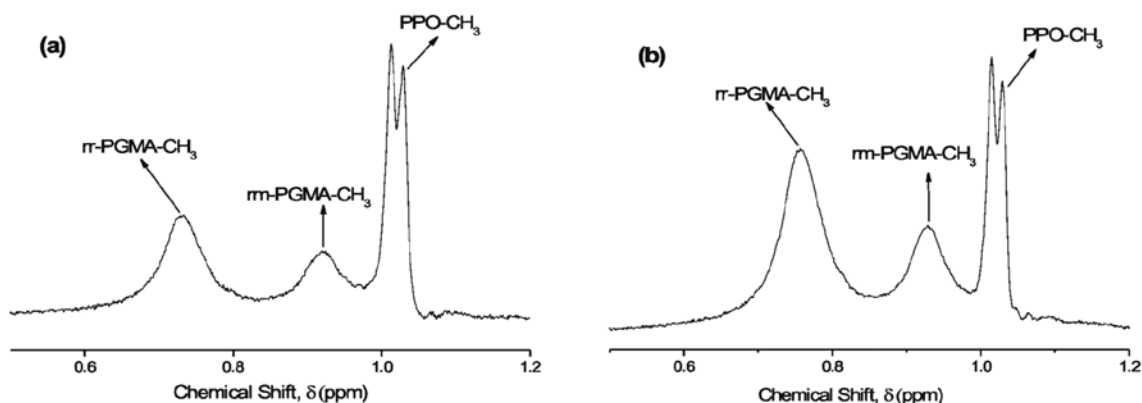


Figure 4.7 ¹H NMR spectra at 200 MHz of 7 g/L polymer in DMSO-*d*₆ at 25 °C (a) PB1 and (b) PB2.

The usual splitting of the PPO methyl protons peak at 1.02 ppm is due to *J* coupling of the methyl group to the methine group and can be noticed clearly in both spectra.²²

Figure 4.8 compares the systematic changes in the ¹H NMR spectra with temperature for the PPO-CH₃ and PGMA-CH₃ resonance signals of the two copolymers above cmc in D₂O.

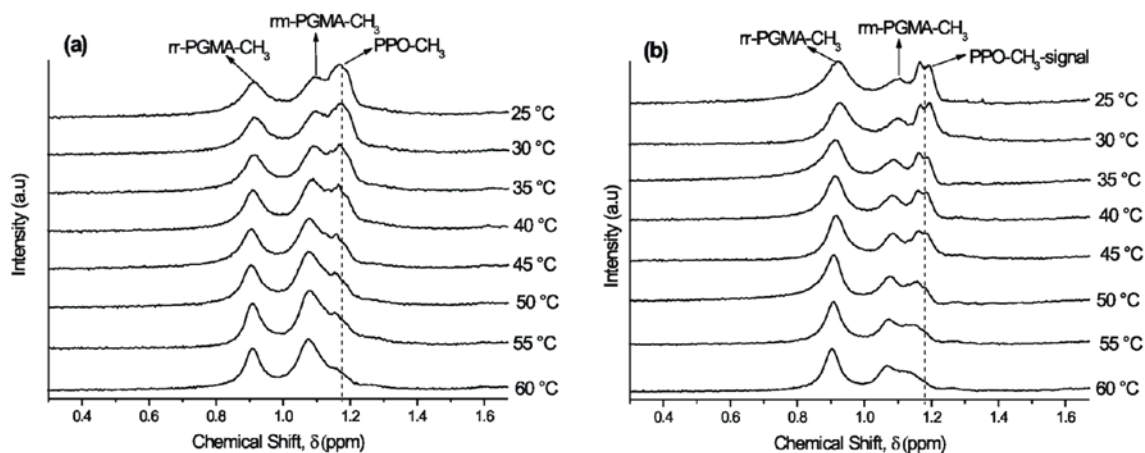


Figure 4.8 ^1H NMR spectra at 200 MHz of 7 g/L of: (a) PB1 and (b) PB2 in D_2O at different temperatures, showing the PGMA- CH_3 and PPO- CH_3 signals. The dashed line represents the position of the PPO methyl protons at 25 °C.

The temperature-dependent residual HDO resonance signal was corrected for each temperature in accordance with earlier studies by Gottlieb et al.³⁵ In Figure 4.8a it is clearly evident that the PPO- CH_3 resonance signal intensity of PB1 at 25 °C is highly attenuated relative to the PGMA- CH_3 signals when this spectrum is compared to the counterpart spectrum obtained in $\text{DMSO}-d_6$ at the same temperature (see Figure 4.7a). Also, the usual splitting of the PPO- CH_3 resonance signal has completely disappeared and the signal broadened as well. Attenuation, broadening and disappearance of the splitting of the PPO- CH_3 signal are due to the reduced mobility of the PPO block.^{22,24} These significant changes in the PPO- CH_3 resonance signal of PB1 indicate a change in the chemical environment of the methyl protons and signify that the majority of the PPO block is already in the relatively hydrophobic microenvironment of a micelle core.^{22,36} This agrees with the DLS results which revealed only single micelles in aqueous solution of PB1 of similar concentration at 25 °C.

Similarly, the PB2 spectrum in D_2O at 25 °C in Figure 4.8b when compared to the spectrum obtained in $\text{DMSO}-d_6$ (see Figure 4.7b) also shows attenuation and broadening of the PPO- CH_3 resonance signal relative to the PGMA- CH_3 signals. Although weak, the splitting of the PPO- CH_3 resonance signal can still be noticed. It can therefore be deduced that, at the given concentration and temperature micellization has already set in, but some block copolymer chains still have their PPO blocks in aqueous environment. The constitution of such polymer chains could originate from micelles which are in their transitional regime as proposed in the micellization mechanism discussed in the next section. With increasing

temperature, the PPO resonance signal intensity gradually decreases, and its splitting character completely disappears above 45 °C. This signifies incorporation of the PPO blocks of such chains into the microenvironment of a micelle core.

A clear observation in the ^1H NMR spectra of the block copolymers in D_2O is the shifting of the resonance signal of the PPO- CH_3 upfield with increasing temperature while the PGMA- CH_3 resonance signals remains at relatively the same position. The upfield shift is due to the change in magnetic susceptibility around the PPO- CH_3 protons, owing to the deshielding effect caused by removal of water molecules around the protons.³⁹ Thus, with increasing temperature the PPO block becomes increasingly dehydrated and hydrophobic.^{20,29,37} Almgren et al.³⁸ as well as Goldmints et al.²⁹ have established experimentally the existence of significant quantities of water within the PPO core of poloxamers micelles based on small-angle neutron scattering measurements (SANS). Since at 25 °C almost all the PPO block of PB1 exist in the micelle core and considering the fact that PPO of similar molar mass has an LCST at around 15 °C,³⁹ it implies some water will be trapped within the core. With increasing temperature, further de-shielding of the PPO protons and, consequently, upfield shifting occurs but because the core is liquidlike the signal response of the PPO- CH_3 protons will still be significant. Eventually, the PPO- CH_3 signal completely overlaps with the *rr*-PGMA- CH_3 signal, resulting in a broader intense single peak at 1.07 ppm at 60 °C (Figure 4.8a). It can be clearly seen from Figure 4.8b that this overlap effect is less pronounced in the ^1H NMR spectrum of PB2 at 60 °C. This is because the presence of the highly hydrophobic F_9 segments within the micelle cores of PB2 creates a well-dehydrated solidlike environment within the core. Hence, the signal response of the PPO- CH_3 protons in this case is relatively weak. Likewise, at 60 °C there is an overlap of the PPO- CH_3 and the *rr*-PGMA- CH_3 signals, but the cumulative effect is very weak compared to PB1. In fact, this simple analyses of the temperature-dependent ^1H NMR spectra of the two block copolymers conveniently upholds the existence of significant amount of water within micelle cores composed of only PPO as has been proven by SANS measurements.^{29,38,40,41} Similar ^1H NMR spectra observations regarding partially hydrated PPO cores of PPO-PGMA micelles in aqueous solution at high temperatures have been reported by Save et al.³⁹

Careful examination of the *rr*-PGMA- CH_3 resonance peaks at ~0.91 ppm (25 °C) in Figure 4.8 shows a gradual narrowing of the resonance signals width with increasing temperature for both block copolymers. This suggests that the mobility in the PGMA corona chains increases with temperature for PB1 and PB2 micelles. In ^1H NMR spectroscopy

measurements, the degree of mobility of a polymer chain in solution is usually assessed by the half-height width, $\Delta\nu_{1/2}$ (the line width at half-height of the highest signal point). Figure 4.9 shows variation of $\Delta\nu_{1/2}$ in hertz as a function of temperature for the rr-PGMA-CH₃ signals of both block copolymers.

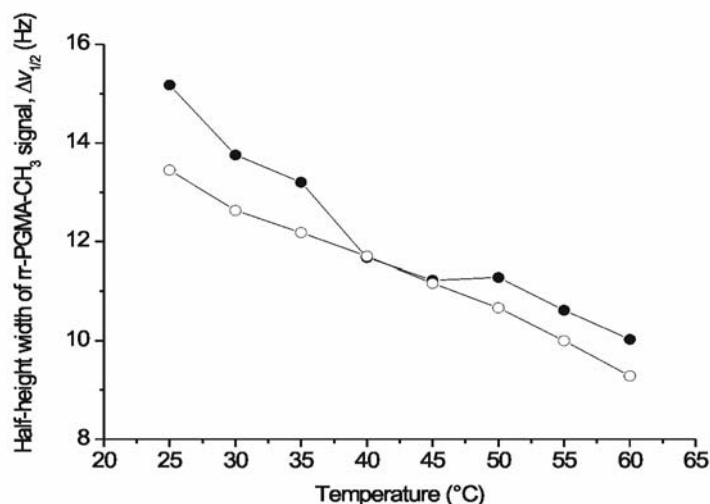


Figure 4.9 Variation of half-height width of the rr-PGMA-CH₃ resonance signal as a function of temperature for 7 g/L D₂O solutions of PB1 (○) and PB2 (●).

Generally, $\Delta\nu_{1/2}$ decreases linearly with temperature for PB1 solution, which implies the mobility of the PGMA coronal chains increases with temperature as a result of H-bonding breaking between the OH groups of the PGMA blocks. This is in agreement with the earlier results of the ¹⁹F NMR spectroscopy measurements of the PB1 solution shown in Figure 4.6. On the other hand, PB2 shows significantly larger $\Delta\nu_{1/2}$ than PB1 at 25 °C which decreases rapidly until 40 °C and exhibits a transition between 40 and 50 °C. This indicates that mobility of the PGMA corona chains of PB2 micelles are more restricted than that of PB1 micelles. The higher restriction in mobility of the PGMA blocks in PB2 micelles can be ascribed, in addition to the general H-bonding effect, to the formation of micelle aggregates as observed in the DLS studies. Thus, the closeness of the coronal chains of the component micelles within the aggregate causes further mobility restriction. At 60 °C, when only single micelles exist in solution for both block copolymers as observed by DLS, $\Delta\nu_{1/2}$ for PB1 and PB2 micelles are 9.3 and 10 Hz, respectively. This is an indication that the mobility of the PGMA corona blocks are still more restricted in PB2 micelles than PB1 counterpart, presumably, due to the looping effect of the PB2 PGMA blocks as they do so to sequester the F₉ segments (see ¹⁹F NMR discussion).

4.3.4 Aggregation Mechanism and Loop Formation

Information gathered from DLS and NMR (^1H and ^{19}F) spectroscopy at 25 °C indicates that PB2 in aqueous solution above cmc forms micelles and aggregates of micelles with the PPO block and the F_9 segments forming the cores of the micelles. On the basis of this information the following aggregation mechanism is proposed. At concentrations above cmc but less than $\sim 43 \mu\text{M}$, unimers are increasingly transferred from the unimer-cluster to form micelles with increasing concentration. Formation of the micelles proceeds by first looping of the PGMA blocks to form an aggregated fluorocarbon inner core followed by collapsing of the PPO blocks around the fluorocarbon core to form an outer core. This results in a “flowerlike” micelle structure as illustrated in Figure 4.10a.

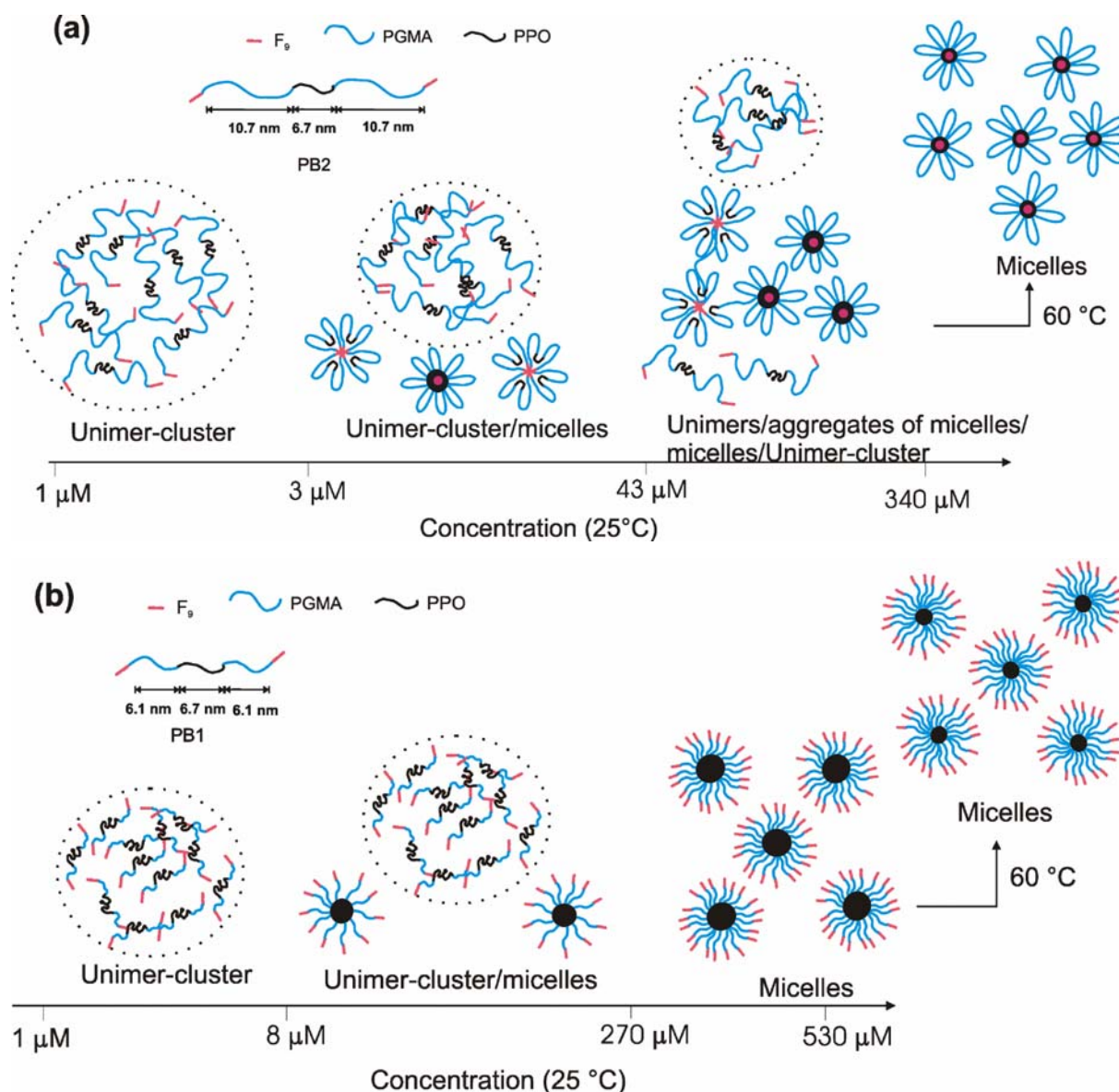


Figure 4.10 schematic representations of micelle structures obtained as a result of increasing polymer concentration and temperature of aqueous solutions of (a) PB2 and (b) PB1. The length scales shown below the single chains denote the contour lengths of the respective blocks. In PB1, the short length of the PGMA blocks prevent it from looping, therefore the F_9 segments cannot be sequestered from the aqueous environment.

Above $\sim 43 \mu\text{M}$, connectivity through the PGMA chains takes place between the micelles. As schematized in Figure 4.10a, it can be assumed that although micellization is initiated by the F_9 segments, the PPO blocks must completely collapse onto the fluorocarbon core to give the complete inner core-outer core-corona micelle. Further dehydration of the PPO blocks is therefore required to render them hydrophobic enough to collapse onto the highly hydrophobic F_9 core. This further dehydration can be achieved by increasing temperature

which leads to obvious dehydration of the PPO block or increase in polymer concentration which leaves less water molecules available for the PPO block hydration. Consequently, it leads to the creation of a solidlike core environment which results in the weak signal response of the PPO block at high temperature as realized in the ^1H NMR spectra studies. Thus, micelle structures with the PPO blocks not adequately dehydrated to collapsed onto the F_9 core (transitional regime) will still have some mobility in their PPO blocks as observed in the ^1H NMR spectra of PB2 solutions at temperatures below 45 °C. It is reasonable to conclude that at high temperature the dehydration and simultaneously contraction of the PPO blocks results in stretching of the interconnecting PGMA chains of the micelle aggregates. However, because the block length of the PGMA chains is not too long, it becomes entropically unfavorable for the interconnectivity to be maintained at high temperature. Eventually, the F_9 segment is expelled, and the PGMA block loops back to incorporate the F_9 segment into the micelle core where the PGMA block is chemically attached. The whole process will lead to the generation of basically only single compact “flowerlike” micelles of PB2 in solution at high temperature, as depicted in Figure 4.10a.

On the other hand, DLS and NMR (^1H and ^{19}F) spectroscopy information obtained leads to the conclusion that, above cmc at 25 °C, PB1 in aqueous solution forms spherical micelles with a core composed of mainly PPO. The PGMA block and the F_9 segments are exposed to the aqueous medium serving as the coronae which stabilize the core. Similar to PB2, unimers of PB1 are increasingly transferred from the unimer-cluster to form micelles with increasing concentration. During the micellization process, the PPO blocks of the copolymer chains simply assemble to form the core of the micelle as schematized in Figure 4.10b. Thus, the PGMA blocks of PB1 are unable to loop to sequester the F_9 segments into the core.

In studying CAB triblock copolymer analogue of the structure, α -fluorocarbon- ω -hydrocarbon end-capped poly(*N*-acylethylenimine), with degree of polymerization, *N*, for the hydrophilic poly(*N*-acylethylenimine) block being 25, Weberkirch and co-workers⁴ realized by ^{19}F NMR spectroscopy measurements in aqueous solution that the micelle formed by this block copolymer is composed of a hydrocarbon core and fluorocarbon end-capped poly(*N*-acylethylenimine) corona. However, with increasing degree of polymerization of the hydrophilic block, specifically *N* = 35, 57, and 75, they found that the micelle structure formed in this case is composed of a core containing both the hydro- and fluorocarbon segments.⁵ Thus, short hydrophilic block length prevents looping and that accounts for the absence of the fluorocarbon block in the micelle core. A Similar effect of the middle block

length on loop formation of BAC triblock copolymer upon micellization has also been observed by other authors.⁴²

There are two opposing thermodynamic parameters that determine loop formation: increase of free energy due to looping of the hydrophilic middle block, ΔG_{bend} , and the free energy decrease as a result of the hydrophobic effect (aggregation of hydrophobic segments from the solvent to the micelle core), ΔG_{phobic} . If the magnitude of the former is less than the latter, the loop formed will be stable.⁴³ In this respect, these parameters are assessed in terms of the transfer of the outer F_9 segment into the micelle cores for the copolymers under investigations. For simplicity, if the enthalpy of mixing between PGMA and water and the repulsive interactions between the F_9 and PPO blocks are ignored, then the free energy of loop formation of the PGMA block can be estimated from⁴³

$$\Delta G_{\text{loop}} = \Delta G_{\text{bend}} + \Delta G_{\text{phobic}} \quad (2)$$

On the basis of the end-to-end distribution probability for a Gaussian chain, Alami et al.²⁶ derived

$$\Delta G_{\text{bend}} = -2.6RT + 1.5RT \ln N \quad (3)$$

Furthermore, the free energy gain for transfer of a CH_2 group from water into a micelle core is about $-0.4RT$ per CH_2 group.²⁶ Since $1\text{CF}_2 \approx 1.7\text{CH}_2$ ⁴⁷ and there are 4 CH_2 groups linking the F_9 segment to the PGMA block, ΔG_{phobic} for the F_9 segment is therefore estimated as $-7.7RT$. The triazole ring between the PGMA and the F_9 segments is neglected in the estimation because a recent study has proven its hydrophilic contribution as a linker.⁴⁸ Substitutions into eqs yield ΔG_{loop} values of -5.5 and $-4.7RT$ for PB1 and PB2, respectively. These results derived from the Gaussian statistical model predict that it is thermodynamically feasible for the hydrophilic blocks of both copolymers to loop upon micellization and even more feasible for PB1 to loop than PB2. Based on the model, the results are perfectly reasonable because smaller N of the PGMA block of PB1 implies a smaller end-to-end distance, r ($r \sim N^{1/2}$), hence, higher probability of the two ends of the PGMA block finding each other.^{44,45,46} However, for polymers with low N , as investigated here, the chains are short and therefore semiflexible. The loop formation dynamics of such polymer chains is mainly dominated by needs to overcome the bending energy cost.⁴⁹ It then becomes important to take the intrinsic stiffness of the chain into account. The Kuhn length, b , which also closely corresponds to the persistence length, l_p ($b = 2l_p$), characterizes the stiffness of a given polymer chain.⁵⁰ Stiffer

chains have larger values of b and vice versa. Jun et al.⁵¹ in their analytical results regarding the dynamics of loop formation for a polymer chain with two reactive ends, taking into account intrinsic chain stiffness, concluded that the time required for loop formation, τ_c (closing time), approaches infinity when the length of the polymer chain, $L < 3-4l_p$. Monte Carlo simulation by Chen et al.⁵² led to $L < 2.9l_p$, and recent simulation by Toan et al.⁵³ gave $4l_p$. These results seem to agree and imply that when $L < 3-4l_p$ the bending energy cost is too high for the polymer chain to loop and thus never forms a loop which leads to $\tau_c \rightarrow \infty$.

In this context one can compute the Kuhn length, $b = lC_\infty$, of the hydrophilic PGMA block using $l = 2.54 \text{ \AA}$ as the length of the monomeric unit and, the characteristic ratio, $C_\infty \sim 12$, typical for poly(ethylene glycol methacrylate) in polar solvents is adopted because of its structural similarity to PGMA.^{43,54} This gives a value of 3 nm for b and subsequently 1.5 nm as l_p of the PGMA block. Furthermore, computing the contour length, $L = Nl$, of the PGMA blocks give 10.7 and 6.1 nm for PB2 and PB1, respectively, which in turn gives $7l_p$ and $4l_p$, respectively. This means PB1 with its L within the regime where bending energy cost becomes very significant will find it difficult to loop to sequester the F_9 segment into the core. Thus, the analytical and simulation results of literature data discussed above support the micellization behavior of the block copolymers under investigation.

4.3.5 AFM and TEM Investigations on Polymer Aggregates

The structures formed by coating aqueous solutions of the block copolymers on solid supports are also investigated by TEM and AFM. Figure 4.11a shows the TEM image obtained by coating 0.014 g/L (0.86 μM) aqueous polymer solution of PB2 on a carbon-coated copper grid and evaporation of the water at room temperature.

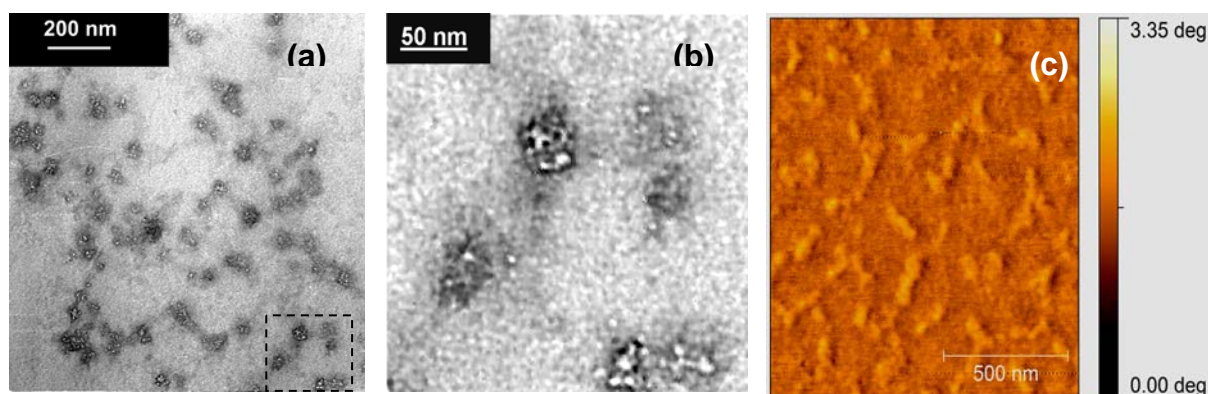


Figure 4.11 (a) TEM image of PB2 obtained after coating a carbon copper grid with 0.014 g/L aqueous polymer solution and evaporation of water at room temperature (b) High-magnification image of the area indicated in (a), (c) Phase image of PB2 obtained after coating a silicon substrate with 1.4 g/L aqueous polymer solution for 2 min, followed by washing with bidistilled water and evaporation at room temperature.

Although, the concentration of the solution used is slightly below cmc, it should be realized that as water slowly evaporates from the surface the cmc threshold will be passed and micelles or well-defined aggregates will be formed during this process. This preparative method was adopted because initial attempts using solution with concentration much higher than cmc resulted in TEM images showing only polymer films. The image shows clustering of spherelike aggregates of micelle cores with a diameter size ranging from 20 to 80 nm. AFM phase image of PB2, shown in Figure 4.11c, reveal structures with morphology similar to that observed in the TEM image. Figure 4.11b provides a magnified image of the square marked in Figure 4.11a. One of such a well-defined aggregate with a diameter of about 50 nm is shown in the upper part of this image. This aggregate shows segregated dark domains of an average diameter of 5.4 nm. Aggregated fluorocarbons domains are known to create a dark contrast in TEM images because of their high electron density.^{55,56} The dark domains in Figure 4.11b can therefore be attributed to the aggregated F₉ segments forming an inner core, and the white surrounding outer core matrix is obviously caused by the PPO. By careful inspection of the aggregate, one can notice the non-continuity in the white PPO outer cores as a result of the barriers created by the gray PGMA contrast. This suggests that the aggregate, indeed, consists of individual micelles which are composed of distinct F₉ inner core, PPO outer core and PGMA corona as depicted schematically in Figure 4.10a. Obviously, the segregation is the result of the immiscibility between the perfluoro segments and the PPO blocks.^{57,58} It results in the formation of a compartmentalized core.³ The gray contrast

emanating from the hydrophilic PGMA blocks can be noticed on the surface and the peripherals of the aggregates.

Contrary to PB2, the TEM image of PB1 in Figure 4.12a shows large spherical gray aggregates of a diameter between 80 and 400 nm with isolated dark spots. The sample was prepared under conditions identical to PB2.

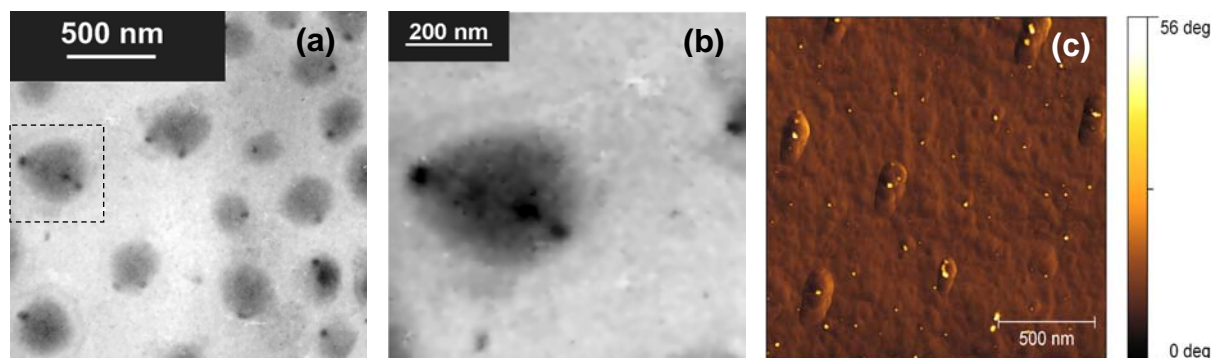


Figure 4.12 (a) TEM image of PB1 obtained after coating a carbon coated copper grid with 0.014 g/L aqueous polymer solution and evaporation of water at room temperature, (b) the high-magnification image of the aggregate marked with a square in (a) and (c) AFM phase image of the same sample used in (a).

A close look at one of the aggregates marked with a square in Figure 4.12a and enlarged in Figure 4.12b shows that the diameter of the dark spots is $\sim 35\text{--}40$ nm. As indicated above, the dark spots in the TEM image can be attributed to aggregated perfluoro F_9 segments of PB1. An AFM phase imaging carried out on the polymer-coated grid used for the TEM is shown in Figure 10c. Although within this scan area the aggregates are embedded in a polymer film with an irregular shape, the isolated spots can still be noticed as white spots on the aggregates. It is known that phase contrast in AFM imaging is due to differences in viscoelastic properties of the material.⁵⁹ Thus, the hard aggregated perfluoro domains of PB1 appear as the white spots in the AFM phase image. At the moment, the exact mechanism behind formation of such large aggregates is not clear. However, it seems that the initially formed PB1 micelles in an attempt to reduce the interfacial energy between their fluorophilic surfaces and the hydrophobic support cluster to form such aggregates. The nonergodic character of PB1 micelles in solution as observed in the DLS studies may also contribute as well since such behavior is known to lead also to the formation of large compound micelles.^{26,59}

4.3.6 TFB Uptake-Capabilities of Block Copolymer Micelles

Preliminary experiments showed that micelles of PB1, PB2 as well as the amphiphilic diblock copolymer, PPO₂₇-PGMA₄₄ are all capable of solubilizing substantial amount of the perfluorocarbon-based benzene molecule, TFB, as shown in Figure 4.13. A simple qualitative test at 25 °C showed that the PPO homopolymer is soluble in TFB, hence, the ability of these PPO core bearing micelles to solubilize significant amount of the hydrophobic TFB in aqueous solution. Interestingly, PB2 micelles showed the highest solubilization capacity which is approximately four times higher than that of PB1 or PPO₂₇-PGMA₄₄ micelles. This indicates that the presence of the perfluoro F₉ segments within the micelle core of PB2 enhances its solubilization capability. Moreover, the fact that PB1 micelles show solubilization capabilities comparable to that of the PPO₂₇-PGMA₄₄ micelles further confirms that the perfluoro F₉ segments do not form part of the PB1 micelle core.

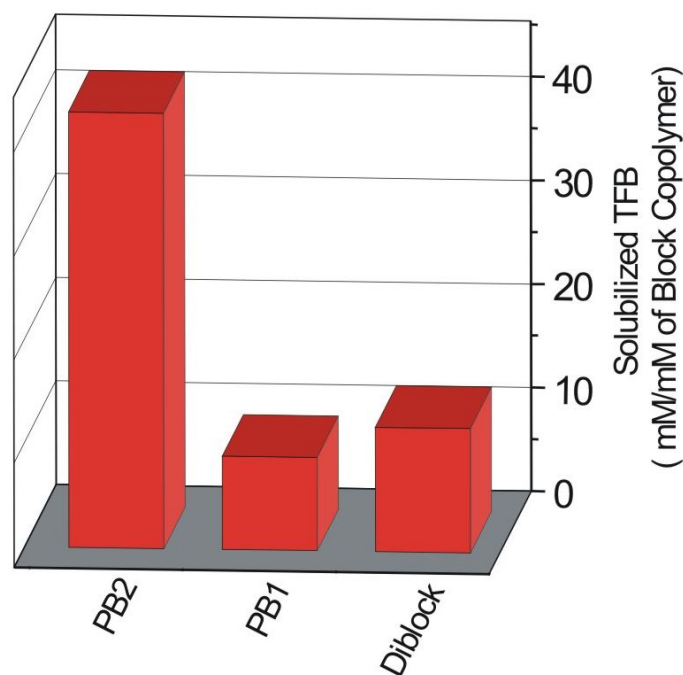


Figure 4.13 Solubilization of tetrafluorobenzene (TFB) at 25 °C by 5 mg/mL D₂O solutions of the triphilic block copolymers PB2 and PB1, and the amphiphilic block copolymer, PPO₂₇-PGMA₄₄ (Diblock).

4.4 Conclusions

The aggregation behavior of the two synthesized CABAC pentablock copolymer analogues, F₉-PGMA₂₄-PPO₂₇-PGMA₂₄-F₉ (PB1) and F₉-PGMA₄₂-PPO₂₇-PGMA₄₂-F₉ (PB2), in water have been compared. The two block copolymers differ only in the degree of polymerization of the hydrophilic PGMA blocks. In aqueous solution, above cmc, PB2 formed micelles and aggregates of micelles which disintegrated into single micelles at high temperature. For the PB2 micelles, the PGMA blocks formed the corona while the PPO block and the F₉ segments formed the core. The immiscibility between the F₉ segments and the PPO blocks within the core resulted in a compartmentalized core where they formed the inner and the outer cores, respectively.

In contrast, single spherical micelles with PPO core and F₉ terminated PGMA coronal chains were formed by PB1 in aqueous solution above cmc. Evidence of the perfluoro F₉ segments forming part of the coronal chains was obtained from ¹⁹F NMR spectroscopy. The effect of the presence or the absence of the F₉ segments within the micelle cores of the two block copolymers was reflected in the temperature-dependent ¹H NMR behavior of their PPO blocks.

The lack of the F₉ segments within the core of PB1 micelles is due to the inability of their short rigid PGMA blocks to loop. This observation is in agreement with theoretical prediction of loop formation by semiflexible polymer chain and accounts for the strong difference in aggregation behavior of these two structurally similar block copolymers. AFM and TEM investigations of the structures formed on solid supports after solvent evaporation also confirmed the aggregation behavior of the two block copolymers. Due to the compartmentalized core of PB2 micelles, they showed about 4 fold enhanced tetrafluorobenzene uptake-capability compared PB1 micelles owing to the absence of the fluorophilic F₉ segments within the micelle core of the latter.

4.5 References

- (1) Li Z.; Hillmyer M.A.; Lodge T. P. *Langmuir* **2006**, *22*, 9409.
- (2) Zhou Z.; Li Z.; Ren Y.; Hillmyer M. A.; Lodge T.P. *J. Am. Chem. Soc.* **2003**, *125*, 10182.
- (3) Thünemann A.F.; Kubowicz S.; Berlepsch H.v.; Möhwald H. *Langmuir* **2006**, *22*, 2506.
- (4) Weberkirch R.; Preuschen J.; Spiess H.W.; Nuyken O. *Macromol. Chem. Phys.* **2000**, *201*, 995.
- (5) Kubowicz S.; Thünemann A. F.; Weberskirch R.; Möhwald H. *Langmuir* **2005**, *21*, 7214.
- (6) Mao J.; Ni P.; Mai Y.; Yan D. *Langmuir* **2007**, *23*, 5127.
- (7) Lodge T. P.; Hillmyer M. A.; Zhou Z. *Macromolecules* **2004**, *37*, 6680.
- (8) (a) Zhao Y.; Liu Y.-T.; Lu Z.-Y.; Sun C.-C. *Polymer* **2008**, *49*, 4899.
(b) Zhang H.; Ni P.; He J.; Liu C. *Langmuir* **2008**, *24*, 4647.
- (9) Lodge T. P.; Rasdal A.; Li Z.; Hillmyer M. A. *J. Am. Chem. Soc.* **2005**, *127*, 17608.
- (10) Ott C.; Hoogenboom R.; Hoepfener S.; Wouters D.; Gohy J.-F.; Schubert U.S. *Soft Matter*, **2009**, *5*, 84.
- (11) Kubowicz S.; Baussard J.-F.; Lutz J.-F.; Thünemann A. F.; Berlesch H.; Laschewsky A. *Angew. Chem. Int. Ed.* **2005**, *44*, 5262.
- (12) Skrabania K.; Laschewsky A.; Berlepsch H.v.; Böttcher C. *Langmuir* **2009**, *25*, 7594.
- (13) Berlepsch H.v.; Böttcher C.; Skrabania K.; Laschewsky A. *Chem. Comm.* **2009**, 2290.
- (14) Kyeremateng S. O.; Amado E.; Blume A.; Kressler J. *Macromol. Rapid Commun.* **2008**, *29*, 1140.
- (15) He J.; Ni P.; Liu C. *J. Polym. Sci., Part A: Polym. Chem.* **2008**, *46*, 3029.
- (16) (a) Kyeremateng S.O.; Amado E.; Kressler J. *Euro. Polym. J.* **2007**, *43*, 3380.
(b) Amado E.; Augsten C.; Mäder K.; Blume A.; Kressler J. *Macromolecules* **2006**, *39*, 9486.
- (17) (a) Alexandridis P.; Athanassiou V.; Fukuda S.; Hatton T.A. *Langmuir* **1994**, *10*, 2604.
(b) Alexandridis P.; Holzwarth J. F.; Hatton T. A. *Macromolecules* **1994**, *27*, 2414.
(c) Wanka G.; Hoffmann H.; Ulbricht W. *Macromolecules* **1994**, *27*, 4145.
- (18) Fang L.; Brown W. *Macromolecules* **1990**, *23*, 3284.

- (19) Madsen J.; Armes S. P. *Biomacromolecules* **2009**, *10*, 1875.
- (20) Hvidt S.; Trandum C.; Batsberg W. *J. Colloid Interface Sci.* **2002**, *250*, 243.
- (21) Zhu Z.; Xu J.; Zhou Y.; Jiang X.; Armes S. P.; Liu S. *Macromolecules* **2007**, *40*, 6393.
- (22) Cau F.; Lacelle S. *Macromolecules* **1996**, *29*, 170.
- (23) Pezron E.; Leibler L.; Ricard A.; Lafuma F.; Audebert R. *Macromolecules* **1989**, *22*, 1169.
- (24) Riess G. *Prog. Polym. Sci.*, **2003**, *28*, 1107.
- (25) Balsara N.P.; Tirrell M.; Lodge T.P. *Macromolecules* **1991**, *24*, 1975.
- (26) Alami E.; Almgren M.; Brown W. *Macromolecules* **1996**, *29*, 2229.
- (27) Won Y.-Y.; Bates F. S. *In Giant Micelles, Properties and Applications*, Zana R., Kaler E.W., Eds.; CRC Press: Boca Raton Florida, 2007; p 418.
- (28) Kositzka M. J.; Bohne, C.; Alexandridis, P.; Hatton, T. A.; Holzwarth, J. F. *Macromolecules* **1999**, *32*, 5539.
- (29) Goldmints I.; Yu G.-E.; Booth C.; Smith K. A.; Hatton T. A. *Langmuir* **1999**, *15*, 1651.
- (30) Preuschen J.; Menchen S.; Winnik M.A.; Heuer A.; Spiess H.W. *Macromolecules* **1999**, *32*, 2690.
- (31) Zhang H.; Pan J.; Hogen-Esch T.E. *Macromolecules* **1998**, *31*, 2815.
- (32) Carriere P.; Grohens Y.; Spevacek J.; Schultz J. *Langmuir* **2000**, *16*, 5051.
- (33) Chen G.; Zhu X.; Cheng Z.; Lu J.; Chen J. *Polym Int.* **2004**, *53*, 357.
- (34) Wang J-S.; Matyjaszewski K. *Macromolecules* **1995**, *28*, 7901.
- (35) Gottlieb H.E.; Kotlyar V.; Nudelman A. *J. Org. Chem.* **1997**, *62*, 7512.
- (36) Ma J-H.; Guo C.; Tang Y-L.; Liu H-Z. *Langmuir* **2007**, *23*, 9596.
- (37) Guo C.; Liu H.Z.; Chen J.Y. *Colloid Polym. Sci.* **1999**, *277*, 376.
- (38) Almgren M.; Brown W.; Hvidt S. *Colloid Polym. Sci.* **1995**, *273*, 2.
- (39) Save M; Weaver J. V. M.; Armes S. P.; McKenna P. *Macromolecules* **2002**, *35*, 1152.
- (40) Yang L.; Alexandridis P.; Steyler D.C.; Kositzka M.J.; Holzwarth J.F. *Langmuir* **2000**, *16*, 8555.
- (41) Pedersen J. S.; Gerstenberg M. C. *Colloids Surf., A* **2003**, *213*, 175.
- (42) Cai Y.; Armes S. P. *Macromolecules* **2004**, *37*, 7116.
- (43) Maiti S.; Chatterji P.R. *J. Phys. Chem. B* **2000**, *104*, 10253.
- (44) Sperling L. H. *Introduction to Physical Polymer Science*, 3rd Ed.; John Wiley & Sons: New York 2001.
- (45) Brinke G.; Hadziioannou G. *Macromolecules* **1987**, *20*, 486.
- (46) Raspaud E.; Lairez D.; Adam M.; Carton J.-P. *Macromolecules* **1994**, *27*, 2956.

- (47) Hussain H.; Busse K.; Kressler J. *Macromol. Chem. Phys.* **2003**, *204*, 936.
- (48) Reuter S.; Busse K.; Radics U.; Niclas H.-J.; Kressler J. *J. Colloid Interface Sci.* **2009**, *340*, 276.
- (49) Santo K.P.; Sebastian K.L. *Phys. Rev. E: Stat., Nonlinear, Soft Matter Phys.* **2006**, *73*, 0319231.
- (50) Strobl G. *The Physics of Polymers*, 2nd Ed.; Springer-Verlag: Berlin Heidelberg 1996.
- (51) Jun S.; Bechhoefer J.; Ha B.-Y. *Europhys. Lett.* **2003**, *64*, 420.
- (52) Chen J. Z. Y.; Tsao H.-K.; Sheng Y.-J. *Europhys. Lett.* **2004**, *65*, 407.
- (53) Toan N. M.; Morrison G.; Hyeon C.; Thirumalai D. *J. Phys. Chem. B* **2008**, *112*, 6094.
- (54) Bohdanecky, M.; Tuzar, Z. *Collect. Czech. Chem. Commun.* **1969**, *34*, 3318.
- (55) Kubowicz S.; Baussard J.-F.; Lutz J.-F.; Thünemann A. F.; Berlesch H.; Laschewsky A. *Angew. Chem. Int. Ed.* **2005**, *44*, 5262.
- (56) Busse K.; Kressler J.; Eck D.; Höring S. *Macromolecules* **2002**, *35*, 178.
- (57) Zhou Z.; Li Z.; Ren Y.; Hillmyer M. A.; Lodge T. P. *J. Am. Chem. Soc.* **2003**, *125*, 10182.
- (58) Li. Z.; Kesselman E.; Talmon Y.; Hillmyer M. A.; Lodge T. P. *Science* **2004**, *306*, 98.
- (59) Njikang G.; Han D.; Wang J.; Liu W. *Macromolecules* **2008**, *41*, 9727.

Chapter 5

Aggregation Behavior of Triphilic CAB Triblock Copolymer Analogues in Water: Comparison with Triphilic CBA and Amphiphilic BA Counterparts

5.1 Introduction

In the last chapter it was observed that when the hydrophilic PGMA block length-A block is long enough, the CABAC pentablock copolymer analogue forms micelles with compartmentalized core. The compartmentalization of the micelle core is the result of the immiscibility or incompatibility between the fluorophilic perfluoroalkyl segment, C, and the lipophilic PPO block, B.^{1,2,3,4} Infact, it was established that for both entities to fully co-exist in the micelle core, the PPO blocks must be rendered highly hydrophobic through dehydration at temperatures well above its lower critical solution temperature (LCST).

This chapter investigates the difference in the aqueous solution behavior of the triphilic CAB triblock copolymer analogues compared to the triphilic CBA counterpart and the amphiphilic BA diblock copolymer. Due to the linking sequence of the hydrophobic components (C and B), it is obvious that for the CBA architecture both the fluorophilic and lipophilic components should form the core structure when aggregation occurs because they are covalently linked to each other.⁵ However, in the case of the CAB architecture where the hydrophilic A block is sandwiched between the fluorophilic and lipophilic components, two possibilities exist during aggregation as illustrated in Figure 5.1. One involves the looping of the hydrophilic middle block to incorporate both the fluorophilic and lipophilic components into the same core, thus, forming a compartmentalized flowerlike micelle.^{6,7,8,9} The other involves the adaptation of a two-compartment network with spatially distinct fluorophilic and lipophilic core domains as illustrated in Figure 5.1.¹⁰

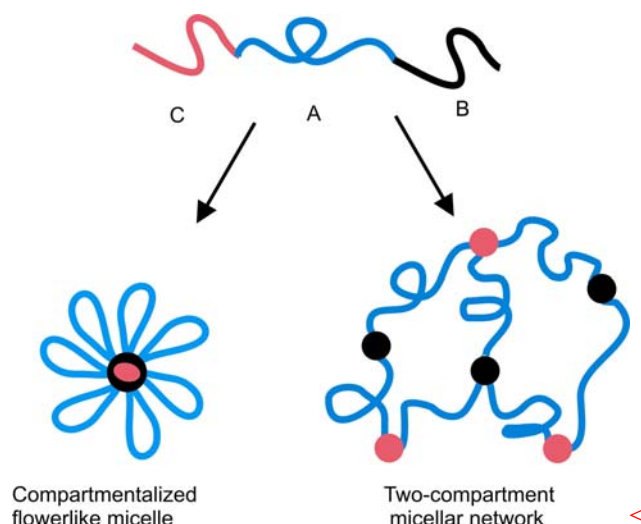


Figure 5.1 Possible aggregation structures formed by triphilic CAB triblock copolymer analogue in water

Weberkirch et al.¹¹ using the triphilic CAB triblock copolymer analogue of the structure, α -fluorocarbon- ω -hydrocarbon end-capped poly(*N*-acylethylenimine), found that at high concentration the copolymer forms a two-compartment network with hydrophilic poly(*N*-acylethylenimine) bridges. However, using a larger length of the hydrophilic poly(*N*-acylethylenimine) block, Kubowicz et al. found that the middle block in this case loops to form cylindrical micelles with a compartmentalized core.⁷ Shunmugam et al. prepared fluorophilic-hydrophilic-lipophilic polymethacrylate-based CAB triblock copolymers, investigated their behavior in water, and showed that these copolymers formed hydrogels ostensibly due to two-compartment network formation.¹² More recently, Taribagil et al. investigated the morphology of hydrogels formed by triphilic CAB block copolymer based on poly(perfluoropropylene oxide) (PFPO), poly(ethylene oxide) (PEO), and poly(1,2 butadiene) (PB), respectively.^{13,14} They established through SANS and cryogenic scanning electron microscopy (cryo-SEM) measurements that the PFPO-PEO-PB copolymer self-assembles into a compartmentalized network in which PFPO blocks form disk-shaped assemblies which are embedded in thin bicontinuous PB sheets with both faces of the sheets covered by looped PEO brushes. The authors reasoned that the disk-shaped adaptation over spherical-shaped by the assembled PFPO blocks is due to the strong hydrophobicity, large interfacial tension, and rodlike behavior exhibited by fluorocarbon molecules in aqueous environment. They further argued that in order to circumvent the enthalpic penalty associated with formation of disk edges in aqueous solution, the PFPO-PEO-PB system associates the fluorocarbon disk domains with the less hydrophobic PB chains to form PB sheets.

Thus, while exclusive bridging of mid-blocks might be naively expected for any triphilic CAB network, the interplay of the interactions among the three components and water can offset the significance of the incompatibility between the lipophilic and the fluorophilic end-components and give rise to a different microstructure.¹⁴ Particularly, we demonstrate this by using thermoresponsive PPO block as the lipophilic B component in our case. The C and A components of our system are a perfluoroalkyl segment and PGMA, respectively. The PPO homopolymer with molecular weight ~ 2000 g/mol has an LCST around 15 °C in water.¹⁵ Thus, below the LCST the PPO chains are hydrated and behave as hydrophilic entities. Conversely, at temperatures above the LCST they become dehydrated (insoluble) and as such behave as hydrophobic entities.¹⁶ It implies that, at temperatures below the LCST of the PPO block, the copolymer will behave as an amphiphile because it has the perfluoroalkyl segment as the only hydrophobic component, while the hydrophilic component consists of PGMA and PPO. Meaning, the copolymer can form micelle composed of fluorocarbon core stabilized by the PGMA and PPO as the hydrophilic corona. The question then is what happens when the PPO component becomes hydrophobic as temperature is raised above its LCST. Will the middle PGMA block loop to incorporate the hydrophobic PPO chains into the micelle core or will the PPO chains form hydrophobic junctions leading to the formation of a two-compartment network?

Thus, the two synthesized CAB triblock copolymer analogues, F_{10} -PGMA₆₆-PPO₃₄ and F_{10} -PGMA₈₅-PPO₃₄, are investigated for aggregation behavior in aqueous solution. Furthermore, the CBA triblock analogue, F_9 -PPO₂₇-PGMA₉₄ and the amphiphilic BA diblock, PPO₃₄-PGMA₆₆, are also investigated for comparative purposes. The characterization techniques used for the investigations include surface tension measurement, DLS, AFM and TEM

5.2. Experimental Part

5.2.1 Materials

The two CAB triblock copolymer analogues, F_{10} -PGMA₆₆-PPO₃₄ and F_{10} -PGMA₈₅-PPO₃₄, hereafter referred to as CAB1 and CAB2, were synthesized by ATRP and CuAAC ‘click’ reaction as already discussed in Chapter 2. CAB1 and CAB2 have molar masses of 13300 and 16300 g/mol, respectively, as calculated from ¹⁹F NMR spectroscopy using α,α,α -trifluorotoluene as internal reference standard. Their polydispersities obtained from size

exclusion chromatography (SEC) are 1.3 and 1.4, respectively. The CBA triblock copolymer analogue with switched lipophilic and hydrophilic sequence, F₉-PPO₂₇-PGMA₉₄, hereafter referred to as CBA, was also synthesized by similar procedure as described in Chapter 2. Its molar mass and polydispersity are 17400 g/mol and 1.4 as determined from spectroscopy and SEC, respectively. The diblock copolymer, PPO₃₄-PGMA₆₆, with molar mass of 12600 g/mol as determined from ¹H NMR and polydispersity of 1.4 as determined from ¹H NMR SEC, hereafter referred to as BA, was synthesized by ATRP as described in Chapter 2.

5.2.2 Characterization

5.2.2.1 Surface Tension Measurement

The surface tension (γ) of the aqueous solutions of the samples at different polymer concentrations was measured by the Wilhelmy plate method using the automated DCAT11 tensiometer (Data Physics Instruments GmbH, Filderstadt, Germany). Stock solutions of 2.5 g/L were prepared by dissolution of the polymer in bidistilled water, stirred overnight at room temperature, and filtered through 0.45 μm pore-size PTFE prior to use. The tensiometer works by automatically injecting predetermined volumes of the stock solution into a thermostated glass vessel containing initially only distilled water. Following each injection, the surface tension is then measured after 10 min of stirring and a 3 h waiting period. For samples which showed phase-separation at room temperature, solutions of different concentrations were prepared at 5 °C and measurements were carried out at 8 °C.

5.2.2.2 Dynamic Light Scattering (DLS)

DLS measurements of aqueous solutions of the polymers were performed using an ALV-NIBS/HPPS automatic goniometer from ALV-Laser (Langen, Germany), in the scattering angle range of 30° to 130°. The light source was a neodymium:YAG DPSS-200 laser ($\lambda = 532$ nm) with a power output of 200 mW. Intensity time correlation functions were measured with an ALV-5000E multiple- τ digital correlator. The CONTIN algorithm was applied to obtain distribution functions from the obtained autocorrelation function. The apparent diffusion coefficient, D_{app} , is related to the reciprocal of the characteristic decay rate, Γ and the scattering vector, q as $D_{app} = \Gamma/q^2$ [where $q = (4\pi n_o/\lambda)\sin(\theta/2)$, with n_o = refractive index of the medium, λ = wavelength of the light, θ = scattering angle]. The corresponding apparent

hydrodynamic radii, R_h , were obtained via the Stokes-Einstein equation $R_h = kT/(6\pi\eta D_{app})$, where k is the Boltzmann constant and η is the viscosity of the solvent, water in this case, corrected at the absolute temperature T . Aqueous polymer solutions were prepared by dissolution in bidistilled water at room temperature and stirring overnight. The solutions were filtered directly into the dust-free light scattering cells through a 0.45 μm pore size filter. For samples which showed phase-separation at room temperature, solution preparation and filtration were carried out at 5 °C.

5.2.2.3 Atomic Force Microscopy (AFM)

AFM images were obtained on a NANOWIZARD I (JPK Instruments, Berlin) operated in tapping mode with silicon cantilevers at a scan rate of 1 Hz. The cantilevers (Arrow, NanoWorld, Neuchâtel) had a resonance frequency of ~285 kHz and a force constant of ~42 N/m.

5.2.2.4 Transmission Electron Microscopy (TEM)

The TEM images were obtained from a JEOL 100CX microscope, operating at an acceleration voltage of 100 kV. Sample was prepared by drop-coating 0.014 g/L aqueous solutions of polymer sample on carbon-coated copper grids and allowed to dry under ambient conditions.

5.3 Results and Discussion

5.3.1 Surface Tension Measurements

For low-molar-mass surfactant or amphiphilic block copolymers that self-assemble in solution, the critical micellization concentration (cmc) is an important physical parameter that characterizes such systems. Surface tension measurement over a wide range of concentration is one of the several methods used for the cmc determination. Therefore, surface tension measurements are carried out on aqueous solutions of the block copolymers in order to obtain information on micelle formation. The surface tensions, γ , are measured as a function of polymer concentrations at 25 °C for CBA and BA. Plotting γ versus polymer concentration yields the cmc, indicated by intersection of the extrapolation of the two linear regimes where

the curve show abrupt change in slope as depicted in Figure 5.2 for both copolymers. The value obtained by this method for CBA and BA are 1.3 (0.02 g/L) and 12.4 μM (0.16 g/L), respectively. Although CBA has relatively larger hydrophilic PGMA block content, its cmc value is significantly lower than that of BA. This can be attributed to the presence of the highly hydrophobic perfluoro segment at the end of the PPO block in the case of CBA.

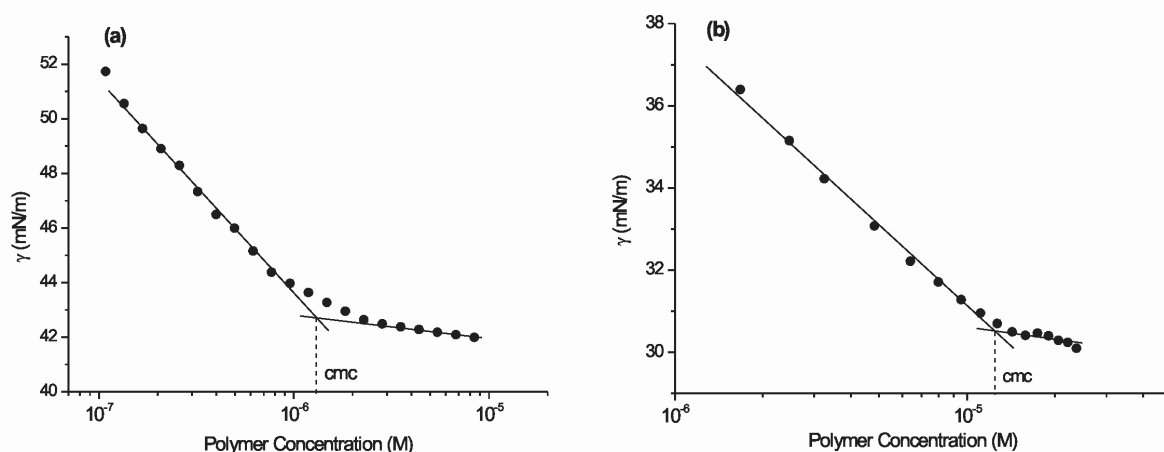


Figure 5.2 Critical micellization concentration (cmc) determinations of (a) CBA and (b) BA from surface tension measurements as a function of concentration at 25 °C.

Interestingly, whereas the aqueous stock solutions of CBA and BA are clearly transparent at 25 °C, that of CAB1 and CAB2 showed phase-separation behaviors (see DLS discussions). Therefore, the γ measurements were carried out at 8 °C to ascertain whether micelles are formed at temperature below the LCST of the PPO component. The γ measurement curve shown in Figure 5.3 for CAB1 exhibits an abrupt slope change at 0.8 μM , indicating that micelles are indeed formed at this temperature. This suggests that, at temperature below the LCST of PPO (around 15°C for the given molar mass),¹⁵ the highly hydrophobic perfluoro segments at the ends of the PGMA blocks are able to aggregate to form fluorocarbon core micelles.¹⁷

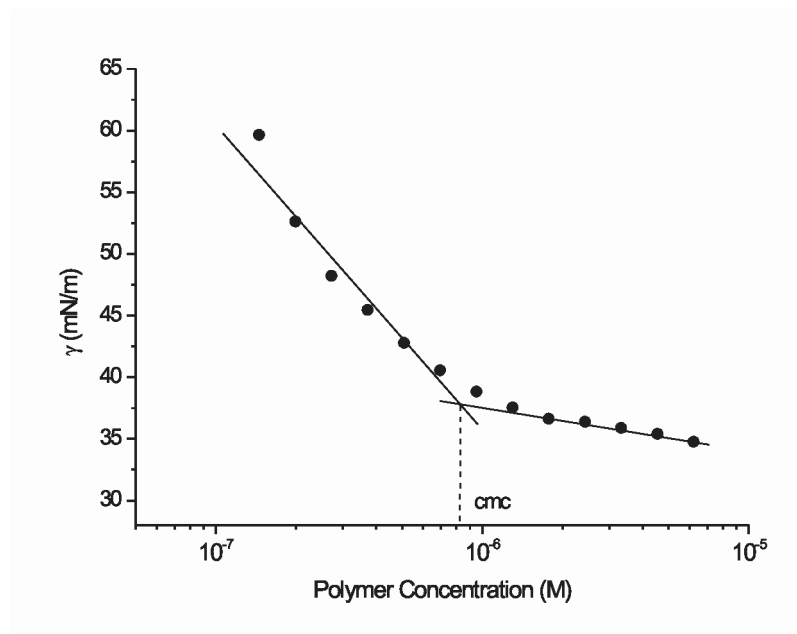


Figure 5.3 Critical micellization concentration (cmc) determination of CAB1 aqueous solution from surface tension measurements as a function of concentration at 8 °C.

Similarly, γ measurements on the aqueous solution of CAB2 at 8 °C also yielded a cmc value of 0.9 μ M. Measurements carried out on aqueous solution of the diblock copolymer, BA, at 8 °C showed only a continuous decrease of γ without any abrupt change in slope, an indication of lack of micelle formation at this temperature (see Figure 5.4). Indeed, this confirms that the ability of CAB1 and CAB2 to micellize in aqueous solution at 8 °C is due to the presence of the perfluoro segments at the ends of their PGMA blocks.

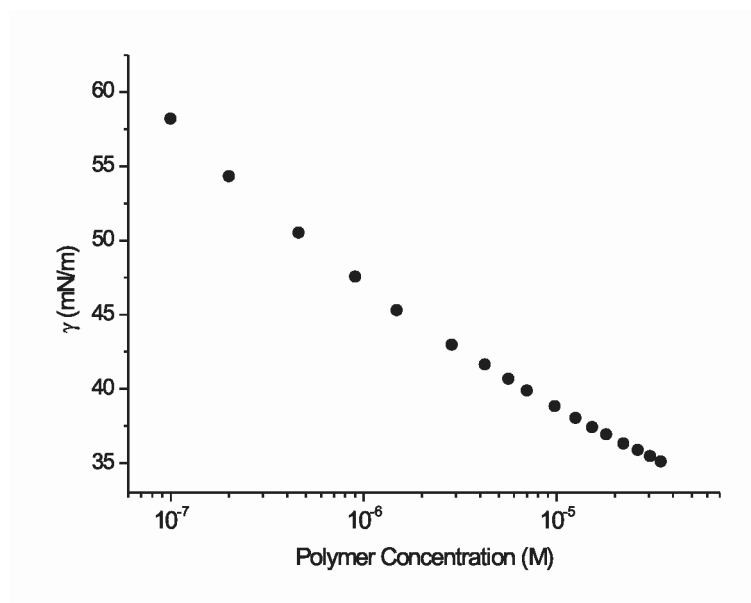


Figure 5.4 Surface tension measurements of BA aqueous solution as a function of concentration at 8 °C.

5.3.2 DLS Studies

In order to understand the influence of the thermoresponsiveness of the PPO block on the aggregation behavior and size of aggregates formed, comparative temperature-dependent DLS measurements were performed on aqueous solutions of BA and CAB1 because both copolymers have the same PPO and PGMA content except for the presence of the perfluoro segment at the end of the PGMA block of CAB1. Besides, the aqueous solution behavior of CAB2 was found to be very similar to that of CAB1. The chosen concentration is at least an order of magnitude higher than their cmc values determined from the surface tension measurements. Figure 5.5a shows the evolution of the R_h distribution with temperature for 1.4 g/L aqueous solution of BA.

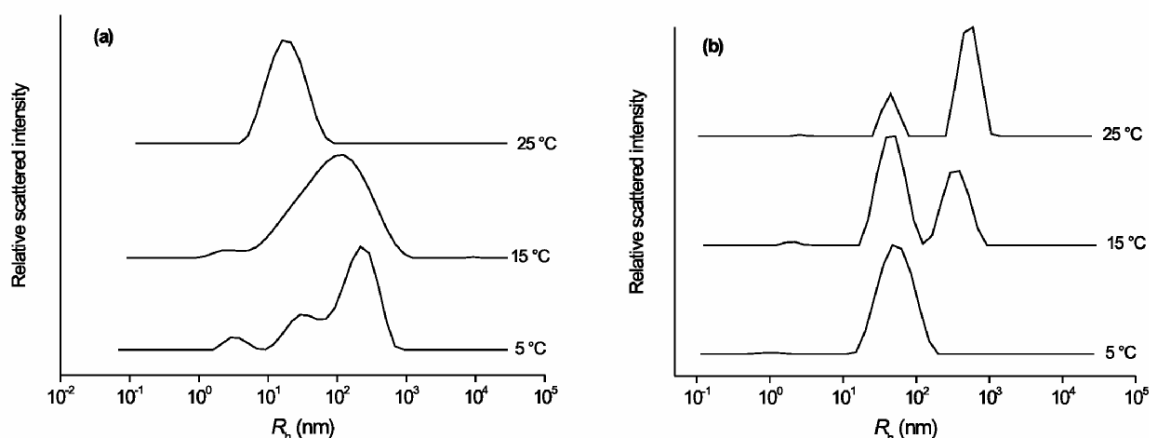


Figure 5.5 DLS data obtained at $\theta = 90^\circ$ for hydrodynamic radii (R_h) distributions as a function of temperature for 1.4 g/L aqueous solution of (a) BA and (b) CAB1.

At 5 °C a multi-modal R_h peak distribution was obtained. The peak with R_h at 3.4 nm corresponds to unimer species while the broad bimodal peak distribution at 186 nm is a result of aggregates formed by unimer-clustering through H-bonding of the hydroxyl groups of the PGMA block.¹⁸ On increasing temperature to 15 °C, the unimer peak diminishes and the aggregate peak transforms into a mono-modal peak with $R_h = 80$ nm. These changes signify the beginning of the concerted transition of block copolymer chains into micelles as the PPO blocks become hydrophobic. By 25 °C, only a single narrow peak distribution with R_h of 18 nm is obtained in solution. This distribution corresponds to micelles which are composed of hydrophobic PPO core stabilized by hydrophilic PGMA chains which serve as coronae.

On the contrary, 1.4 g/L of CAB1 aqueous solution at 5 °C showed mainly a mono-modal peak distribution with R_h of ~50 nm as can be seen in Figure 5.5b. This suggests that while the PPO component is still hydrophilic at 5 °C, the block copolymer chains are able to form micelles through aggregation of the perfluoro segments at the ends of the PGMA blocks. The observation is in agreement with the above discussions on the surface tension behavior of CAB1 at temperature below the solubility of the PPO component. Increasing the temperature to 15 °C, around the LCST of the PPO component, leads to appearance of a new peak distribution with $R_h = 460$ nm as seen in Figure 5.5b. The new peak continues to increase in intensity and size ($R_h = 546$ nm) at the expense of the micelle peak on increasing temperature to 25 °C. Visual observation of the polymer solution at this point confirmed a phase-separated solution. The increase of scattered light intensity as a function of the temperature at a fixed angle of 90° was used to determine the LCST for 5 g/L aqueous solution of CAB1.¹⁹ The LCST is determined as the inflection point of the curve which is obtained from the maxima of the first derivative of the curve as depicted in Figure 5.6. A value of 13 °C is determined for the CAB1 solution by this method. Similarly, under the same experimental conditions, a value of 15 °C is determined as the LCST of CAB2 solution. Certainly, the higher LCST value of CAB2 is due to its longer hydrophilic block-length.

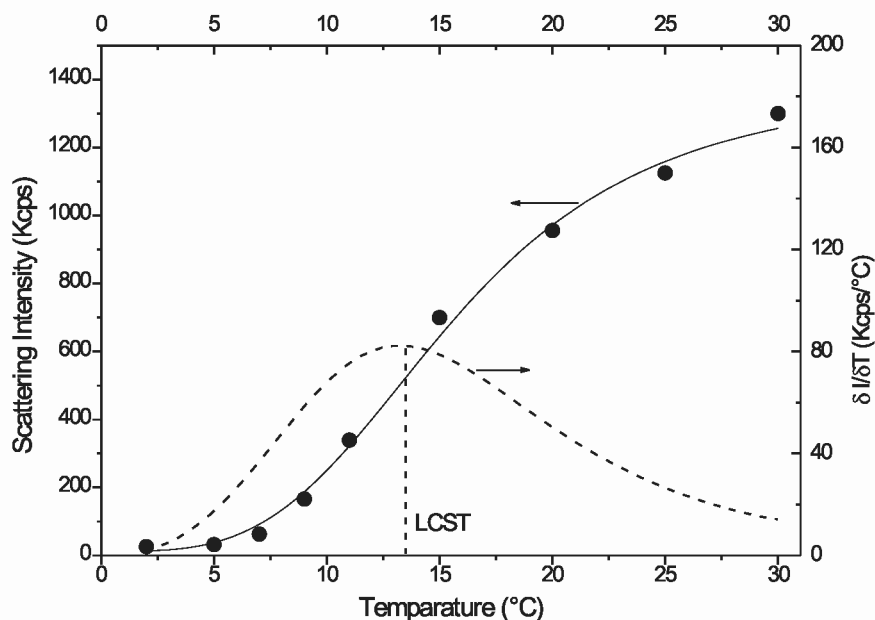


Figure 5.6 Temperature dependence of scattered light intensity at $\theta = 90^\circ$ for 5 g/L aqueous solution of CAB1 (●). The solid line curve is obtained from the data fitting while the dash line curve is the corresponding derivative from which the LCST is taken as the maxima.

As schematically illustrated in Figure 5.7, at temperatures where the PPO block is hydrophilic alongside the PGMA block, the presence of the highly hydrophobic perfluoro segments at the ends of the PGMA blocks causes micellization of the CAB1 block copolymer in solution. Thus, the PGMA-PPO blocks serve as the corona of the formed fluorocarbon core micelle. However, as temperature is increased the PPO blocks become increasingly hydrophobic. Eventually, around 13 °C, the PPO chains of the micellar corona collapse and aggregate leading to clustering of the micelles which is macroscopically manifested as phase-separation.

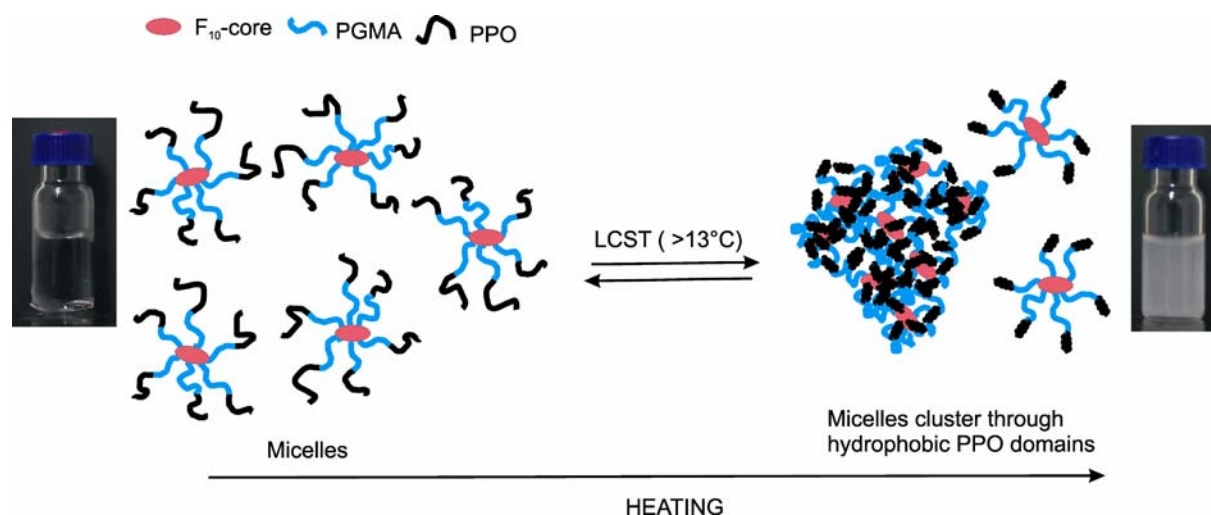


Figure 5.7 Schematic representations of micelle structures and aggregates obtained as a result of increasing temperature of aqueous solution of CAB1.

The critical solution concentration above which the phase-separation occurs can be determined by measuring the increase of the scattered light intensity as a function polymer concentration at fixed angle. Figure 5.8 shows the plot obtained for CAB1 by such measurements at 25 °C. It can be seen that the scattered light intensity remains nearly constant till 11 μM . Interestingly, this concentration is very close to the cmc of the amphiphilic diblock counterpart, BA, at 25 °C. Above this concentration, the intensity begins to increase very sharply indicating the onset of phase-separation. Interestingly, a critical look at the plot in the concentration region of 0.13 to 5.3 μM (see inset) reveals that a relatively weak increase in the scattered light intensity occurs above 0.5 μM . This concentration is close the 0.8 μM concentration where the perfluoro segments of CAB1 aggregate to form fluorocarbon core micelles as determined from the surface tension measurement. The slight difference in these

two concentrations can perhaps be attributed to the different temperatures at which both measurements were performed. It therefore suggests that fluorocarbon core micelles are indeed formed prior to the critical concentration above which phase-separation occurs. It can be summarized that at 25 °C the aggregation behavior of CAB1 solution with increasing concentration proceeds in two stages. During the first stage, at very low concentration, the copolymer chains aggregate to form fluorocarbon core micelles. With increasing concentration to the range where the PGMA-PPO component is capable of forming micelles alone, the second stage occurs which is associated with phase-separation. Thus, the phase-separation behavior of CAB1 aqueous solution at temperatures above to the LCST of the PPO block component is indeed due to clustering of the fluorocarbon core micelles through the hydrophobic PPO domains.

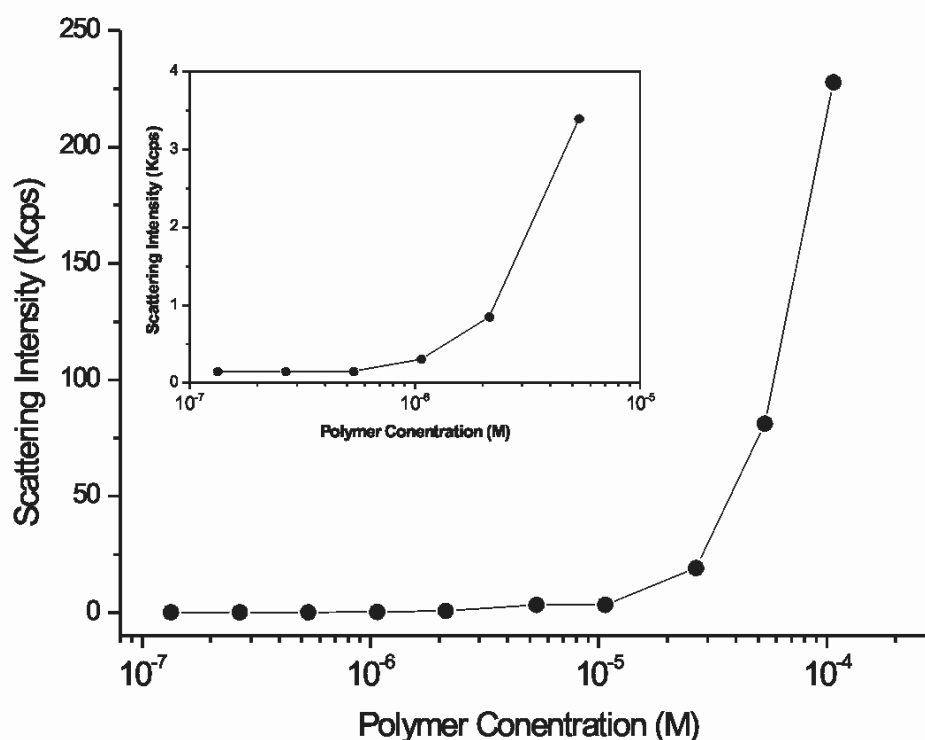


Figure 5.8 Plot of scattered light intensity at $\theta = 90^\circ$ as a function of polymer concentration at 25 °C for CAB1. The inset shows the plot for the concentration region of 1.3×10^{-7} to 5.3×10^{-6} M.

By considering the aqueous solution behavior of the triphilic CAB to that of the BAB-type amphiphilic triblock copolymers (B and A represent PPO and PEO, respectively), some comparison can be made. For the BAB-type of block copolymers in dilute aqueous solution above cmc, flowerlike micelles composed of hydrophobic B cores and looped A coronae are

formed.²⁰ With an increase in concentration and the resulting increase in the number density of these micelles, the middle block can overcome the entropic penalty of looping by bridging to another micelle core.²¹ With more bridging, the viscosity of the solution increases and a gel phase is formed. The gel phase typically occurs in the concentration range of 18-40 wt%.²² At much higher concentrations, above ~60 wt% phase-separation occurs then.²³ The phase-separation is governed by competition between osmotic repulsion among micelles and attraction resulting from the increase in configuration entropy of the system when bridges form between micelles. Thus, phase-separation sets in when the attraction is sufficiently large to overcome the repulsion.²⁴

Comparatively, for CAB1 phase-separation is observed at concentration above 0.015 wt% (11 μ M), which is an extremely low concentration. It therefore suggests that the thermodynamic driving force associated with the phase-separation of CAB1 aqueous solution is different from that of the BAB-type block copolymers.

As it was established in the last chapter, for both the PPO block and the perfluoro segment to fully co-exist in the same core, the PPO blocks must be rendered highly hydrophobic through dehydration at temperatures well above its lower critical solution temperature (LCST). Given this condition, it means when the PPO blocks become insoluble at temperatures just above its LCST, they will still be forced to stay outside the fluorocarbon core micelles even though it is permissible for the middle PGMA blocks to loop. Preferentially, the insoluble PPO blocks of the micelles start to interact with each, which in principle, should lead to formation of a two-compartment micellar network. However, it seems the hydrophilic PGMA blocks are ineffective in stabilizing this micellar network, thus, resulting in the phase-separation. Two reasons could possibly account for the inability of the hydrophilic PGMA to stabilize the two-compartment micellar network in this case;

(i) studies have revealed that hydroxyl bearing hydrophilic polymers such PGMA and the polyoxyalkylene analogue, poly(glycidol) (PG), interact less effectively with water at 25 °C, behaving as polymer coils in marginal solvent.^{25,26} This can be attributed to the effect of self-association through H-bonding that occurs among the hydroxyl groups, thus, limiting the number of hydroxyl sites available for effective interaction with water.²⁵

(ii) fluorocarbon-based micelles in water adopt flat disklike interface due to strong interfacial tension that exist between the fluorocarbon core and water.^{27,28} It has been argued that hydrophobic disk edges are enthalpically unfavorable in aqueous environment. To circumvent the enthalpic penalty of fluorocarbon core/water interface, the fluorocarbon core may crowd

its surface with PGMA chains, thereby expelling water from the interface.¹⁴ This will also lessen the effective interaction of the PGMA chains with water.

5.3.3 AFM and TEM Investigations on Polymer Aggregates

Additional information about the shape and size of the self-assembled structures formed by CAB1 and BA were obtained from AFM measurements at room temperature. Figure 5.9a shows the height image of BA aggregates obtained after coating a silicon substrate with 1.4 g/L aqueous polymer solution for 2 min, followed by washing with bidistilled water and drying under ambient conditions overnight.²⁹ The image reveals spherical structures with diameter of 28-32 nm which is slightly smaller than the micellar diameter of 36 nm ($R_h = 18$ nm) observed for aqueous BA solution at 25 °C. The smaller diameter size observed in the AFM measurement is due to the fact that the micelles now exist in a “dry state” with desolvated PGMA coronae.³⁰

Figure 5.9b shows the height image of aggregated structures formed by CAB1. The sample was prepared under conditions similar to BA, except that coating was done at 5 °C. Large irregular aggregates with size ranging from 200 to 400 nm can be seen embedded in double layered sheets with thickness of ~2.5 nm each. The observed sheets can be attributed to formation of the two-compartment micellar network.¹⁴ As opposed to what was observed in bulk aqueous solution, it seems that the presence of the solid support helps stabilize the initially formed network structure to form the sheets. Nonetheless, some regions of the network remain unstable and thus aggregate into the large irregular structures observed in the image.

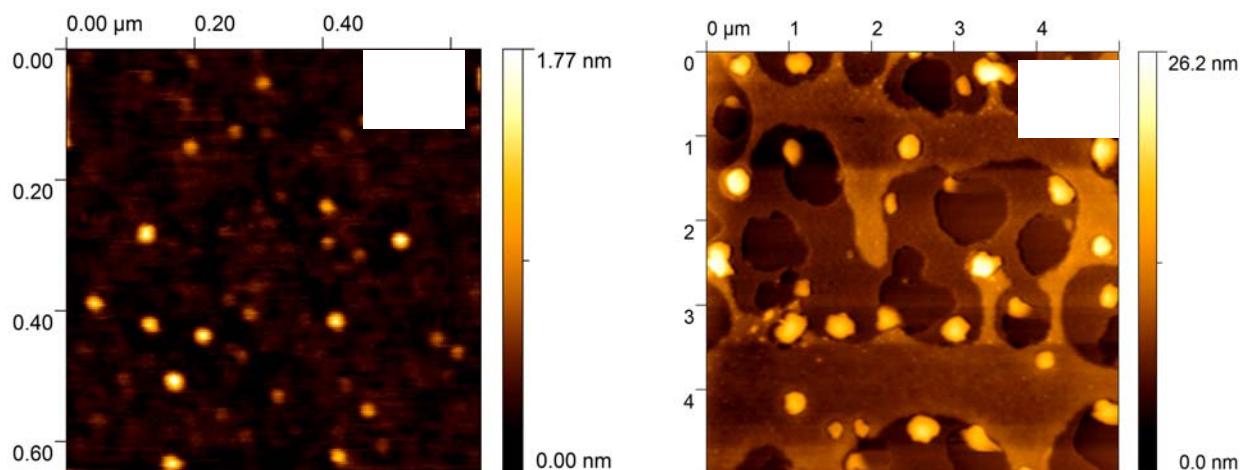


Figure 5.9 Height image obtained after coating a silicon substrate with 1.4 g/L aqueous polymer solution of (a) BA at 25 °C, and (b) CAB1 at 5°C for 2 min, followed by washing with bidistilled water and evaporation at room temperature.

Due to the linking sequence and the incompatibility between the perfluoro segment and PPO, CBA is expected to segregate into fluorocarbon- and PPO-rich domains when it self-assembles. Therefore, TEM imaging was carried out on the CBA copolymer. Figure 5.10 shows the TEM image obtained on a copper grid solid support after coating with 0.014 g/L aqueous polymer solution followed by evaporation of water at room temperature.

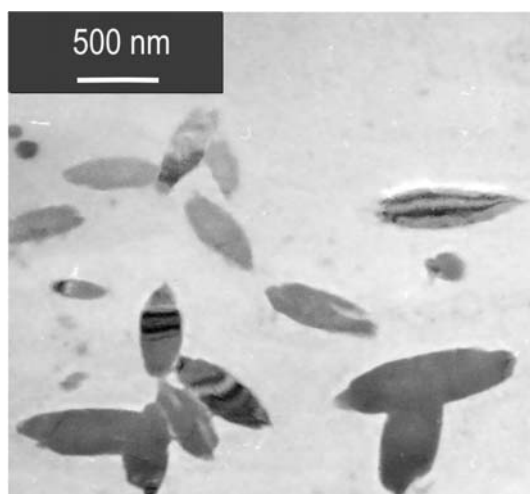


Figure 5.10 Transmission electron microscopy (TEM) image of CBA obtained after coating a carbon copper grid with 0.014 g/L aqueous polymer solution and evaporation of water at room temperature.

Although, the concentration of the solution used is slightly below cmc, it should be realized that as water slowly evaporates from the surface the cmc threshold will be passed and

micelles or well defined aggregates will be formed during this process. This preparative method was adopted because initial attempts using solution with concentration much higher than cmc resulted in TEM images showing only polymer films. The image shows large supramolecular structures with length in the range of 300-900 nm. The driving forces responsibly for the supramolecular self-organization of CBA into such structures are, multiple intra- and interchain hydrogen bonds in the hydrophilic PGMA blocks,³¹ lipophilic association of the PPO blocks, and fluorophilic association of the perfluoro segment. During the self-organization because the PPO and perfluoro segments are hydrophobic, they self-assemble inside the structure formed to minimize contact with water. However, due to the incompatibility between them, they segregate microscopically to give ~30 nm thick fluorocarbon-rich domains which appear as dark stripes in the TEM image.³² The PPO and PGMA components of the aggregate appear as white and gray contrast, respectively, in the image. In fact, the behavior of the perfluoro segments is in agreement with theoretical predictions by Semenov, Khokhlov and co-workers who identified a new regime of phase behavior that they dubbed “superstrong segregation”.^{33,34} In this regime, the repulsive interactions between two adjoining blocks become so strong that the interfacial energy overwhelms the conformational entropy or coronal crowding, as such, the minor block becomes nearly stretch out completely.³³

5.4. Conclusions

In this chapter the aggregation behavior of the synthesized CAB triblock copolymer analogues, F₁₀-PGMA₆₆-PPO₃₄ (CAB1) and F₁₀-PGMA₈₅-PPO₃₄ (CAB2), in water have been investigated and compared with PPO₃₄-PGMA₆₆ (BA) and F₉-PPO₂₇-PGMA₉₄ (CBA). It is found that while BA and CBA formed clear micellar solutions at 25 °C, the CABs solutions exhibited phase-separation at this temperature. However, at temperatures below the LCST of the PPO block component, the CABs form clear solutions containing fluorocarbon core micelles. As observed by DLS, the phase separation is due to formation of large micellar clusters with $R_h \sim 546$ nm at temperatures above the LCST of the PPO component. It seems the clustering effect is due to the inability of the hydrophilic PGMA blocks to stabilize the resulting two-compartment micellar network formed through hydrophobic PPO junctions between the fluorocarbon core micelles.

Comparatively, the CBA architecture cannot form such two-compartment micellar network because the perfluoro alkyl segment and the PPO the block are covalently linked. However, they segregate into fluorocarbon and PPO-rich domains when they self-assemble as observed in the TEM image.

5.5 References

1. Kyeremateng S.O., Henze T., Busse K., Kressler J. *Macromolecules* **2010**, *43*, 2502.
2. Thünemann A.F.; Kubowicz S.; Berlepsch H.v.; Möhwald H. *Langmuir* **2006**, *22*, 2506.
3. Zhou Z.; Li Z.; Ren Y.; Hillmyer M. A.; Lodge T. P. *J. Am. Chem. Soc.* **2003**, *125*, 10182.
4. Li. Z.; Kesselman E.; Talmon Y.; Hillmyer M. A.; Lodge T. P. *Science* **2004**, *306*, 98.
5. Zhou Z.; Li Z.; Ren Y.; Hillmyer M. A.; Lodge T.P. *J. Am. Chem. Soc.* **2003**, *125*, 10182.
6. Zhang H.; Ni P.; He J.; Liu C. *Langmuir* **2008**, *24*, 4647.
7. Kubowicz S.; Thünemann A. F.; Weberskirch R.; Möhwald H. *Langmuir* **2005**, *21*, 7214.
8. Berlepsch H.v.; Böttcher C.; Skrabania K.; Laschewsky A. *Chem. Comm.* **2009**, 2290.
9. Skrabania, K.; Berlepsch, H. V.; Böttcher, C.; Laschewsky, A. *Macromolecules* **2010**, *43*, 271.
10. Hillmyer, M. A.; Lodge, T. P. *J Polym. Sci., A: Polym. Chem.* **2002**, *40*, 1.
11. Weberkirch R.; Preuschen J.; Spiess H.W.; Nuyken O. *Macromol. Chem. Phys.* **2000**, *201*, 995.
12. Shunmugam, R.; Smith, C.; Tew, G. *J Polym. Sci., A: Polym. Chem.* **2007**, *45*, 2601.
13. Taribagil, R. R.; Hillmyer, M. a.; Lodge, T. P. *Macromolecules* **2009**, *42*, 1796.
14. Taribagil, R. R.; Hillmyer, M. a.; Lodge, T. P. *Macromolecules*. **2010**, *43*, 5396.
15. Save M; Weaver J. V. M.; Armes S. P.; McKenna P. *Macromolecules* **2002**, *35*, 1152.
16. Xu, J.; Ge, Z.; Zhu, Z.; Luo, S.; Liu, H.; Liu, S. *Macromolecules* **2006**, *39*, 8178.
17. Li Z., Kyeremateng S. O., Fuchise K., Kakuchi R., Sakai R., Kakuchi T., Kressler J. *Macromol. Chem. Phys.* **2009**, *210*, 2138.
18. Kyeremateng S.O.; Amado E.; Kressler J. *Euro. Polym. J.* **2007**, *43*, 3380.
19. De Santis, S.; Diana Ladogana, R.; Diociaiuti, M.; Masci, G. *Macromolecules* **2010**, *43*, 1992.
20. Zhou, Z.; Chu, B. *Macromolecules* **1994**, *27*, 2025.
21. Tae, G.; Kornfield, J.A.; Hubbell, J.A.; Johannsmann, D.; Hogen-Esch T.E. *Macromolecules* **2001**, *34*, 6409.
22. Mortensen, K.; Brown, W.; Joergensen, E. *Macromolecules* **1994**, *27*, 5654.

23. Van Vlimmeren, B.; Maurits, N.; Zvelindovsky, A.; Sevink, G.; Fraaije, J. *Macromolecules* **1999**, *32*, 646.
24. Semenov, A.; Joanny, J.; Khokhlov, A. *Macromolecules* **1995**, *28*, 1066.
25. Wang C.; Yu B.; Knudsen B.; Harmon J.; Moussy F.; Moussy Y. *Biomacromolecules* **2008**, *9*, 561.
26. Rangelov, S.; Trzebicka, B.; Jamroz-Piegza, M.; Dworak, A. *J. Phys. Chem. B* **2007**, *111*, 11127.
27. Rogers, S. E.; Eastoe, J.; Hudson, L.; Gold, S.; Heenan, R. K.; Grillo, I. *J. Colloid Interface Sci.* **2009**, *330*, 437.
28. Eastoe, J.; Rogers, S. E.; Martin, L. J.; Paul, A.; Guittard, F.; Guittard, E.; Heenan, R. K.; Webster, J. R. **2006**, *22*, 2034.
29. Rakhmatullina, E.; Braun, T.; Chami, M.; Malinova, V.; Meier, W. *Langmuir* **2007**, *23*, 12371.
30. Shell, R.; Gohy, J.; Willet, N.; Varshney, S.; Zhang, J.; Je, R. *Angew. Chem.* **2001**, *113*, 3314.
31. Rangelov, S.; Almgren, M.; Halacheva, S.; Tsvetanov, C. *J. Phys. Chem. C* **2007**, *111*, 13185.
32. Hussain H.; Busse K.; Kressler J. *Macromol. Chem. Phys.* **2003**, *204*, 936.
33. Semenov, A. N.; Nyrkova, I. A.; Khokhlov, A. R. *Macromolecules* **1995**, *28*, 7491.
34. Nyrkova, I. A.; Khokhlov, A. R.; Doi, M. *Macromolecules* **1993**, *26*, 3601.

Chapter 6

Summary

Novel PPO-based amphiphilic diblock copolymers and triphilic multiblock copolymer analogues of the architectures BA, CBA, CAB, and CABAC have been successfully synthesized by combination of atom transfer radical polymerization (ATRP) and copper(I)-catalyzed alkyne-azide cycloaddition (CuAAC) ‘click’ post-polymerization reaction. ATRP is the method of choice due to the simple synthetic procedure and commercial availability of all necessary reagents. The CuAAC ‘click’ reaction is a convenient post-polymerization coupling method because of the facility with which the halogen end groups inherent to ATRP can be substituted with azide groups.

The A, B, and C components of the block copolymers comprised of hydrophilic poly(glycerol monomethacrylate) (PGMA), lipophilic poly(propylene oxide) (PPO), and perfluorocarbon segment, respectively. Molar mass values of the polymers were obtained from ^1H and ^{19}F NMR spectroscopy measurements. Size exclusion chromatography (SEC) analysis confirmed unimodal molar mass distribution with generally low polydispersities ($1.2 \leq M_w/M_n \leq 1.5$).

The aggregation behavior of the copolymers in aqueous solution was studied by temperature-dependent ^1H and ^{19}F NMR, isothermal titration calorimetry (ITC), dynamic light scattering (DLS), small angle neutron scattering (SANS), atomic force microscopy (AFM), and transmission electron microscopy (TEM).

The self-assembly of the amphiphilic PPO/PGMA diblock copolymer into micelles was studied and compared to the most widely studied amphiphilic block copolymer system, PPO/PEO. This was done to assess the comparative influence of the hydrophilic PGMA block on the micellization behavior. It was found that replacing the hydrophilic PEO block with PGMA influences very significantly the micellization process but not the final spherical-shaped micelles formed by both block copolymer systems, as evidenced by SANS investigations. The replacement of PEO with PGMA leads to comparatively smaller critical micellization concentration (cmc) and smaller values of the standard free energy $\Delta G^\circ_{\text{mic}}$, standard enthalpy, $\Delta H^\circ_{\text{mic}}$, and standard entropy, $\Delta S^\circ_{\text{mic}}$, of the micellization process. It also leads to comparatively larger PPO core size of the PPO/PGMA micelles as determined from the SANS measurements. These significant differences stem from the partial self-association

through H-bonding which occurs among the PGMA blocks. The self-association effect leads to lesser interactions with water molecules giving PGMA a lesser hydrophilic character than PEO. Consequently, this lesser hydrophilic character is responsible for the comparatively lower cmc , ΔG°_{mic} , ΔH°_{mic} , and ΔS°_{mic} for the micellization of the PPO/PGMA block copolymer in water.

The aggregation of the triphilic block copolymers analogues, CBA, CAB, and CABAC in aqueous solution showed intriguing structures. The structures they formed were governed by the strong immiscibility between the lipophilic PPO blocks and the fluorophilic perfluorocarbon segments as well as the blocks sequence and length. It was observed that the CBA copolymer formed clear micellar solution at room temperature. TEM investigation revealed that CBA block copolymer segregate into fluorocarbon and PPO-rich domains when they self-assemble due to the strong immiscibility between the lipophilic and fluorophilic components. Interestingly, the copolymer with the reversed architecture, CAB, formed a phase-separated solution at room temperature. However, at temperatures below the LCST of the PPO block component, a clear solution composed of fluorocarbon core micelles was formed. Information obtained from temperature-dependent DLS measurements indicated that the phase-separation is due to formation of large micellar clusters with $R_h \sim 546$ nm at temperatures above the LCST of the PPO component. AFM investigations also confirmed the formation of micellar clusters. The clustering effect is most likely due to the ineffectiveness of the hydrophilic PGMA blocks to stabilize the resulting two-compartment micellar network formed via hydrophobic PPO junctions between the fluorocarbon core micelles.

For the CABAC copolymers, a tremendous influence of the hydrophilic block-A length on the aggregation behavior was observed. The two CABAC copolymers investigated in this work namely, F_9 -PGMA₂₄-PPO₂₇-PGMA₂₄-F₉ (PB1) and F_9 -PGMA₄₂-PPO₂₇-PGMA₄₂-F₉ (PB2), differ only in the degree of polymerization of the hydrophilic PGMA blocks. Their aggregation behavior studied in aqueous medium by temperature-dependent DLS measurements showed that PB1 forms only spherical micelles with hydrodynamic radius, R_h , of ~ 18 nm in solution at all temperatures while PB2 forms mainly aggregate of micelles with R_h of 40 nm at 25 °C. The aggregate disintegrate into compact single flowerlike micelles with R_h of ~ 17 nm at high temperatures.

The aggregation behavior in aqueous medium studied by ^{19}F NMR spectroscopy revealed that the fluorocarbon component forms part of the micelle corona of PB1, while in PB2 it aggregates to form part of the micelle core. The immiscibility between the F_9 segments and the

PPO blocks within the PB2 micelle core resulted in a compartmentalized core where they formed the inner and the outer cores, respectively.

The effect of the presence or the absence of fluorocarbon component within the micelle cores of the two block copolymers was reflected in the temperature-dependent ^1H NMR behavior of their PPO blocks. For PB2 micelles the presence of the highly hydrophobic fluorocarbon component within the micelle cores created a well-dehydrated solidlike core environment which eventually leads to a weak signal response from the protons of the PPO block. In contrast, the core environment of PB1 micelles is liquidlike due to the absence of the fluorocarbon component, thus, leading to significant signal response from the protons of the PPO block.

The lack of the fluorocarbon component within the core of PB1 micelles is due to the inability of their short rigid PGMA blocks to loop. This observation is in agreement with theoretical prediction of loop formation by semiflexible polymer chain and accounts for the strong difference in aggregation behavior of these two structurally similar block copolymers. AFM and TEM investigations of the structures formed on solid supports after solvent evaporation also confirmed the aggregation behavior of the two block copolymers.

Due to the compartmentalized core structure of PB2 micelles, they showed about 4 fold enhanced tetrafluorobenzene uptake-capability compared PB1 micelles owing to the absence of the fluorocarbon component within the micelle core of the latter.

Chapter 7

Experimental Procedures for Synthesis of Block Copolymers

7.1 Materials

All chemicals were bought from Sigma-Aldrich unless otherwise stated. Toluene (99%) and pyridine (99%) were dried over calcium hydride overnight, distilled under normal atmospheric condition and stored over molecular sieve. Triethylamine (Et₃N) (99.8%), dimethylformamide (DMF) (99.8%) and anisole (Alf-Aesar, 99%) were dried over calcium hydride overnight, distilled under reduced pressure and kept over molecular sieve. Anhydrous dichloromethane (CH₂Cl₂), (99.8%), *n*-hexane (97%), diethyl ether (98%), 1,4-dioxane (99%), methanol (99.8%), ethanol (99.8%) monohydroxy terminated poly(propylene oxide) (PPO-OH) [M_n (SEC) ~2500 g mol⁻¹, M_n (¹H NMR) ~2000 g mol⁻¹] and poly(propylene oxide) [M_n (SEC) ~2000 g mol⁻¹, M_n (¹H NMR) ~1600 g mol⁻¹] were used as received. Tetrahydrofuran (THF) (99.5%) was distilled from potassium hydroxide and stored over molecular sieve. Copper bromide (CuBr) (99%) was purified by stirring in glacial acetic acid under nitrogen for 24 h to dissolve the Cu(II) species, filtered, washed several times with ethanol and dried under vacuum. Copper chloride (CuCl) (99 %), *N*-ethyl-diisopropylamine (DIPEA) (98%), tris-(benzyltriazolylmethyl)amine (TBTA) (97%), sodium azide (NaN₃) (99.5%), hex-5-ynoic acid (97%), 2-bromoisobutryl bromide (BIB) (98%) nonadecafluoro-1-decanol (C₉F₁₉CH₂OH) (97%), heneicosafuoro-1-undecanol (C₁₀F₂₁CH₂OH) (95%), *N,N'*-(dicyclohexyl)carbodiimide (DCC) (99%), 2,2'-bipyridine (bpy) (Merck, 99.5%), α,α,α -trifluorotoluene (TFT) (99%) and 4-(dimethylamino) pyridine (DMAP) (99%) were used without further purification.

7.2 Synthesis of Monomer (Solketal Methacrylate)

Freshly distilled triethylamine (59.7 g, 0.61 mol) was mixed in 200 mL benzene solution of solketal (isopropylidene glycerol) (80.4 g, 0.61 mol). The solution was cooled to about 0°C in a water-ice bath. Methacryloyl chloride (47.7 g, 0.46 mol) was vacuum distilled ($T_b \sim 44^\circ\text{C}$, 70 mbar), diluted in 100 mL benzene and added dropwise to the solution for 2 h with stirring in a water-ice bath under argon atmosphere. The mixture was stirred for 20 h more at room temperature. It was filtered to remove the precipitated triethylamine hydrochloride, washed

twice with 250 mL distilled water and dried with anhydrous sodium sulphate to give a pale orange liquid. After filtration from anhydrous Na_2SO_4 , 0.5 g methylene blue was added and benzene was evaporated under reduced pressure. The product was purified by fractional distillation at 66-80 °C (5 mbar) to give 65.8 g (0.32 mol) of the monomer solketal methacrylate (SMA) as a colorless liquid.¹ Yield = 72%. ^1H NMR (400 MHz, $\text{DMSO}-d_6$): δ (ppm) = 6.0 and 5.65 (s, $\text{H}_2\text{C}=\text{CCH}_3$), 4.30-3.65 (m, $-\text{CH}_2\text{CHCH}_2-$), 1.86 (s, $\text{H}_2\text{C}=\text{CCH}_3$), 1.28 and 1.23 [s, $-\text{C}(\text{CH}_3)_2$].

7.3 ATRP Initiators Synthesis

Heneicosafuoro-1-undecyl 2-bromoisobutanoate (perfluoroalkyl-initiator) ($\text{F}_{10}\text{-Br}$)

In a round bottom flask 2.5 g (4.5 mmol) of $\text{C}_{10}\text{F}_{21}\text{CH}_2\text{OH}$ was dissolved in 10 mL of freshly distilled THF at room temperature. 0.71 g (9 mmol) of pyridine was added to the stirring solution and the flask kept in an ice bath. 2.7g (9 mmol) of BIB was dissolved in 10 mL THF and added slowly over a 30 min period after which an additional 1 h was allowed before the ice bath was removed. The reaction was allowed to proceed at room temperature for 48 h. The reaction products was diluted with excess THF and filtered through glass cotton. THF was removed via rotary evaporation and the residue dissolved in diethyl ether. The ethereal solution was washed with distilled water, followed by 0.5 M NaOH solution and finally with distilled water. Traces of water were removed from the ethereal solution by drying with anhydrous magnesium sulphate, followed by removal of the diethyl ether via rotary evaporation. Final purification was by column chromatography using hexane:diethyl ether 10:1(v/v).² Yield = 91%. ^1H NMR (400 MHz, CDCl_3): δ (ppm) = 4.65 [t, $-\text{CF}_2-\text{CH}_2-$], 1.95 [s, $-\text{C}(\text{Br})-(\text{CH}_3)_2$]. ^{19}F NMR (200 MHz, CDCl_3): δ (ppm) = -126.51 [$-(\text{CF}_2)_7-\text{CF}_2-\text{CF}_3$], -122.21 [$-(\text{CF}_2)_7-\text{CF}_2-\text{CF}_3$], -119.78 [$-\text{CH}_2-\text{CF}_2-(\text{CF}_2)_7-$], -81.18 [$-(\text{CF}_2)_7-\text{CF}_2-\text{CF}_3$].

α,ω -2-Bromoisobutanoate poly(propylene oxide) (difunctional macroinitiator) (Br-PPO-Br)

In a 100 mL two-necked round bottom flask containing 5 g of HO-PPO-OH (2.5 mmol, $M_n \sim 2000 \text{ g mol}^{-1}$), 30 mL of toluene was added. Azeotropic distillation of the solution was carried out using the Dean and Stark apparatus. The solution was allowed to cool and 0.76 g (7.5 mmol) of Et_3N added. The flask was then placed in a water-ice bath and 1.72 g (7.5 mmol) of BIB added dropwise and slowly over a 30 min period. Reaction was carried out at room temperature for 48 h. Purification was achieved by first filtering off the $(\text{Et}_3\text{NH})^+\text{Br}^-$

salt formed, followed by removal of toluene by rotary evaporation under reduced pressure. The polymer was dissolved in 120 mL methanol/water solution and NaOH solution (0.25 N) was added with vigorous shaking until neutral pH. Methanol was removed and the polymer extracted with dichloromethane. The extract was decolourised with activated charcoal, dried with anhydrous MgSO_4 and dichloromethane removed under reduced pressure to afford difunctional macroinitiator, Br-PPO-Br.³ Yield = 70%. ^1H NMR (400 MHz, CDCl_3): δ (ppm) = 1.0-1.28 [m, $-\text{CH}(\text{CH}_3)-\text{CH}_2-$], 1.9 [s, $-\text{C}(\text{Br})-(\text{CH}_3)_2$], 3.27-3.41 [m, $-\text{CH}(\text{CH}_3)-\text{CH}_2-$], 3.44-3.73 [m, $-\text{CH}(\text{CH}_3)-\text{CH}_2-$].

α -Azido- ω -2-bromoisobutanoate poly(propylene oxide) (heterofunctional macroinitiator) (N_3 -PPO-Br)

Similar to the preparation of the difunctional macroinitiator, the monofunctional macroinitiator was prepared by partial acylation of the dihydroxy-terminated PPO in a molar ratio [PPO]:[BIB]:[Et_3N]; 1:1.3:1.3. Thin layer chromatography (TLC) showed the product did not contain unacylated PPO. Based on this knowledge, it was estimated from analysis of the ^1H NMR spectrum that the product contains about 15 mol-% of completely acylated PPO; i.e., 85 mol-% of the PPO is end capped with a free OH group. The terminal Br group of the chains was then replaced with N_3 through azidation reaction with NaN_3 according to a method reported elsewhere.⁴ The terminal free OH of the PPO chains were further acylated with BIB using the same method as mentioned above, but replacing Et_3N with pyridine and dichloromethane with diethyl ether, to afford 85 mol-% heterofunctional macroinitiator, Br-PPO- N_3 , and 15 mol-% α,ω -diazido-terminated poly(propylene oxide) (N_3 -PPO- N_3). Yield = 77%. ^1H NMR (400 MHz, CDCl_3): δ (ppm) = 1.0-1.28 [m, $-\text{CH}(\text{CH}_3)-\text{CH}_2-$], 1.4 [s, $-\text{C}(\text{N}_3)-(\text{CH}_3)_2$], 1.9 [s, $-\text{C}(\text{Br})-(\text{CH}_3)_2$], 3.27-3.41 [m, $-\text{CH}(\text{CH}_3)-\text{CH}_2-$], 3.44-3.73 [m, $-\text{CH}(\text{CH}_3)-\text{CH}_2-$].

Bromoisobutanoate poly(propylene oxide) (monofunctional macroinitiator) (PPO-Br)

In a 100 mL two-neck round bottom flask containing 14 g of $\text{PPO}_{34}\text{-OH}$ (7 mmol, $M_n \sim 2000 \text{ g mol}^{-1}$), 60 mL of toluene was added. Azeotropic distillation of the solution was carried out using the Dean and Stark apparatus. The solution was allowed to cool and 2.5 g (32 mmol) of pyridine added. The flask was then placed in a water-ice bath and 4.65g (20 mmol) of BIB added drop wise and slowly over 30 min period. Reaction was carried out at room temperature for 48 h. Purification was achieved by first filtering off the pyridium salt formed followed by removal of toluene by rotary evaporation under reduced pressure. The

polymer was dissolved in 120 mL methanol/water solution and NaOH solution (0.5 M) was added with vigorous shaking until neutral pH. Methanol and water were removed under reduced pressure and the polymer dissolved in diethyl ether. Then the ethereal solution was washed several times with distilled water, dried with anhydrous magnesium sulfate and the diethyl ether finally removed under reduced pressure to give the purified monofunctional macroinitiator, PPO-Br. Yield = 85 %. ^1H NMR (400 MHz, CDCl_3): δ (ppm) = 1.0-1.28 [m, $-\text{CH}(\text{CH}_3)-\text{CH}_2-$], 1.9 [s, $-\text{C}(\text{Br})-(\text{CH}_3)_2$], 3.27-3.41 [m, $-\text{CH}(\text{CH}_3)-\text{CH}_2-$], 3.44-3.73 [m, $-\text{CH}(\text{CH}_3)-\text{CH}_2-$].

7.4 Synthesis of Alkyne-End Functionalized Compounds

Nonadecafluoro-1-decyl hex-5-ynoate ($\text{F}_9\text{C}\equiv\text{H}$)

Synthesis of $\text{F}_9\text{C}\equiv\text{H}$ was accomplished in two steps. First, hex-5-ynoic acid was reacted with 1,3-(dicyclohexyl)carbodiimide (DCC) in anhydrous dichloromethane to afford hex-5-ynoic anhydride. In the second step, the anhydride was esterified with nonadecafluoro-1-decanol using THF as a solvent in the presence of pyridine and 4-(dimethylamino) pyridine.⁵ Purification of the crude product was by column chromatography using hexane:ether (10:1) Yield = 93%. ^1H NMR (400 MHz, CDCl_3): δ (ppm) = 1.83-1.90 (m, $-\text{CH}_2-\text{CH}_2-\text{CH}_2-$), 1.96 (s, $\text{HC}\equiv\text{C}-$), 2.27 (t, $\equiv\text{C}-\text{CH}_2-\text{CH}_2$), 2.56 [t, $\text{CH}_2-\text{CH}_2-\text{C}(\text{O})-$], 4.58 (t, $\text{O}-\text{CH}_2-\text{CF}_2-$). ^{19}F NMR (200 MHz, $\text{DMSO}-d_6$): δ (ppm) = -126.13 [$-(\text{CF}_2)_6-\text{CF}_2-\text{CF}_3$], -122.06 [$-(\text{CF}_2)_6-\text{CF}_2-\text{CF}_3$], -118.93 [$-\text{CH}_2-\text{CF}_2-(\text{CF}_2)_6-$], -80.63 [$-(\text{CF}_2)_6-\text{CF}_2-\text{CF}_3$].

Poly(propylene oxide) hex-5-ynoate ($\text{PPO}-\text{C}\equiv\text{H}$)

This was synthesized by esterification of hex-5-ynoic anhydride with PPO-OH. In brief, to a 30 mL anhydrous dichloromethane solution containing 5 g (2 mmol) of the polymer was added 0.316 g (4 mmol) of pyridine and 0.449 g of DMAP. 0.825 g (4 mmol) of the anhydride was added dropwise and slowly at room temperature. After complete addition, the solution was allowed to stir at room temperature for 48 h. Dichloromethane was removed under vacuum and the residue dissolved in diethyl ether, washed twice with 0.5 M NaOH, twice with distilled water, and the organic layer dried over anhydrous MgSO_4 . Diethyl ether was removed under reduced pressure to give the alkyne terminalized poly(propylene oxide), $\text{PPO}-\text{C}\equiv\text{H}$. Final purification was by column chromatography with THF as eluent. Yield = 92 %. ^1H NMR (400 MHz, CDCl_3): δ (ppm) = 1.0-1.28 [m, $-\text{CH}(\text{CH}_3)-\text{CH}_2-$], 1.9 [s, $-\text{C}(\text{Br})-(\text{CH}_3)_2$], 3.27-3.41 [m, $-\text{CH}(\text{CH}_3)-\text{CH}_2-$], 3.44-3.73 [m, $-\text{CH}(\text{CH}_3)-\text{CH}_2-$],

2.42 [t, $-\text{C}(\text{O})-\text{CH}_2-\text{CH}_2-$], 2.24 [t, $-\text{C}(\text{O})-\text{CH}_2-\text{CH}_2-$], 1.96 [s, $-\text{CH}_2-\text{C}\equiv\text{CH}$], 1.84 [m, $-\text{CH}_2-\text{C}\equiv\text{CH}$].

7.5 Synthesis of BA ABA and CA Block Copolymers by ATRP

BA (PPO-PSMA): As a typical example for the general experimental procedure, 16 mg (0.11 mmol) of CuBr and 53 mg (0.34 mmol) of bpy were placed in a dry schlenk flask equipped with a stir bar. The flask was evacuated under high vacuum and back-filled with nitrogen three times before leaving it under nitrogen. 1 mL of previously degassed anisole was introduced into the flask via a nitrogen-purged syringe. The solution was stirred at room temperature for 30 min to enable homogenization and formation of the catalyst-ligand complex. This was followed by addition 525 mg (2.6 mmol) of degassed SMA via a nitrogen-purged syringe. 300 mg (0.11 mmol) of the mono- or heterofunctional macroinitiator was dissolved in 1 mL of degassed anisole and introduced into the flask via a nitrogen purged-syringe. Degassing was carried out for 15 min after which polymerization was carried out at 40 °C. After 20 h the flask was opened to air, allowed to cool and excess THF added. The polymer was purified by column chromatography, followed by precipitation into excess hexane and dried under high vacuum for 48 h at room temperature.

ABA (PSMA-PPO-PSMA): Exactly the same procedure above was followed with 16 mg (0.11 mmol) of CuBr and 53 mg (0.34 mmol) of bpy, 250 mg (0.11 mmol) of the difunctional macroinitiator and 1.32 g (6.6 mmol) of SMA. Polymerization was carried out at 40 °C for 90 min. Yield based on monomer conversion: PPO-PSMA (71%), PSMA-*b*-PPO-PSMA (85%). ^1H NMR (both, 400 MHz, DMSO- d_6): δ (ppm) = 0.60-0.99 (m br., $-\text{C}-\text{CH}_3$), 1.02-1.06 (m, $-\text{CH}-\text{CH}_3$, PPO), 1.17-1.39 [d, $-\text{C}-(\text{CH}_3)_2$], 1.38 [s, $-\text{C}(\text{N}_3)-(\text{CH}_3)_2$] (BA from heterofunctional initiator), 1.86 [s, $-\text{C}(\text{Br})\text{CH}_3$], 1.52-2.09 (s br., $-\text{CH}_2-\text{C}-\text{CH}_3$), 3.14-3.56 (m, $-\text{O}-\text{CH}_2-\text{CH}-\text{CH}_3$, PPO), 3.76-4.11 ($-\text{CH}_2-\text{CH}(\text{O})-\text{CH}_2-$), 4.14-4.32 ($-\text{CH}_2-\text{CH}(\text{O})-\text{CH}_2-$).

Determination of degree of polymerization (DP): The DP of the PSMA blocks of the PPO-PSMA copolymers were determined from the ^1H NMR spectra in DMSO- d_6 using the relation $I_e/I_c \times n$, with I_e/I_c being the integral ratio of the PSMA backbone and PPO methyl protons peaks, and n being the DP of the PPO block. For the PSMA-PPO-PSMA copolymers, the total DP of the PSMA blocks determined from the ^1H NMR spectra was divided by two.

CA (F₁₀-PSMA): As an example for the general experimental procedure, 28 mg (0.29 mmol) of CuCl, 90 mg (0.57 mmol) of bpy and 200 mg (0.287 mmol) of the perfluoro-initiator were placed in a dry schlenk flask equipped with a stir bar. The flask was evacuated under high vacuum and back-filled with nitrogen three times before leaving it under nitrogen. 2 mL of previously degassed α,α,α -trifluorotoluene was introduced into the flask via a nitrogen-purged syringe. The solution was stirred for 30 min to enable homogenization and formation of the catalyst-ligand complex. This was followed by addition 1.72 g (8.6 mmol) of degassed solketal methacrylate (SMA) via a nitrogen-purged syringe. Further degassing was carried out for 15 min after which polymerization was carried out at 50 °C. After 40 mins the flask was opened to air, allowed to cool and excess THF added. The polymer was purified by column chromatography, precipitated into excess *n*-hexane, and dried under high vacuum for 48 h at room temperature. Yield based on monomer conversion: 70 %. ¹H NMR (400 MHz, DMSO-*d*₆): δ (ppm) = 0.60-0.99 (m br., -C-CH₃), 1.17-1.39 [d, -C-(CH₃)₂], 1.52-2.09 (s br., -CH₂-C-CH₃), 3.76-4.11 (-CH₂-CH(O)-CH₂-), 4.14-4.32 (-CH₂-CH(O)-CH₂-). ¹⁹F NMR (200 MHz, DMSO-*d*₆): δ (ppm) = -131.20 [-(CF₂)₇-CF₂-CF₃], -126.87 [-(CF₂)₇-CF₂-CF₃], -124.46 [-CH₂-CF₂-(CF₂)₇-], -85.88 [-(CF₂)₇-CF₂-CF₃].

Determination of degree of polymerization (DP): The DP of the PSMA blocks of the F₁₀-PSMA-N₃ polymers was estimated from the ¹⁹F NMR spectra recorded in DMSO-*d*₆ solutions which contained 0.2 vol% TFT as an internal reference standard, using the following formula

$$DP = A \times \frac{5I_p}{3I_{TFT}} \quad (1)$$

where *A* represents the integral ratio of the CF₃ peak of TFT to that of the polymer in the ¹⁹F NMR spectrum. *I_p* and *I_{TFT}* denote the integral values of the backbone methyl protons of the polymer and the phenyl protons of TFT, respectively, in the ¹H NMR spectrum.

7.6 Replacement of Br Chain-End Functionality with N₃ (Azidation Reaction)

The bromine (Br) chain end-functionality of the CA and ABA copolymers were replaced with the azido (N₃) functionality. The replacement simply involves reaction of the polymers with excess NaN₃ in DMF at room temperature. For a typical experimental procedure, 950 mg of ABA (0.08 mmol) was dissolved in 6 mL of freshly distilled DMF and 20 mg (0.31 mmol) of NaN₃ was added. The reaction vessel was sealed and the reaction was allowed to proceed for 24 h under stirring. Afterwards, 250 mL of diethyl ether was added and the reaction mixture was filtered. This was followed by washing of the ethereal solution with distilled

water until it became transparent. The ethereal solution was then dried over anhydrous MgSO_4 . The solution was then concentrated with rotary evaporation and polymer precipitated into excess *n*-hexane. Under high vacuum, the polymer was dried at room temperature for 48 h. Yield = 80%. ^1H NMR (400 MHz, $\text{DMSO-}d_6$): δ (ppm) = 0.60-0.99 (m br., $-\text{C}-\text{CH}_3$), 1.02-1.06 (m, $-\text{CH}-\text{CH}_3$, PPO), 1.17-1.39 [d, $-\text{C}-(\text{CH}_3)_2$], 1.38 [s, $-\text{C}(\text{N}_3)-(\text{CH}_3)_2$], 1.52-2.09 (s br., $-\text{CH}_2-\text{C}-\text{CH}_3$), 3.14-3.56 (m, $-\text{O}-\text{CH}_2-\text{CH}-\text{CH}_3$, PPO), 3.76-4.11 ($-\text{CH}_2-\text{CH}(\text{O})-\text{CH}_2-$), 4.14-4.32 ($-\text{CH}_2-\text{CH}(\text{O})-\text{CH}_2-$).

7.7 Copper(I)-Catalyzed Alkyne-Azide Cycloaddition (CuAAC) ‘Click’ Reactions

The azido end-functionalized block copolymers, N_3 -PPO-PSMA and N_3 -PSMA-PPO-PSMA- N_3 , were ‘clicked’ with $\text{F}_9\text{C}\equiv\text{H}$ to afford F_9 -PPO-PSMA (CBA) and F_9 -PSMA-PPO-PSMA- F_9 (CABAC), respectively. Similarly, the azido end-functionalized polymers, F_{10} -PSMA- N_3 were ‘clicked’ with $\text{PPO}-\text{C}\equiv\text{H}$ to afford F_{10} -PSMA-PPO (CAB). The same experimental conditions were used for all the ‘click’ reactions. The general experimental procedure for one of the polymers is as follows;

In a schlenk flask containing 570 mg (0.03 mmol, $M_n \sim 18700 \text{ g mol}^{-1}$) of N_3 -PSMA-PPO-PSMA- N_3 and 72 mg of $\text{F}_9\text{C}\equiv\text{H}$ (0.12 mmol), 5 mL of freshly distilled THF was added and stirred for complete dissolution. The solution was degassed for 15 min with nitrogen followed by addition of 3 mg CuBr (0.02 mmol), 16 mg DIPEA (0.12 mmol) and 3.2 mg TBTA (0.006 mmol). Further degassing was carried out for additional 10 min and the flask placed in an oil bath at 50 °C for 20 h.⁵ Purification of the product was by column chromatography with silica stationary phase and THF as eluent, followed by precipitation into excess *n*-hexane.

Yield = 95%. ^1H NMR (400 MHz, $\text{DMSO-}d_6$): δ (ppm) = 0.60-0.99 (m br., $-\text{C}-\text{CH}_3$), 1.02-1.06 (m, $-\text{CH}-\text{CH}_3$, PPO), 1.17-1.39 [d, $-\text{C}-(\text{CH}_3)_2$], 1.78 (s, $-\text{N}-\text{C}-\text{CH}_3$), 1.52-2.09 (s br., $-\text{CH}_2-\text{C}-\text{CH}_3$), 2.29 [s, $-\text{O}-\text{C}(\text{O})-\text{CH}_2-$], 2.63 (s, $-\text{CH}_2-\text{C}=\text{CH}$), 3.14-3.56 (m, $-\text{O}-\text{CH}_2-\text{CH}-\text{CH}_3$, PPO), 3.76-4.11 [$-\text{CH}_2-\text{CH}(\text{O})-\text{CH}_2-$], 4.14-4.32 [$-\text{CH}_2-\text{CH}(\text{O})-\text{CH}_2-$], 7.95 ($-\text{CH}_2-\text{C}=\text{CH}-$).

7.8 Acidic Hydrolysis of the Acetonide Groups of the Block Copolymers

The acetonide groups of the hydrophobic PSMA blocks of the copolymers were removed by acidic hydrolysis to yield hydrophilic poly(glycerol monomethacrylate) (PGMA) blocks. In a typical procedure 200 mg of F_9 -PPO-PSMA was dissolved in 10 mL of 1,4 dioxane in an

open single neck round bottom flask. 1 mL of 1 N HCl solution was added dropwise and slowly via a syringe. The transparent solution was left to stir for 48 h at room temperature after which it was dialyzed against water for 48 h, and then freeze-dried to give F₉-PPO-PGMA block copolymer as white solid. Yield = 95 %. ¹H NMR (400 MHz, DMSO-*d*₆): δ (ppm) = 0.60-0.99 (m br., -C-CH₃), 1.02-1.06 (m, -CH-CH₃, PPO), 1.80 [s, -N-C-(CH₃)₂], 1.52-2.09 (s br., -CH₂-C-CH₃), 2.29 [s, -O-C(O)-CH₂-], 2.63 (s, -CH₂-C=CH), 3.14-3.12 [m, -O-CH₂-CH-CH₃ from PPO and -CH₂-CH(O)-CH₂-], 4.69 [s, -CH(OH)-CH₂(OH)], 4.95 [s, -CH(OH)-CH₂(OH)], 7.95 (-CH₂-C=CH-).

7.9 References

1. Kyeremateng, S.O.; Amado, E.; Kressler, J. *Euro. Polym. J.* **2007**, *43*, 3380.
2. Kyeremateng, S. O.; Amado, E.; Blume, A.; Kressler J. *Macromol. Rapid Commun.* **2008**, *29*, 1140.
3. Liu, S.; Armes, S.P. *J. Am. Chem. Soc.* **2001**, *123*, 9910.
4. Coessens, V.; Nakagawa, Y.; Matyjaszewski, K. *Polym. Bull.* **1998**, *40*, 135.
5. Binder, W. H.; Sachsenhofer, R.; Straif, C. J.; Zirbs R. *J. Mater. Chem.* **2007**, *17*, 2125.

Appendix

Appendix 1: NMR Spectra of ATRP Initiators

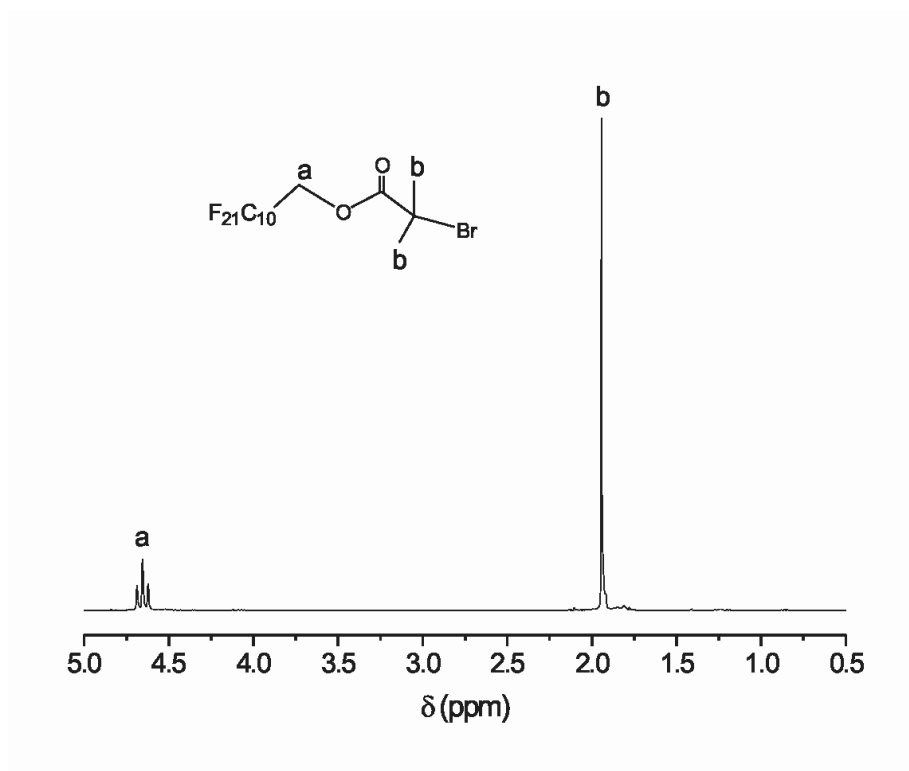


Figure A1.1 ^1H NMR spectrum of perfluoro-initiator ($\text{F}_{10}\text{-Br}$) in CDCl_3 (400 MHz)

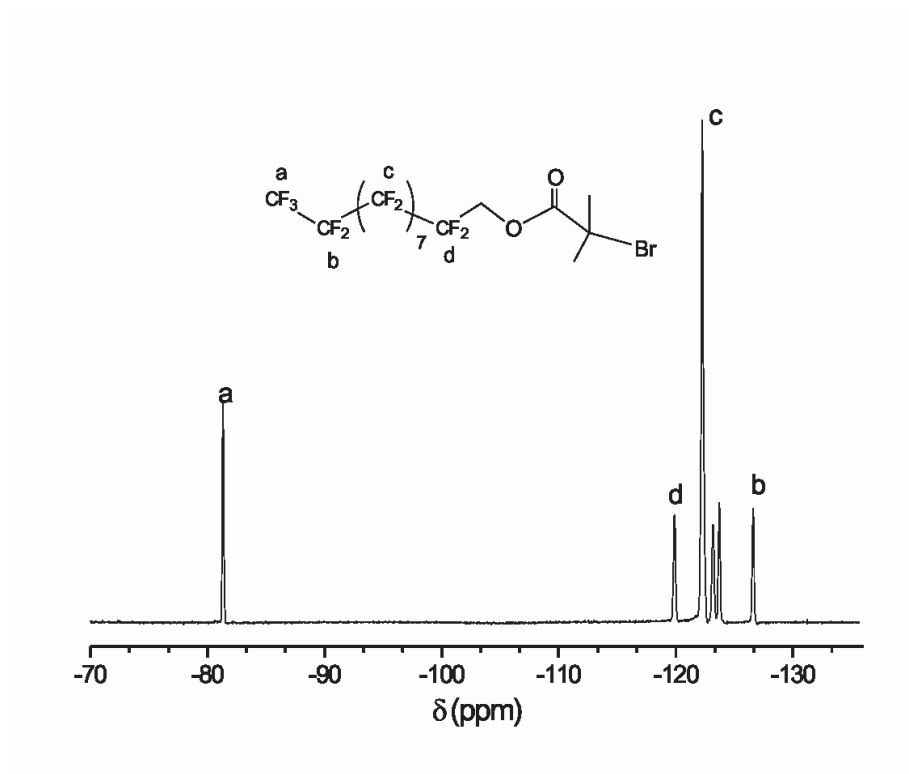


Figure A1.2 ^{19}F NMR spectrum of perfluoro-initiator ($\text{F}_{10}\text{-Br}$) in CDCl_3 (200 MHz)

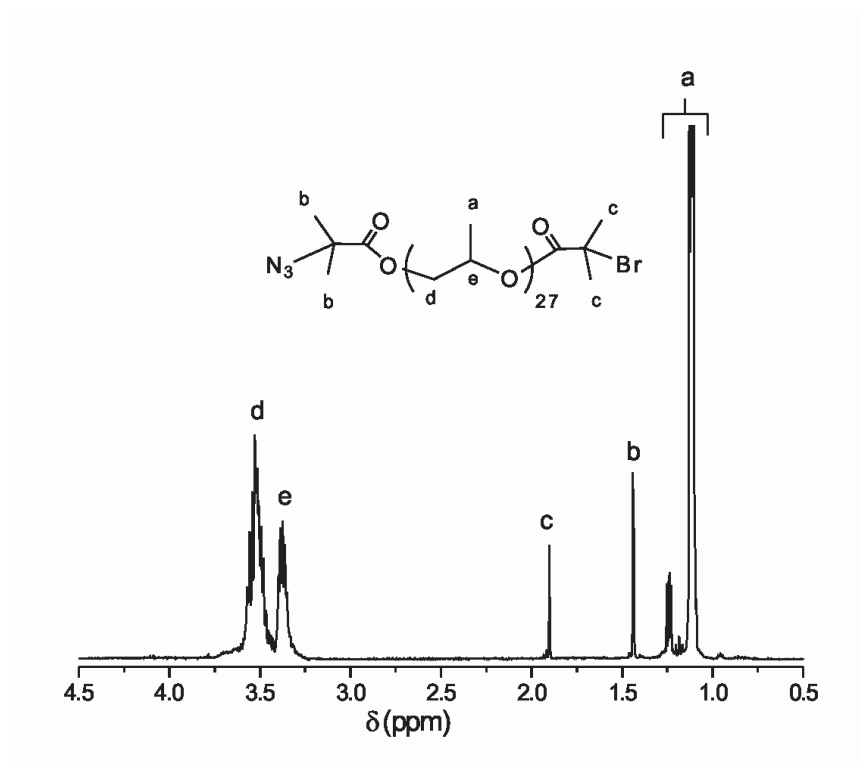


Figure A1.3 ^1H NMR spectrum of heterofunctional PPO macroinitiator ($\text{N}_3\text{-PPO-Br}$) in CDCl_3 (400 MHz)

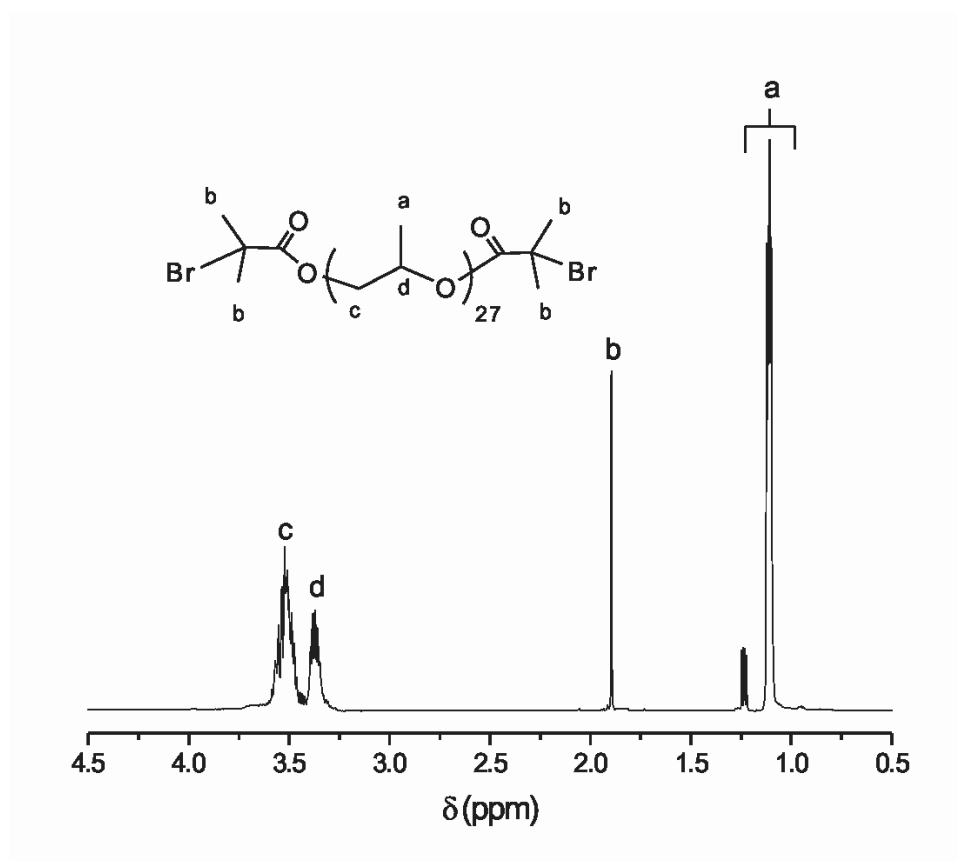


Figure A1.4 ^1H NMR spectrum of difunctional PPO macroinitiator ($\text{N}_3\text{-PPO-Br}$) in CDCl_3 (400 MHz)

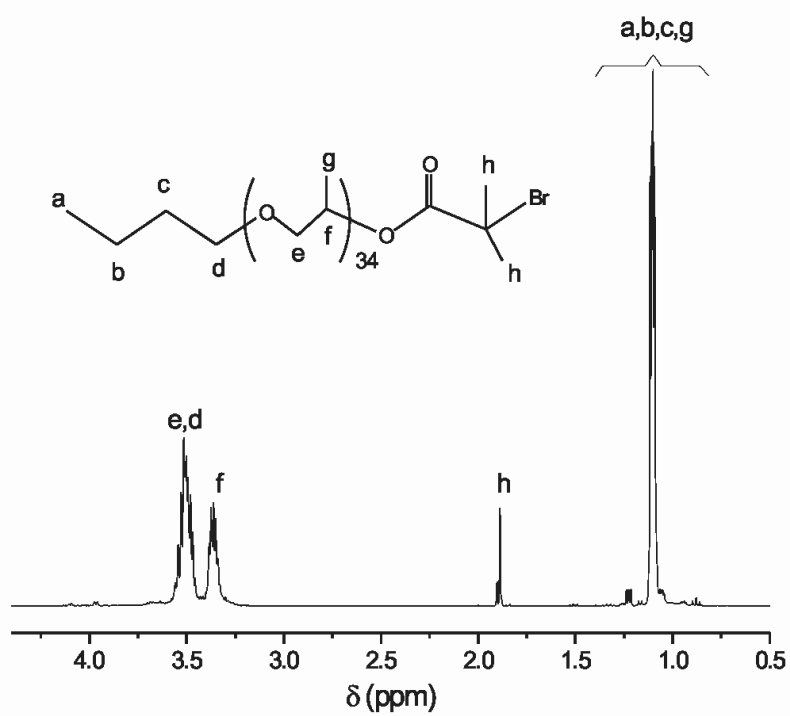


Figure A1.5 ^1H NMR spectrum of monofunctional PPO macroinitiator (PPO-Br) in CDCl_3 (400 MHz)

Appendix 2: NMR Spectra of Alkyne-End Functionalized Compounds

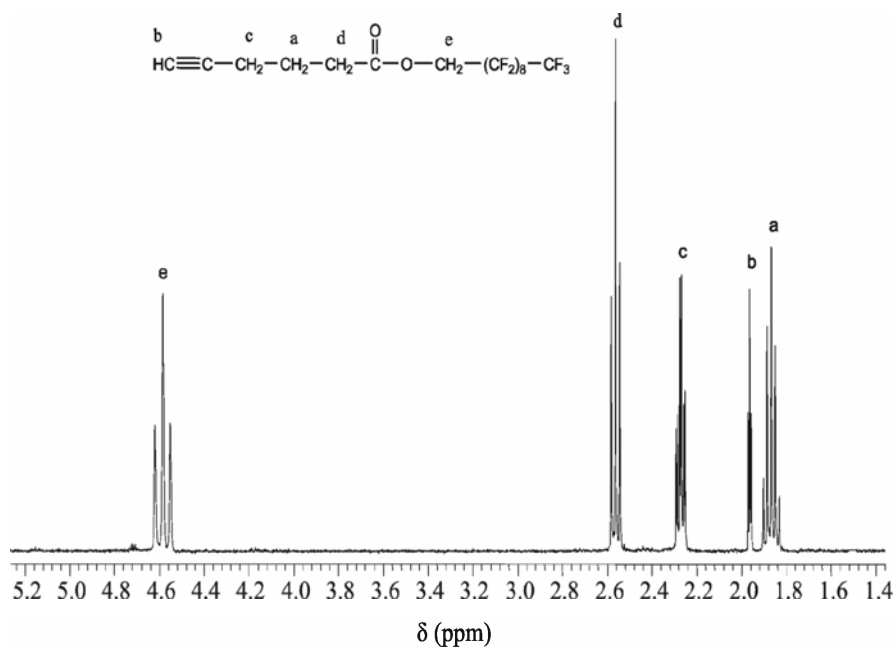


Figure A2.1 ^1H NMR spectrum of nonadecafluoro-1-decyl hex-5-ynoate ($\text{F}_9\text{C}\equiv\text{H}$) in CDCl_3 (400 MHz)

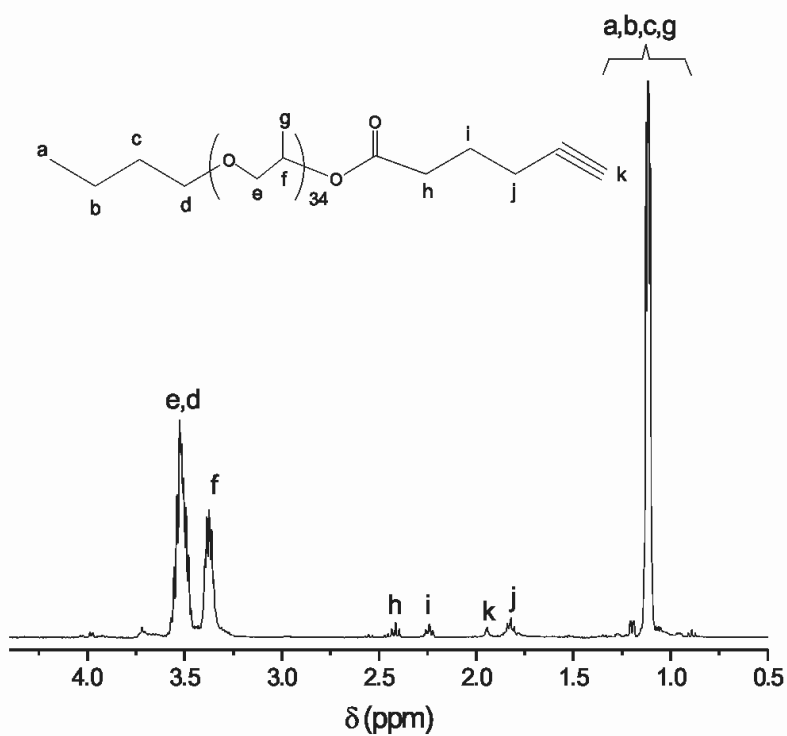


Figure A2.3 ^1H NMR spectrum of poly(propylene oxide) hex-5-ynoate ($\text{PPO-C}\equiv\text{H}$) in CDCl_3 (400 MHz)

Appendix 3: SEC Chromatogram of Polymers

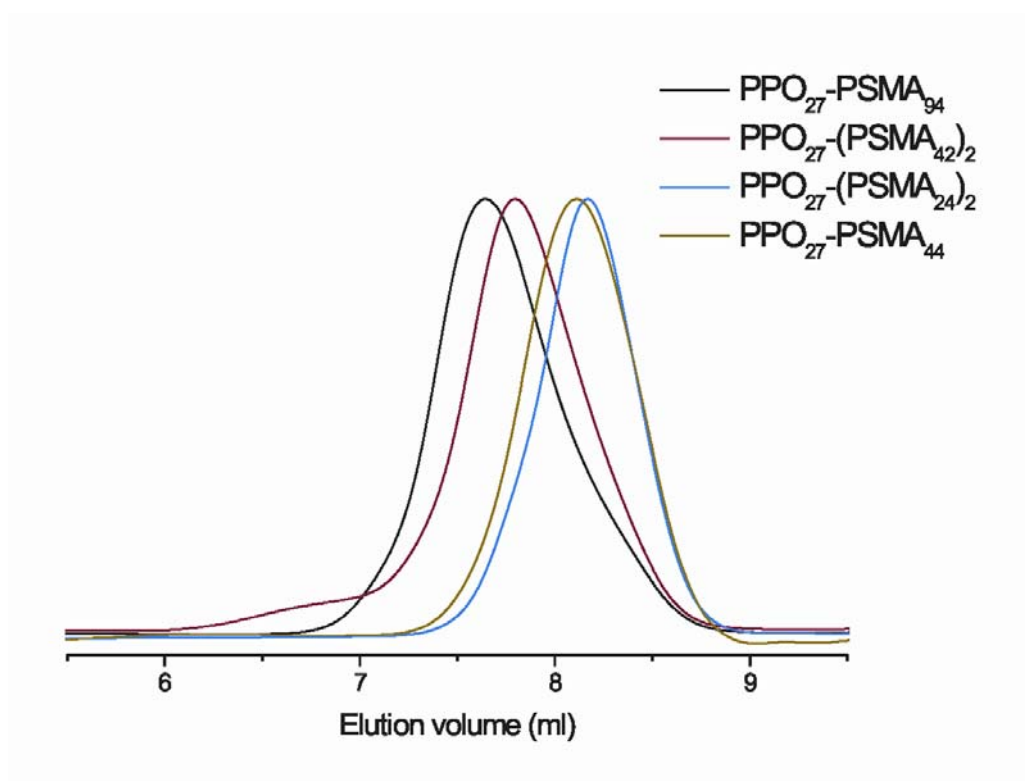


Figure A3.1 SEC traces of precursor polymers for synthesis of amphiphilic BA and triphilic CBA and CABAC copolymers.

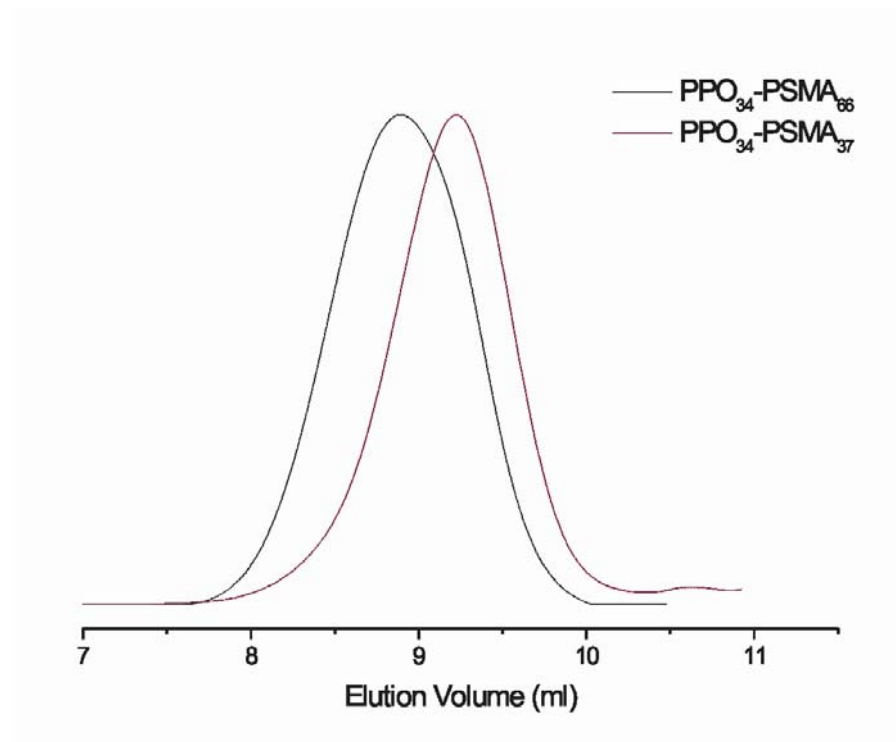


Figure A3.2 SEC traces of precursor polymers for synthesis of amphiphilic BA copolymers.

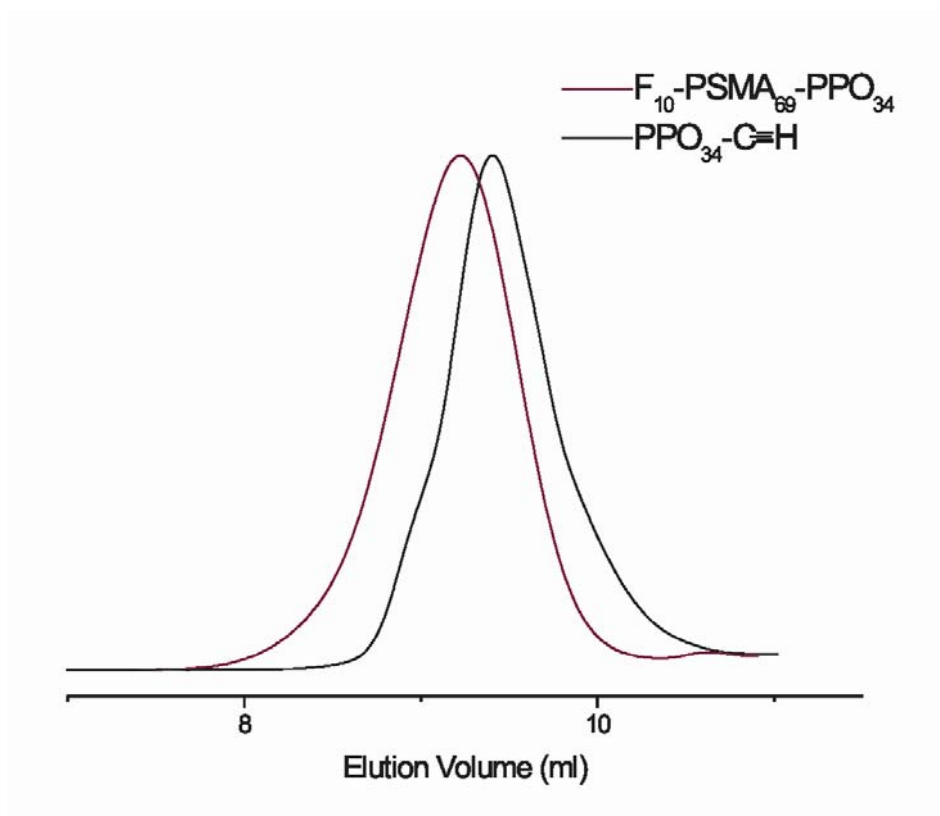


Figure A3.3 SEC trace of $\text{PPO-C}\equiv\text{H}$ and after 'clicking' with $F_{10}\text{-PSMA}_{69}\text{-N}_3$ to give the precursor polymer for synthesis of triphilic CAB copolymer.

Appendix 4: FT-IR Spectra of Polymers

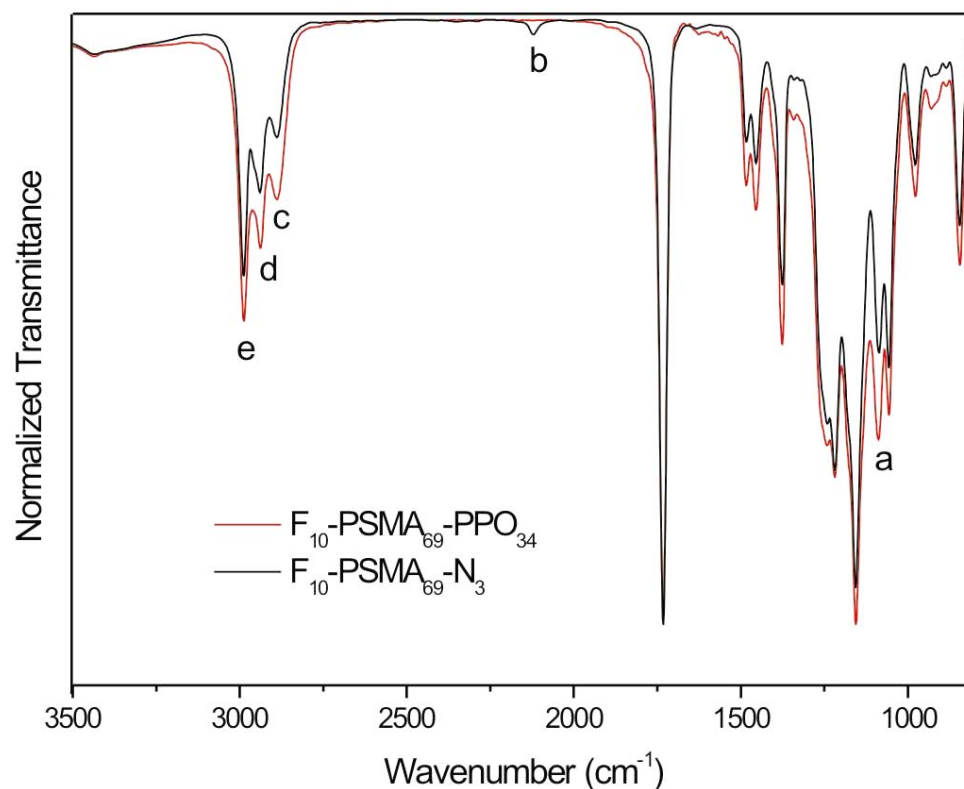


Figure A4.1 Comparison of the FTIR spectrum of F₁₀-PSMA₆₉-N₃ and the corresponding spectrum after coupling with PPO₃₄. The characteristic bands labeled a, b, c, d, and e on the spectra are the stretching vibration from the ether linkages, the stretching vibration due to the terminal N₃, the CH₃ symmetric stretching vibration, the CH₂ stretching vibration, and the CH₃ asymmetric stretching vibration, respectively.

The completion of the 'click' reaction between F₁₀-PSMA₆₉-N₃ and PPO-C≡H was confirmed by the disappearance of the azide band (at 2112 cm⁻¹) in the FT-IR spectrum of the product as shown above. Accordingly, there is a relative increase in the intensities of the CH₃ symmetric and asymmetric stretching vibrations at 2887 and 2988 cm⁻¹, respectively, due to contributions from the coupled PPO block. Furthermore, the CH₂ stretching vibration at 2947 cm⁻¹ and the absorption band at 1085 cm⁻¹ corresponding to the ether linkage also increased in intensities due to the contributions from the PPO block.

ACKNOWLEDGEMENTS

My utmost gratitude goes to GOD ALMIGHTY for the strength, wisdom and courage throughout my studies.

My deepest appreciation goes to the entire staff of Applied Polymer Science International Degree Program at Martin Luther University, Halle-Germany.

I am especially indebted to Prof. Jörg Kressler, coordinator of the program and my supervisor throughout my graduate studies and Ph.D research period. His constructive comments and suggestions have brought me this far as a polymer scientist. Many thanks to all current and previous members of Prof. Jörg Kressler's group especially Dr. Kasrten Busse, Dr. Henning Kausche, Dr. Zofia Funke, Dr. Elkin Amado, Dr. Sergej Kaiser, Dr. Yanjiao Jiang, Dr. Hangsheng Li, Sascha Reuter, Dirk Pfefferkorn, Toufik Naolou, Zheng Li, Miss Claudia Hochbach and Miss Elvira Starke. I would also like to thank Prof. Wolfgang Binder of the Chemistry Department for his invaluable advice for the 'click' reactions. Many thanks to Miss Otten of the Physics Department, Martin Luther University, for her help in carrying out all the infrared spectroscopy measurements during this work.

Finally, I would like to thank my family and friends for their support. Above all, I cannot express my full gratitude to my parents, Stephen Kyeremateng and Rose Addae, for their love, understanding and patience throughout my studies.

Publications

1. Synthesis and characterization of random copolymers of (2,2-dimethyl-1,3-dioxolan-4-yl)methyl methacrylate and 2,3-dihydroxypropyl methacrylate
S. O. Kyeremateng, E. Amado, J. Kressler *Euro. Polym. J.* **2007**, *43*, 3380–3391.
2. Synthesis of ABC and CABAC Triphilic Block Copolymers by ATRP Combined with ‘Click’ Chemistry
S. O. Kyeremateng, E. Amado, A. Blume, J. Kressler *Macromol. Rapid Commun.* **2008**, *29*, 1140–1146
3. The Aggregation Behavior of Poly(N-isopropylacrylamide) Telechelics with a Perfluoroalkyl Segment in Water
Z. Li, S. O. Kyeremateng, J. Kressler, K. Fuchise, R. Kakuchi, R. Sakai, T. Kakuchi *Macromol. Chem. Phys.* **2009**, *210*, 2138-2147
4. Effect of Hydrophilic Block-A Length Tuning on the Aggregation Behavior of α,ω -Perfluoroalkyl End-capped ABA Copolymers in Water
S. O. Kyeremateng, T. Henze, K. Busse, J. Kressler *Macromolecules* **2010**, *43*, 2502-2511
5. Melt Surface Tensions of Miscible Blends of Poly(ethylene oxide)/Poly(methyl acrylate)
D. Pfefferkorn, S. O. Kyeremateng, Z. Funke, H. W. Kammer, J. Kressler *J. Polym. Sci., Part B: Polym. Phys.* **2010**, *48*, 1893-1900

Meeting Abstracts

1. Synthesis of Perfluorinated end-capped Triphilic Block Copolymers by ATRP Combined with ‘Click’ Chemistry.
S. O. Kyeremateng, E. Amado, A. Blume and J. Kressler *Polymer Preprints* **2008**, *49*, 336
2. Structure Formation of Triphilic Block Copolymers and Their Interaction with Phospholipids
S. O. Kyeremateng, E. Amado, J. Kressler *Polymer Preprints* **2010**, *51*, 320

Curriculum Vitae

Personal Details:

Name: Samuel Oppong Kyeremateng
Date of Birth: 21 August 1978
Place of Birth: Kumasi, Ghana
Marital Status: Single

Educational Details:

02/2007-07/2010 Ph.D student at the Institute of Chemistry, Martin-Luther-Universität Halle-Wittenberg, Halle (Saale) in the group of Prof. Jörg Kressler
10/2004-12/2006 *Master of Science (M.Sc.) in Applied Polymer Science (Grade 1.3-“excellent”)*
Martin-Luther-Universität Halle-Wittenberg, Halle (Saale)
08/1998-06/2002 *Bachelor of Science (B.Sc.) in Chemistry (Second Class Upper Division)*
Kwame Nkrumah’s University of Science and Technology, Kumasi, Ghana

Professional Membership: Member of the American Chemical Society (ACS)

Award: DAAD-Prize for Best International Student 2006, Martin-Luther-Universität Halle-Wittenberg, Halle (Saale)

DECLARATION

I hereby declare that I have written and submitted this thesis independently without any help. I have not used any other sources or devices than indicated in this thesis. All quotations from literatures used, to the best of my knowledge, have been duly acknowledged. This thesis has neither been submitted to any other institution nor has it been previously used to apply for a doctorate degree.

.....

Kyeremateng, Samuel Oppong

Halle (Saale), July 2010